PHOTO-DISINTEGRATION OF LIGHT NUCLEI

by

DAVID C. MENZIES

Department of Natural Philosophy
University of Glasgow

Presented to the University of Glasgow September 1959
as a thesis for the degree of Doctor of Philosophy

PREFACE

This thesis describes some experiments designed to study the photo-disintegration of light nuclei. In the first chapter, the experimental results and the current theories of the photo-disintegration process are discussed, with particular reference to the giant resonance. It is shown that, in general, the results can be explained in the case of heavy nuclei, but that the disintegration of light elements has not been studied sufficiently extensively to test the theories. The experiments in this region either refer to a single reaction of several which may occur, or to the energy and angular distributions of the emitted particles without distinguishing the reaction which produced these particles. The cloud chamber technique allows the examination of several reactions simultaneously, and also the positive identification of each reaction.

The second chapter describes the cloud chamber, and associated electronic equipment. This equipment is quite standard, and the description is included for the sake of completeness. The author was responsible for some minor improvements in the system, and for the design of the circuit used to synchronise the 34MeV M.R.C. synchrotron with the cloud chamber. The chamber was adapted for operation at a pressure less than atmospheric by the author in collaboration with D.Balfour.

For the experiments described in the thesis, a rapid and accurate method of detecting and analysing cloud chamber tracks was required./

required. Three methods are described in chapter 3: the third method was devised by the author from a study of the others, and is believed to be superior to either, in that it combines the speed of the first method with the accuracy of the second.

In the fourth chapter, an investigation of the reaction $O^{16}(\gamma,p)N^{15}$ is described. This reaction was first studied through some photographs taken of events in a cloud chamber by I.G.Crawford and I.M.H.Preston: the author assisted in the analysis of these films, and in the compilation of the results from them. A second set of films was exposed by the author to determine the absolute value of the reaction cross-section: the author was entirely responsible for the analysis of these films and for the interpretations presented in this thesis.

The remainder of the thesis is devoted to studies of the disintegration of nitrogen and oxygen. In chapter 5, the results on the disintegration of nitrogen were taken from the results of the analysis of photographs taken and analysed by the author in collaboration with D.Balfour. The photographs of the disintegration of oxygen, in chapter 5 were also taken in collaboration, but the analysis was performed entirely by the author. The discussion and interpretation of these results, which is presented in chapter 6, is largely original, but was developed in part from discussions with Balfour.

In Appendix 1, the published matter on the range energy relations for heavy recoil nuclei is reviewed, and the possible methods of calculating relations are discussed. The derivation of the relations

which/

which were used in the interpretation of the observed results in chapter 5 is then described. The author was responsible for the application of this method to low energy (0 - 10MeV) recoils, and for the calculation of the values used for the effective charge of these ions. The second appendix contains a series of cloud chamber photographs typical of those obtained in the course of the work described throughout the thesis.

ACKNOWLEDGMENTS

The author wishes to express his appreciation of Mr.Balfour's collaboration in the work performed on the disintegration of nitrogen. He is grateful to Professor P.I.Dee, Mr. J.M.Reid, and Mr. J.R.Atkinson for their encouragement and sustained interest in the work described in this thesis. His thanks are also due to Mr.Dixon of Glasgow and to the staff of the M.R.C. synchrotron at Cambridge, and to Dr.McFarlane and the staff of the 340MeV Glasgow synchrotron, for their co-operation. Finally, the author wishes to acknowledge the award of a research studentship by the Department of Scientific and Industrial Research during his period of study.

CONTENTS

C O N T E N T S (Contd)

CHAPTER 1. Introduction

CHAPTER 1 INTRODUCTION

1. 1 Historical

The disintegration of a nucleus by electromagnetic radiation was first observed by Chadwick and Goldhaber (1), who showed that deuterium, when exposed to the γ-rays from thorium C", broke into its constituent nucleons. A short time later, Szillard and Chalmers (2) reported that neutrons were emitted when berillium was exposed to the same radiation. The first comprehensive survey of photo-neutron emission was undertaken by Bothe and Gentner (3), who used the radiation from the 440keV resonance in the reaction $Li^{7}(p,\gamma)Be^{8}$.

The intensity of the radiation used in these early experiments was small, and although the emission of other particles was expected, this was not observed until a more powerful source of radiation had been developed. Such a source was provided by the betatron (4), and in 1944, Huber et al. (5) observed a (γ,p) reaction. In 1946, Baldwin and Klaiber reported an experiment in which (γ,α), and multiparticle events were observed in a cloud chamber (6).

The early experiments were limited by the narrow energy band covered by the photons from a nuclear reaction, and provided little information about the variation of the cross-section with energy. The first measurement of this was carried out by Baldwin and Klaiber (7) in 1948, and revealed a broad pronounced maximum in the cross-section curve for the (γ,n) reaction at about 20MeV. Later work (8) showed that this resonance was a feature of all photon induced reactions,/

reactions, and that its general characteristics were remarkably constant through-out the periodic table.

Since then, this resonance has become known as the "Giant Resonance of Photo-disintegration", and has been studied for a large number of elements, using a variety of techniques. There have also been several attempts to explain the phenomena theoretically, which have met with a varying degree of success. The principal results and theories are reviewed in the following pages.

---

1. 2 Experimental Results

It has already been observed that the most striking feature of the results on photo-disintegration is the giant resonance. Its properties have been studied for a large number of isotopes: the results are reviewed in the following paragraphs.

The energy of the maximum in the cross-section curve varies smoothly from 26MeV in helium (15) to about 11MeV in bismuth (16). The variation has been plotted by Montalbetti et al., from measurements of the (γ, n) reaction in a large number of isotopes(17). Their results are reproduced in figure 1, and show that the energy of the peak in the cross-section decreases as $A^{-1/5}$.

The width of the resonance varies between 4MeV and 10MeV, but does not vary steadily with A. It appears to be related to the number of protons and neutrons in the nucleus: a plot of the width against the number of neutrons shows a number of maxima and minima. In the accompanying diagram (fig.2), which is reproduced from a paper

by/

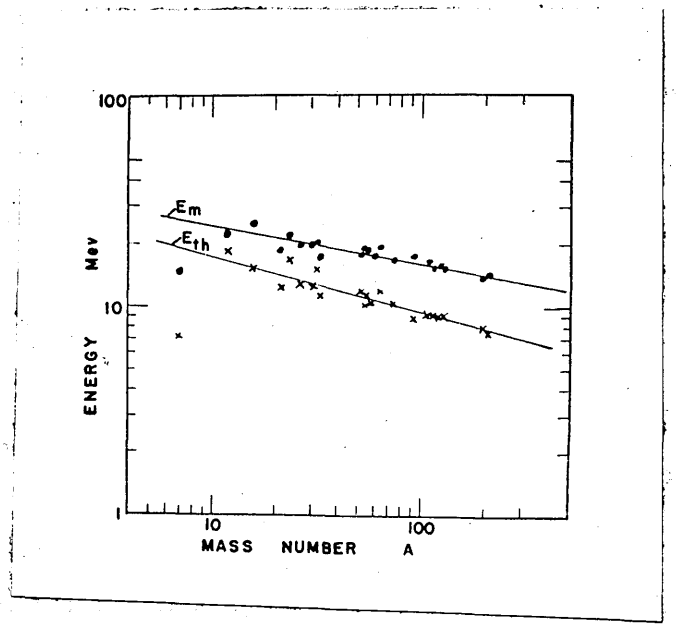

Figure 1

Plot of the energy (E_m) at which the peak in the (γ,n) cross-section occurs, and the threshold energy (E_{th}) for that reaction in the same isotopes (17).

by Osokina (18), it will be seen that the minima co-incide with the proton and neutron "magic numbers". The diagram also shows the correlation between the width of the resonance and the deformation of the nucleus. There have been some reports that the abnormal width of the resonance in deformed nuclei is due to the existence of two maxima in the cross-section curve, which are not normally resolved. In the case of tantalum, two peaks have been detected, using a neutron counting system (19). Other workers (20), however, using an activation technique, observe a single broad resonance, and claim that the second peak is due to the onset of the (γ,2n) reaction, which with a neutron counting system will be indistinguishable from the (γ,n) reaction. This position has not yet been resolved, but it is clear that the width of the giant resonance of deformed nuclei is abnormally large.

The integrated cross-section (σ_{int}) appears to vary smoothly with the mass number of the element concerned, and to be approximately $\propto A$. Kerst and Price (21), and Terwilliger et al. (22) have measured the integrated cross-section of the (γ,n) reaction for a number of elements, and Levinger and Bethe (23) have shown that their data could be fitted with an expression of the form

$$\sigma_{int} = 0.14 \frac{NZ}{A}$$

If the number of neutrons (N) is assumed to be equal to the number of protons (Z), this reduces to

$$\sigma_{int} = 0.07\ A$$

which probably fits the experimental data equally well. It should perhaps/

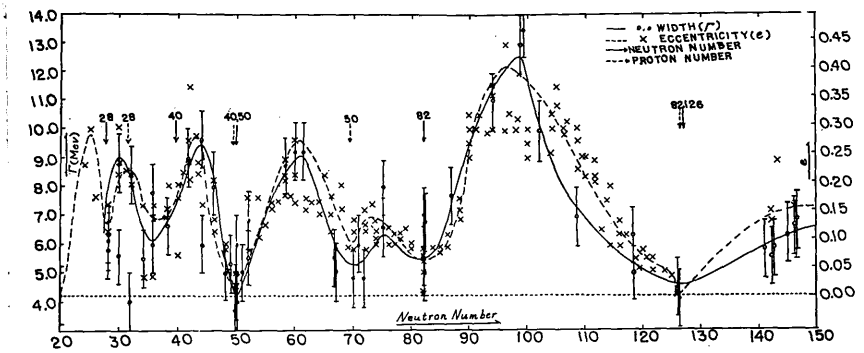

FIG. 1. Correlation between the nuclear eccentricity e and the photonuclear resonance width Γ. Crosses are eccentricities listed i ble I. Open circles are observed resonance widths for nonmagic nuclei; closed circles are for magic nuclei. (See Table IV.) Dashe d solid curves are for eccentricity and for resonance width respectively. Arrows indicate the magic numbers: the solid one is fo utrons and the dashed one is for protons. The dotted straight line indicates the intrinsic width, Γ_0, which is taken in this paper a Mev. The uncertainty of the resonance width is assumed to be 1 Mev; the uncertainty of the eccentricity is from 20 to 30% of it lue.

Figure 2

The width of the giant resonance as a function of the number of neutrons in the nucleus. The proton and neutron magic number nuclei are indicated in the figure. (18).

perhaps be emphasised that these results refer only to the (γ,n) reaction: while it is true to say that this is the only important reactions in heavy elements, in light elements other reactions will account for a large part of the photo-nuclear cross-section, and the fit to the above formula of the (γ,n) integrated cross-section is then found to be poor.

The maximum cross-section for the photo-nuclear process is of the order of several millibarns in most elements, and varies from element to element. The cross-section for the (γ,n) reaction increases with A, but that for the (γ,p) reaction remains substantially constant (24).

The results can be summarised as follows :

(1) The cross-section curve for photo-nuclear processes exhibits a broad resonance.

(2) The energy of the maximum in the cross-section varies from 26MeV to 11MeV, approximately as $A^{-1/5}$.

(3) The width of the resonance is several MeV, and varies from isotope to isotope, being related to the deformation of the nucleus, and to the proton and neutron magic numbers.

(4) The integrated cross-section is proportional to A.

(5) The maximum cross-section is of the order of several millibarns.

At energies below the giant resonance, in some light elements, the cross-section curve is found to exhibit a series of sharp peaks. Wright et al. have observed three such peaks in the cross-section for the/

the reaction N^{14} $(\gamma,p)C^{13}$ between the reaction threshold (7.54MeV) and the upper limit of their measurements (about 11MeV). Studies of the disintegration of oxygen (26-32) all reveal a similar fine structure.

A large volume of work has been devoted to the measurement of the angular distributions of the particles emitted from a target under the influence of radiation. The results can generally be fitted with a curve of the form

$$A + B\sin^2\theta(1+p\cos\theta)^2$$

In general, p is small, and the value of B/A varies from 0 (isotropic distribution) to large values ($\sin^2\theta$ distribution), and for a given reaction, both p and B/A vary with the energy of the particles measured. Some typical values are shown in table 1, which is reproduced from a review article by de Sabbata (33).

Most of these results are subject to the criticism that the reaction causing the emission of the particles cannot be identified with certainty - the observed protons may be due to the (γ,p) reaction, or to the (γ,pn) reaction, and the same applies to the neutrons (if these reactions are all energetically possible).

The above discussion has been mainly concerned with the study of the emission of single nucleons. Recently considerable interest has been aroused in the simultaneous emission of a proton and a neutron. It has been shown that at energies of the order of 100MeV, this process becomes important, and angular correlations have been observed between the directions of the emitted fragments (35,36).

In/

TABLE 1.

Nuclei	p	σ_a/σ_d %	E_{max} (MeV)	Intervallo energetico dei protoni considerati
^{9}Be	0.85÷1	15÷20	30 42 60 80	tutti i protoni
^{12}C	0.25	1	23	tutti i protoni
^{12}C	0.8	13	65	protoni > 14 MeV
^{12}C	0.5÷0.75	5÷11	30 42 60 80	tutti i protoni
^{12}C	0.6	7	35	protoni > 7 MeV
^{12}C	0.6	7	31	protoni > 5.5 MeV
^{12}C	0.3	1.8	20÷40	per protoni di ~ 6 MeV
^{15}N	0.24	1	18.7 e 24.6	9.3÷14 MeV
^{16}O	0.2	0.8	70	protoni > 10.5 MeV
^{27}Al	0.7	10	40 e 65	protoni a più alta energia
^{27}Al	1.35	36	65	protoni > 14 MeV
Si	0.75	11	30	protoni > 7 MeV
Si	0.57	6	30	protoni > 5.5 MeV
^{59}Co	0.5	5	23	tutti i protoni
^{59}Co	1	20	24	tutti i protoni
Ni	1.45	40	65	protoni > 14 MeV
Cu	0.5	5	23	tutti i protoni
Mo	2	80	65	protoni > 14 MeV
^{103}Rh	0.2	0.8	70	7÷10 MeV
^{103}Rh	0.3	1.8	70	10÷16 MeV
In	0.75÷1	11÷20	23	tutti i protoni
^{197}Au	1.0	20	70	11÷17 MeV
^{209}Bi	2	80	24	protoni > 10 MeV

In this energy region, processes involving the fission of the target nucleus into many fragments also become more probable, and in such cases, a fast proton and neutron are often emitted (37).

The study of the photo-fission of a nucleus is rendered difficult by the short range of the fragments, and by their multiplicity. Some reactions have been studied, using loaded nuclear emulsions (38) and cloud chambers (6, 25). The cross-sections are found to be several orders of magnitude less than that for the emission of a single nucleon, in the energy region of the giant resonance.

From the above discussion, it will be seen that

(a) reactions involving the emission of a single nucleon account for a large part of the photo-nuclear cross-section. Proton and neutron emission are equally important in light elements, but the latter process is dominant in heavy elements.

(b) the absorption cross-section rises from the reaction threshold to a maximum value of several millibarns, then falls to about .1mb. The properties of the resonance vary from element to element.

(c) in light elements, the cross-section curve may exhibit a series of sharp maxima below the giant resonance.

(d) the angular distributions of the emitted nucleons can be fitted by curves of the form

$$A + B\sin^2\theta(1 + p\cos\theta)^2$$

(e)/

(e) at high energies (7 50MeV), the disintegration of the nucleus into many particles becomes more probable. The emission of an energetic proton is often accompanied by the emission of a fast neutron, and correlations are observed between the directions of such pairs of nucleons.

---

1. 3 Theories of the Photo-disintegration Process.

1.3.1 Sum Rules

In theoretical studies of the interaction of electromagnetic radiation with matter, it is usual to expand the radiation field in terms of its electric and magnetic multi-pole components. This procedure is also applied in the case of nuclear interactions. It is found that dipole interactions are much stronger than higher multipoles, and electric multipoles are stronger than the corresponding magnetic multipoles. Thus calculations of the reaction cross-sections etc. can deal only with E1 absorption, and ignore the effect of other multipoles, in first order calculations, at least.

Levinger and Bethe (41) calculated the integrated cross-section for dipole absorption, without, in the first instance making any assumptions about nuclear models:

$$\sigma_{int} = \frac{2\pi^2 e^2 h}{Mc} \frac{NZ}{A} \sim \frac{\pi^2 e^2 h}{Mc} \frac{A}{2} = 0.015A \text{ Mev.b}$$

with the obvious significance for the symbols.

This result ignores the effect of exchange forces: it has been shown that such forces will increase the dipole sum (43), and Levinger allowed for the effect by the inclusion of a parameter, χ,

modifying/

modifying the equation to

$$\sigma_{int} = 0.015\ A\ (1 + 0.8\alpha)\ \text{MeV.b}$$

This correction is model dependent, and the coefficient of α was calculated using a degenerate Fermi gas confined in a square well of radius $R = r_o A^{1/3} \times 10^{-13}$ cm, where r_o was taken as 1.5, as the nuclear model.

Levinger and Bethe compared their result with experimental measurements of the (γ, n) cross-section (23), and found that the expression was of the correct form, but its predictions were rather low. The calculated result, however, is of the same order as the integrated cross-section of the giant resonance, and it is therefore reasonable to suppose that the predominant mode of absorption in this region is El.

The method is not capable of detailed predictions as to the shape of the cross-section curve, but can be used to calculate the mean energy, and the harmonic mean energy of the absorbed photons:

r_o	1.2	1.50		Expt.
Mean energy	25MeV	16MeV	for Cu^{63}	25MeV
Harmonic mean energy	5MeV		Cu^{63}	20MeV
	1MeV		U	

The value of the mean energy varies with r_o as r_o^{-2}, but is independent of A, while the harmonic mean energy is independent of r_o. The results disagree with experiment, but the agreement is improved if a model involving strong correlations between small groups of/

of nucleons is assumed (44).

Levinger (45) has also considered the variation of the mean energy ($\overline{W}$) and the harmonic mean energy (W_h) with A. Using an independent particle model, with a harmonic potential well, he finds

$$\overline{W} = W_h = 42A^{-1/3}$$

The inclusion of exchange forces modifies this result to

$$W_h = 60A^{-1/3}$$

This value is still rather smaller than the experimental result, but the agreement is not unsatisfactory.

1.3.2 Collective Models

Sum rule calculations can predict the integrated cross-section, but give no information about the detailed variation of the cross-section with energy. This can only be obtained from studies of a particular model. The earliest models were based on the assumption that the nucleons are strongly bound together in the nucleus, and the interaction of a photon excites a collective motion of the whole nucleus.

Goldhaber and Teller (45) suggested three forms of collective motion which might account for the observed variation of the cross-section. The first motion envisaged an oscillation of all the protons and neutrons about a mean position, and this led to a value for the energy of the maximum in the cross-section which did not vary with A. The second model regarded the protons and neutrons as two interpenetrating imcompressible fluids moving relative to each other. This leads to

a/

a value of the energy of the maximum cross-section given by

$$E_m = 40A^{-1/6},$$

and of the integrated cross-section given by

$$\sigma_{int} = \frac{\hbar^2 e^2 h}{Mc} \frac{A}{2}$$

The peak energy is correct in magnitude, but the variation with A is rather slower than the experimental result. The integrated cross-section agrees with the sum rule result.

The third form of collective motion has been developed in detail by Steinwedel and Jensen (47), and by Danos (48). In this case, it is assumed that the protons and neutrons on the nuclear surface have fixed relative positions, and the internal motion is expressed in terms of changes of density. This leads to a value of $60A^{-1/3}$MeV for the energy of the peak cross-section. The agreement with experiment is improved if a non-uniform initial distribution of protons is assumed - this reduces slightly the $A^{-1/3}$ dependence of the energy (50).

These studies make no detailed predictions as to the width of the resonance, accounting for it as being due to some form of damping of the collective motion. Businaro and Gallone (52) attribute the width to the effect of transferring all the energy of the collective motion to a single nucleon. This leads to a value of 4MeV, which agrees satisfactorily with experiment.

The exceptional width of the resonance in the case of deformed nuclei has been considered by Danos (54), and Okamoto (18).

Danos/

Danos finds that the extension of the hydrodynamic model to non-spherical nuclei leads to two values for the frequency of the dipole resonance. If the separation of the energies of these resonances is sufficient, the cross-section curve will show two peaks, and if the peaks are not resolved, the result is a single broad resonance. Okamoto compares the quadrupole moment of nuclei with the width of the resonance, and shows that there is a strong correlation.

1.3.3 Independent Particle Models

These models are based on an assumption directly opposed to that of the collective model: they assume that the bonds between nucleons in the nucleus are weak, compared with the energy of the incident radiation.

The simplest form of the model describes the nucleus as a gas of nucleons in equilibrium. The absorption of a photon results in the excitation of a new equilibrium state - the compound nucleus state - which can de-excite in a variety of ways, one possibility being the evaporation of a nucleon. The model has been applied to the calculation of the energy distributions of the emitted particles (33a, 55), and satisfactory agreement was obtained at low energies with the experimental results for medium and heavy elements. At high energies, the predicted cross-section falls short of the measured value, and in light elements, the assumption of a statistical state is not valid, since the number of nucleons is small.

Burkhardt (57) has used a more detailed form of the independent particle model, assuming that each nucleon moves in a potential well due to all the others, to calculate the dipole absorption cross-section for Cu^{63}. He compares his result with the cross-section for the (γ,n) reaction, as measured by Katz (11): taking $r_o = 1.5$, he finds that the peak cross-section occurs at an energy of 8.4MeV while the experimental value is 17MeV. This result would be considerably improved by the use of a smaller value of r_o. Burkhardt also calculates the angular distribution, and finds that this should be of the form $A+B\sin^2\theta$, with $B/A < 1$, in good agreement with experiment. Finally, he estimates the relative number of high energy protons as 0.3%, compared with the value of 10% obtained experimentally by Byerly and Stephens (58).

Courant (59) suggests that the excess of high energy particles can be accounted for by a direct photo-effect - the direct ejection of a nucleon without the formation of a compound nucleus state. This leads to a better value for the cross-section at high energies, but his initial result was still an order of magnitude too small. He points out that the use of a wine bottle potential well (instead of a square well), and of a smaller value of r_o would improve the agreement.

Courant also calculated the angular distribution of directly emitted nucleons, and obtains a result of the form

$$A + B\sin^2\theta$$

where/

where the ratio of B : A depends on the initial and final angular momentum states of the emitted particle -

$$\text{for } L \rightarrow L+1, \quad \frac{B}{A} = \frac{1/2\ (L+1)\ (L+2)}{L\ (L+1)}$$

$$L \rightarrow L-1, \quad \frac{B}{A} = \frac{1/2\ L\ (L-1)}{L\ (L+1)}$$

Large anisotropies ($B/A > 1.5$) have been observed in the angular distributions of fast protons from certain nuclei (33a, 60,61), suggesting that these protons can be accounted for by a transition of the type $L=0 \rightarrow L=1$, and the experimental results can be accounted for by an evaporation process at low energies, and a direct mechanism at high energies.

1.3.4 The Shell Model

Shell model wave functions have been successfully applied to the description of the ground states and low lying excited states of nuclei. The model has been extended to higher energies to explain the giant resonance and other photo-disintegration phenomena by Wilkinson (62,63). Weisskopf, in applying the cloudy crystal ball model, has shown that an incident particle can have a relatively long mean free path in nuclear matter ($\sim 2\times10^{-12}$ cm)(64). Wilkinson argues that the mean free path of a nucleon excited by a photon into a higher shell model state will be equally long, and that the subsequent interaction of the nucleon can be described by cloudy crystal ball wave functions.

Since the giant resonance almost exhausts the dipole sum, it is reasonable to assume that the absorption process is E1, and that the/

the shell model transitions involved will be of the type $1p \rightarrow 1d$, $1p \rightarrow 2s$, $1s \rightarrow 2p$, etc. Further, if all such transitions are considered, the dipole sum will be exhausted, and the integrated cross-section obtained will automatically agree with experiment. However, of the above transitions, only those involving nodeless wave-functions are important; these transitions are spread over many MeV, and do not immediately suggest a resonant structure. By the introduction of the concept of parent states (65), it can be shown that all possible final states are not equally probable, and the result is a modification of the cross-section curve to the familiar resonant shape. Fine structure (12, 66, 78) in the giant resonance would not be inconsistent with this picture, but is rather improbable, since the width of each single particle state, based on the mean free path mentioned above, is about 3MeV.

Wilkinson calculated the energy of the peak in the resonance, as a function of A, using a square well, and $r_o = 1.2$. His result is compared in figure 3 with the observed variation: he also calculated the variation on the assumption that the effective mass of a nucleon in the nucleus is half that of a free nucleon - this result is shown by the third curve. Rand (67) has developed a treatment of the shell model using a velocity dependent potential, and finds that good agreement with experiment (for medium and heavy nuclei) is achieved if the effect of the potential is to reduce the mass of a nucleon to 55% of its normal value. It would not be unreasonable to expect that the effective mass of a nucleon in a

light/

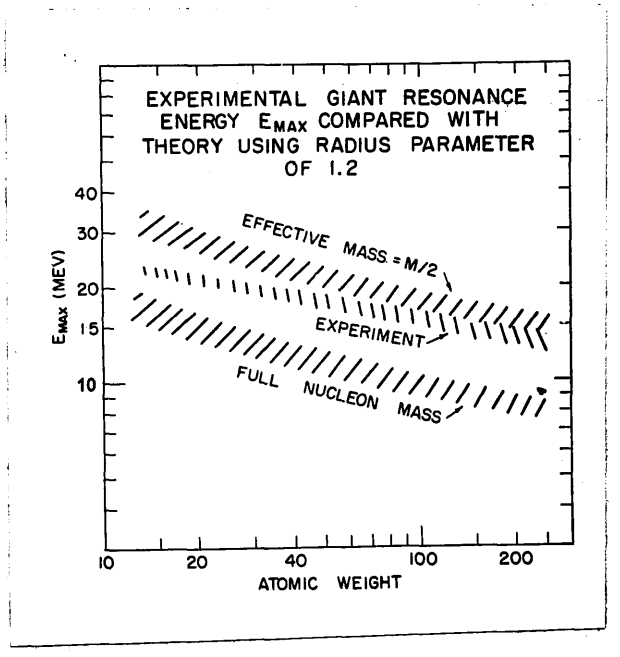

Figure 3

The energy of the maximum in the cross-section of the giant resonance, as plotted by Wilkinson (63). The figure shows the experimental variation, and the variation predicted by shell model considerations for two values of the effective mass of the nucleons in the nucleus.

light nucleus is nearer that of a free nucleon, and this would bring the third curve into line with experimental results.

The width of the resonance can be attributed to two primary factors: the energy spread of the important initial and final states, and the width of each of these states. The resultant width is estimated as about 3-5MeV, in accord with experimental results. The transitions of valency nucleons do not exhibit a resonant structure, and are spread over the whole cross-section curve, tending further to broaden the resonance - this explains the small width of the resonance for magic number nuclei. Lejkin et al. study the photo-protons from copper and nickel (71), and compare their results with shell model predictions. They find that the valency nucleons play a much more fundamental role in the determination of the cross-section than is suggested by Wilkinson, but their results are otherwise consistent with his predictions.

In the case of deformed nuclei (68) it is no longer correct to compute shell model results with a spherically symmetric potential well. Wilkinson points out that if the potential be treated as ellipsoidal, each shell model state degenerates into two separate levels. As a result, the giant resonance consists of two peaks, one due to each set of shell model states which, if not resolved, appear as a single broad resonance.

Wilkinson also considers the angular distributions to be expected from the shell model. Courant has calculated the angular distribution/

distribution of directly emitted nucleons, and Wilkinson estimates the proportion of excitations which result in the direct ejection of a nucleon

$$C = \frac{2kP\ h^2/2MR}{W}$$

where k = the wave number of the nucleon

P = the penetrability of the coulomb and centrifugal barriers

$h^2/2MR$ = the single particle reduced width

W = the imaginary part of the cloudy crystal ball potential

Assuming that the angular distribution of the evaporated nucleons is isotropic, the distribution resulting from El absorption will be of the form

$$1 + C(A + B\sin^2\theta)$$

where A and B are given by Courant's result. This result has been compared with experiment (69, 70), and satisfactory agreement was obtained. Lejkin, however, observes a rather greater asymetry than is predicted by Courant. This has been attributed to interference between emission from protons emitted from $L \rightarrow L+1$ transitions and from $L \rightarrow L-1$ transitions, which Courant does not consider (72). A large number of the observed distributions are not symmetric about 90^o, and this can be accounted for by assuming a small amount of E2 absorption. If the distribution is of the form

$$A + B\sin^2\theta(1 + p\cos\theta)^2$$

then the ratio of quadrupole transitions to dipole transitions is $p^2/5$ (16).

1.3.5/

1.3.5 High Momentum Models

One factor associated with the absorption of a photon by a nucleus has not been mentioned in the above discussion: the momentum of the incident photon. The fact that a photon carries relatively little momentum, compared with its energy, makes the absorption of a photon by a single free nucleon impossible. The difficulty can be overcome by postulating that the momentum of the final state is already present in the ground state of the nucleus. As the energy of the photon increases, however, the observed cross-section decreases much less rapidly than the number of high momentum states associated with the models described above.

High momentum states can exist in the motion of nucleons belonging to a small sub-unit of the nucleus, if the nucleons are sufficiently close together. Levinger (73) has considered such systems in the nucleus, and has performed calculations for a two nucleon system consisting of a proton and a neutron. His model is known as the "quasi-deuteronmodel". It predicts the emission of pairs of energetic nucleons - a proton and a neutron - in coincidence, with a strong correlation between their directions, and this has been observed (36) Levinger was able to account for the observed energy and angular distributions at high excitation energies ($>$ 150MeV). Dedrick (74) extended the treatment to lower energies ($>$50MeV) and found that the agreement with experiment was satisfactory.

1.3.6 Conclusions

The/

The behaviour of nuclear matter under the influence of electromagnetic radiation can be described in several ways. Sum rule calculations established that the dipole absorption cross-section is sufficiently large to account for most of the photo-disintegration cross-section. Two nuclear models have met with considerable success in the energy region of the giant resonance - the collective model and the shell model. These models are based on very different assumptions, but each can be made to fit the experimental data. The shell model is more successful in its predictions of angular distributions, and emission processes at higher energies, but this may be due to the fact that the collective model has not yet been developed sufficiently to describe phenomena involving individual nucleons (68). Brink (75) has shown that the models are formally identical if the nuclear potential is described by a harmonic oscillator potential without damping forces. He suggests that this identity may persist in some form in physical nuclei, and that it is therefore futile to attempt to distinguish the models.

At energies greater than a few tens of MeV (63) the shell model and the collective model lose their usefulness. In this region, the photon can be regarded as interacting with a small sub-unit of the nucleus which is in a high momentum state. The process is satisfactorily described by the quasi-deuteron model.

---

1. 4 Light Nuclei

Several models have been proposed to describe the photo-

nuclear/

nuclear process. These have been tested extensively for medium and heavy nuclei, where the (γ,n) reaction accounts for a large part of the photo-nuclear cross-section. In light elements, several reactions may be important, and tests of nuclear models are much more difficult. A complete test must involve the measurement of the characteristics of all the important reactions.

Experimental measurements of the disintegration of light nuclei are generally not sufficiently comprehensive to provide such a complete test. Some work has been performed using the activation technique to examine the (γ,n) reactions: this provides information about the cross-section of only one reaction, and cannot study the energy and direction of the emitted particles. Other experiments have been directed to the measurement of the energy and angular distributions of the ~~emitted~~ fragments emitted by a target under the influence of radiation. Much information can be obtained in this way, but most of the results cannot be taken as conclusive, since, unless all the fragments of each disintegration are detected, the reaction producing them cannot be identified with certainty.

The last condition mentioned above immediately suggests the use of a cloud chamber, since this technique will ensure the detection of all the charged fragments emitted from each disintegration. The low stopping power of the chamber makes it unsuitable for the study of energetic protons, and neutrons, being uncharged, cannot be detected. On the other hand, some of the important nuclear reactions/

reactions result in the formation of heavy recoil nuclei which have a very short range. Measurements of these recoils will provide as much information about the reactions which caused their formation, as measurements of the emitted nucleons. The use of a cloud chamber would permit the study of these reactions over a very wide range of excitation energies, and would ensure that each reaction was identified with reasonable certainty.

Experiments of this type are described in chapters 5 and 6 of this thesis. The ranges of the recoil nuclei observed were of the order of 1cm, and it was therefore necessary to develop a measurement technique capable of interpreting photographs of cloud chamber tracks rapidly and accurately: This is described in chapter 3.

The cloud chamber is also well suited to the study of slow charged particles. Much interest has centred on the possibility of the existence of some fine structure near the giant resonance, especially in the case of light nuclei. The disintegration of oxygen has been studied at excitation energies greater than 15MeV, using emulsion and other techniques, but there is no published work on the energy region between the threshold for the reaction $O^{16}(\gamma,p)N^{15}$ (12.1MeV) and that energy. It was therefore decided to undertake a study of the (γ,p) reaction in this energy region, and to compare the results with the theories of the photo-disintegration process in the region of the giant resonance. This work is described in chapter 4.

CHAPTER 2. Equipment and Procedure

CHAPTER 2 EQUIPMENT AND PROCEDURE

2. 1 The Operation of an Expansion Cloud Chamber

The operation of a cloud chamber depends on the fact that condensation from a supersaturated vapour will occur preferentially on charged ions. Thus if a charged particle pass through such a vapour, liquid drops will tend to form on the ions it creates, and its track in the gas will become visible. The conditions required for the formation of good tracks in a cloud chamber are :-

1. The supersaturation of the vapour must be sufficient to cause condensation to occur freely on ions, but insufficient to cause spontaneous condensation.

2. The gas must be free of unwanted condensation nuclei since these would tend to obscure any tracks which form.

3. The gas must be free from turbulent motion, which would distort the tracks.

The supersaturation of the gas in a cloud chamber with vapour can be achieved either by the diffusion of a vapour from hot to cold gas layers, making the chamber continuously sensitive in a small region, or by the adiabatic expansion of the gas in the chamber, which makes the whole chamber sensitive for a relatively short time. Since the expansion type of chamber was used exclusively for the investigations described in this thesis, the diffusion type will not be considered.

The three conditions mentioned above can be attained easily in an expansion chamber. The degree of supersaturation is controlled

by/

by varying the ratio of the expanded volume of the chamber to its normal volume - the expansion ratio. Unwanted condensation nuclei are removed in two ways: ions are removed by an electrostatic field across the sensitive part of the chamber, and dust particles are swept out by a series of slow expansions, which create a sufficient degree of supersaturation to cause condensation on macroscopic dust particles. Turbulent motion of the gas after the fast (adiabatic) expansion is reduced to a minimum by expanding the gas through a thick perforated plate.

Since the chamber is only sensitive for a short time (about 1/2 sec.), and only attains its maximum sensitivity some time after a fast expansion (about 100m.sec.), it is necessary to time the formation of the tracks accurately. The clearing field must be switched off before the tracks are formed to prevent distortion. Liquid drops take some time (about 60m.sec.) to grow to a visible size and the chamber must be photographed after this period. The timing of these operations was controlled by the "fast expansion control unit". The automatic operation of the slow expansion cycle was regulated by the "slow expansion control unit". The cloud chamber, and the associated electronic equipment are described in the following paragraphs.

---

2. 2 The Cloud Chamber

Two cloud chambers were used in the investigations described in this thesis. One chamber was designed for operation with the small (30MeV) synchrotron at Glasgow, and the second was intended for studies/

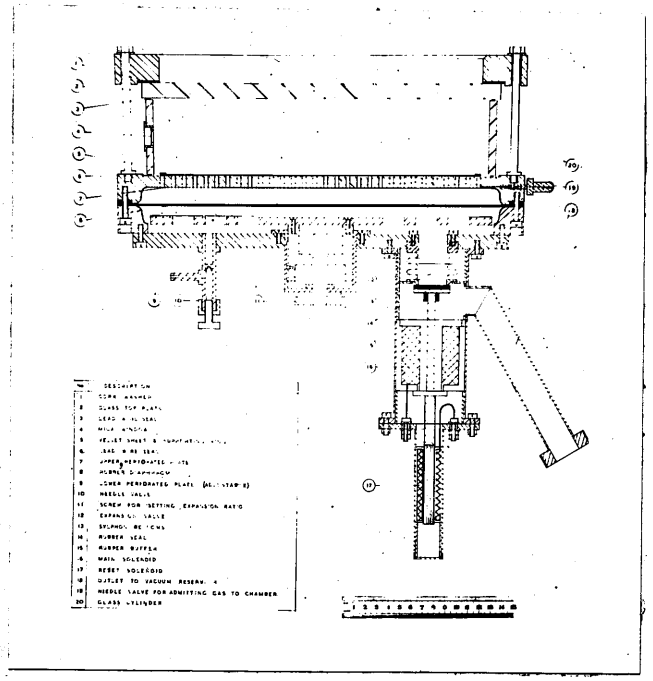

Figure 4

The cloud chamber used in the experiments described in this thesis.

studies of the reactions induced by photons from the 340MeV Glasgow machine. These chambers are identical, apart from the mode of attachment to their respective machines, and will therefore be described as one, the differences being indicated where they occur.

The cloud chamber is shown in the accompanying diagram (figure 4). Essentially, it consists of two volumes, separated by a rubber diaphragm: the tracks are formed in the sensitive volume, and the expansion of this volume is controlled by the pressure in the second. Two magnetic valves were connected to the needle valves; these were activated in turn by the slow expansion control unit to allow a gentle flow of gas to or from the space. The fast expansion valve is shown in the diagram: it will be seen that if the current to the hold-on solenoid is broken, the pressure will break the seal, allowing the rapid escape of gas from the lower volume.

In the experiments using the 340MeV Glasgow synchrotron, the cloud chamber was attached to the machine by means of a special port. This system is described fully by Atkinson et al. (76) and will not therefore be dealt with in detail here. Suffice it to say that the target gas in the chamber was separated from a "clean" photon beam only by a 0.0005" mylar window, and the electron background in the chamber was therefore small. In this work, the chamber was operated at a pressure less than atmospheric, and it was therefore necessary to provide a large evacuated tank to extract the gas from the lower volume.

A slightly different system was used with the 34MeV M.R.C. (Cambridge) synchrotron. This machine is used regularly for X-ray therapy, and the collimation system could not therefore be altered drastically/

drastically to suit the requirements of a cloud chamber. The existing collimator fired a cone of photons into the beam room and, by the choice of a suitable stop, it was found possible to pass the beam through the cylindrical walls of the chamber. At the peak energy at which the machine was operated (17MeV) it was found that the background of electrons, produced by the passage of the beam through the chamber walls, was insufficient to obscure the tracks of heavy particles. A plain glass cylinder was therefore used in this experiment. Since the chamber was operated at a pressure greater than atmospheric it was possible to expand the lower volume into the atmosphere, but a source of compressed air was required to fill it after each expansion.

---

2. 3 Cameras and Photography

A set of three cameras was used to record cloud chamber events. Each camera was fitted with an 80mm F3.5 Ental lens in a focussing mount, and an Agilux shutter. Since the cameras were intended for use as a set with their films all in the same plane, the axis of each lens was displaced from the centre of the image which it formed so that the full width of the film was used.

60mm unperforated recording film (either Ilford 5G91, or Kodak R55) was used. The film was loaded in 25ft lengths, and wound through the camera as it was used, its position being defined accurately by a gate. Since the cameras were intended for use in a

reprojection/

reprojection system (see chapter 3), they were equipped with removable backs, and lamps were designed to illuminate their film gates.

Photographs were taken in the light of two Mullard LSD16 flash tubes, mounted on opposite sides of the chamber. The lamps were triggered by a high frequency pulse from the fast expansion control unit (see below), which caused the discharge of a 300uF condenser bank, charged to 1.5kV through them.

The operation of the cameras was completely automatic. The shutters were opened by activating a solenoid, and photographs were taken by the open flash method. After each exposure, a pulse from the fast expansion control unit caused the film to wind on a distance determined by the operation of a cam on the drive shaft.

---

2. 4 Electronics

The operation of the cameras and the cloud chamber was governed by two electronic control units - the "slow expansion control unit", and the "fast expansion control unit" - the timing of each operation in the fast cycle with the synchrotron pulse was regulated by a decatron timing unit, and power was supplied to all equipment by a multiple power unit, and a 24 volt power unit. Some other circuits were used for special purposes.

2.4.1 The power supplies

The multiple power unit was designed to supply all the power required for the operation of the cloud chamber and associated

electronic/

electronic equipment. A 300v positive stabilised, a 150v negative and a 6.3v A.C. output were provided for the fast expansion control unit. A 400v supply was included, to create the electrostatic field across the cloud chamber, and this was fitted with a potentiometer to vary the strength, and a switch, to change the direction of the field. Finally, an A.C. output was provided, at either 2, or 8v, for a small lamp which was used to illuminate the chamber for testing purposes.

The second power unit supplied 24v D.C. to the fast and slow control units, and, through the fast expansion control unit, to the shutters and wind-on motors of the cameras.

2.4. 2 The slow expansion control unit

This unit (figure 5) was designed to control the slow expansion cycle of the cloud chamber. Separate 300v +, and 150v - supplies were included in the unit, and 24v to operate the relays was drawn from the 24v power pack. This cycle starts immediately after a fast expansion:

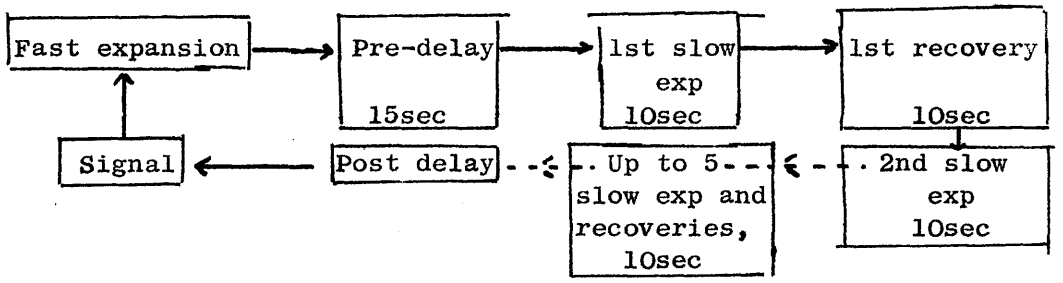

The times involved are regulated by the time constant of C3 (see figure 5) and the high resistances attached to bank 1 of the uniselector./

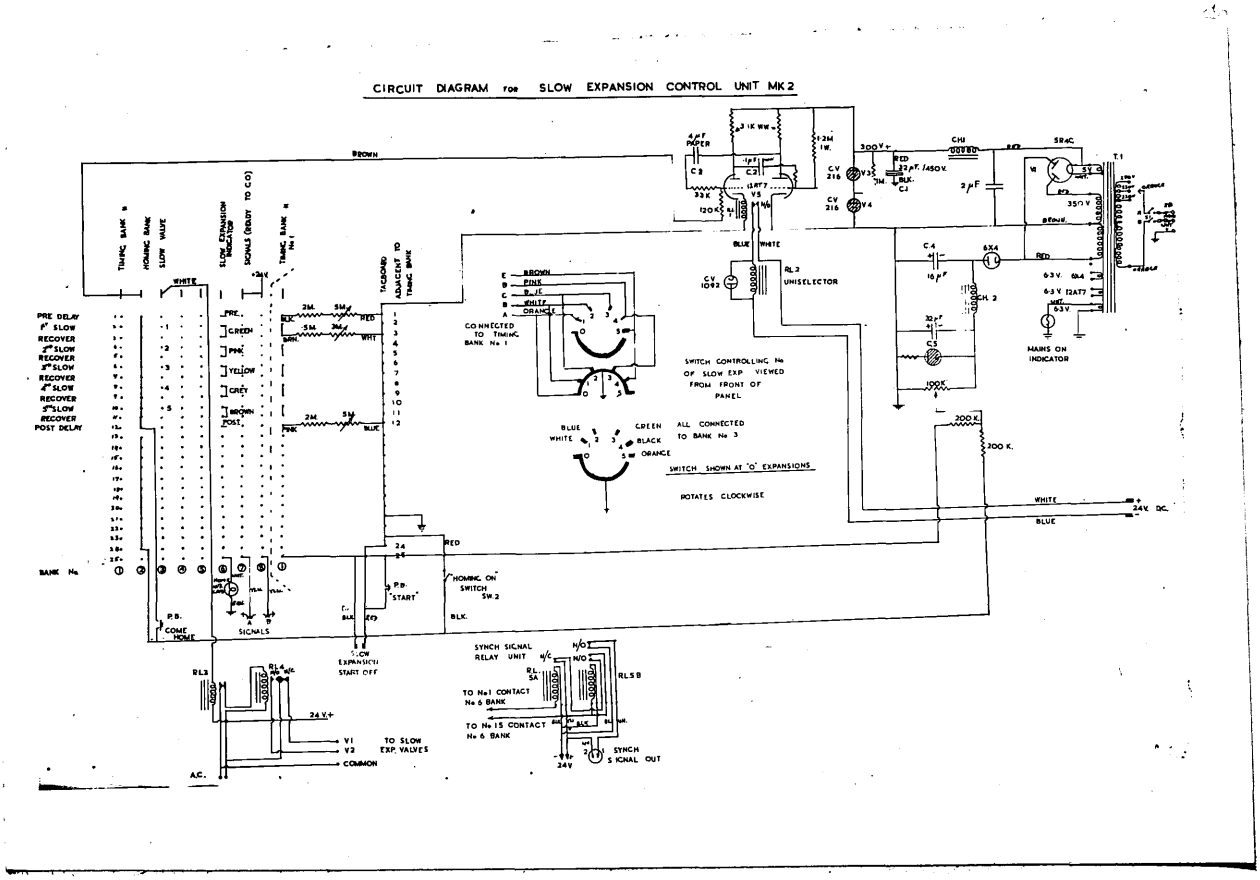

Figure 5

The circuit of the slow expansion control unit.

uniselector. This controls the movement of the uniselector, which in turn controls the operation of the chamber. The circuit is designed so that any number, (up to 5), of slow expansions can be preselected. Pilot lights are included, to indicate the state of the chamber in its slow cycle, and external pulses are available, to indicate the completion of the cycle.

2.4. 3 The fast expansion control unit

This unit (figure 6) was designed to control the fast expansion cycle of the cloud chamber. Two pulses are accepted from a decatron timing unit; the first of these starts the cycle and the second triggers the lamps at a predetermined time:

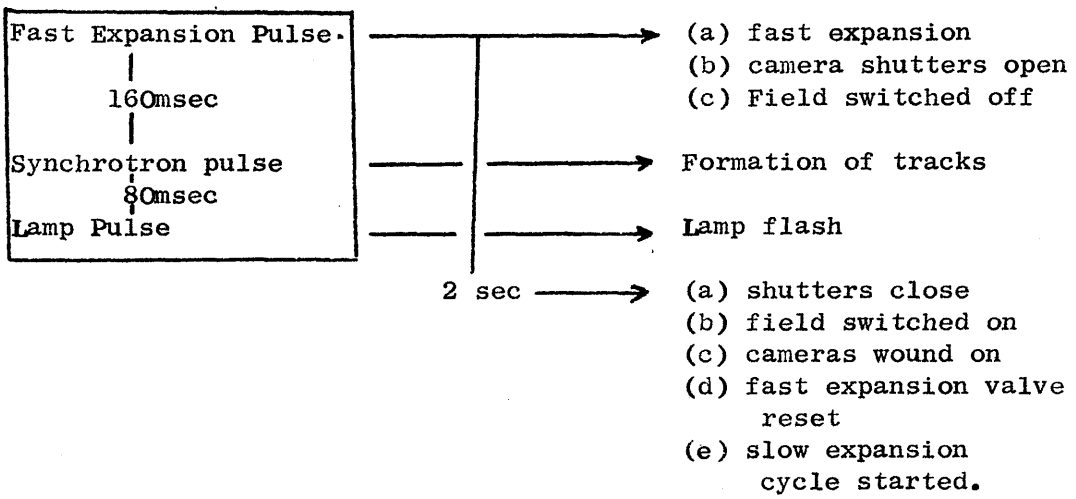

The fast expansion pulse triggers a flip-flop circuit, and at the same time, shuts off the two 6L6 valves which supply the current to the fast expansion valve. The flip-flop operates relay 1, opening the camera shutters, and switching off the field. Some time later the recovery/

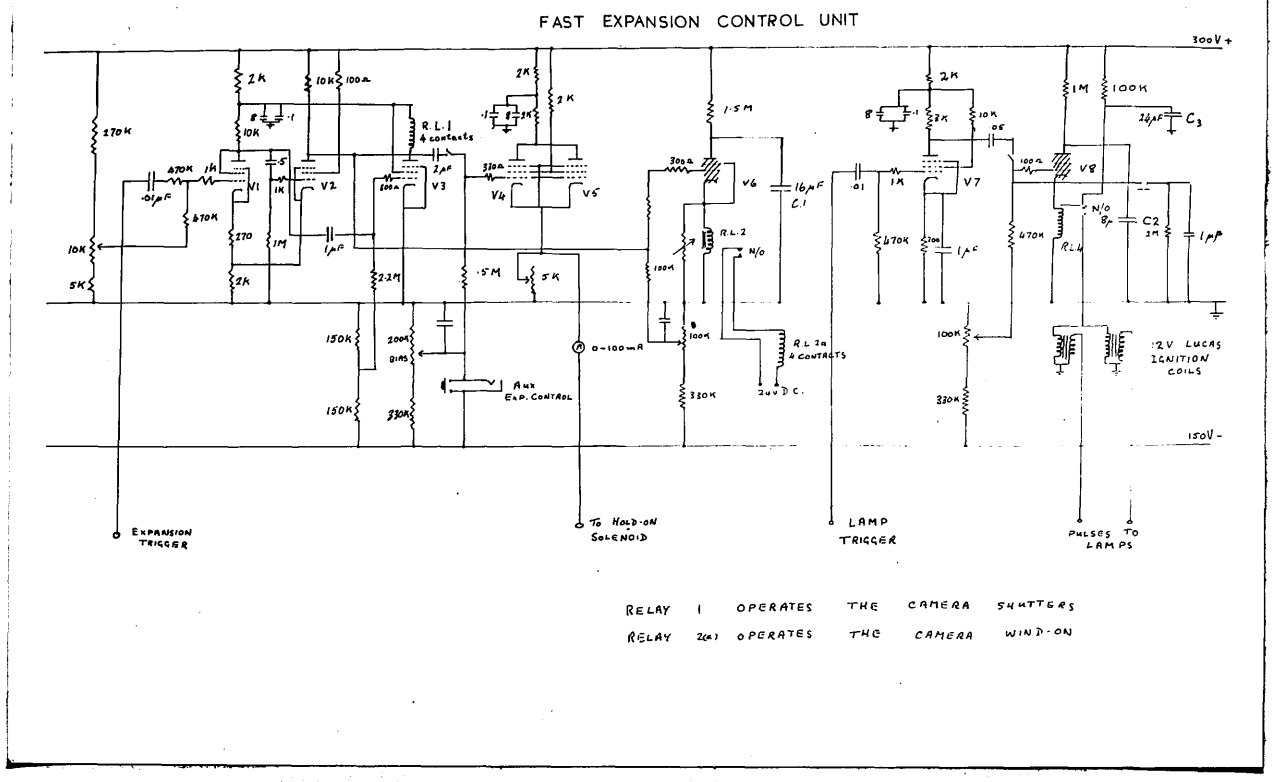

Figure 6

The circuit of the fast expansion control unit.

recovery of the flip-flop closes the shutters, and restores the field; the flip-flop recovery is also used to discharge the condenser (C1) through a thyratron (V6), thus closing relay 2. Relay 2 starts off the slow expansion cycle, and activates relay 2a, which controls the camera wind-on, and the resetting of the fast expansion valve.

The lamp pulse, which is timed to follow about 240msec after the fast expansion pulse, discharges the condenser (C2) through relay 4, allowing C3 to discharge through the two ignition coils. This produces a high frequency pulse, which triggers the lamps.

2.4. 4 Other circuits

(a) The decatron unit: this was used to synchronise the operation of the cloud chamber with the synchroton. Two 12-cathode valves were used, one of which was regulated by a square wave generator, tied to the mains frequency, and the second was triggered by the first. Pulses could be extracted from any of the cathodes, and the unit was therefore capable of timing at intervals of 20msec over a period of about 3 sec.

(b) X-ray trigger circuit: in testing the cloud chamber prior to an experiment, it was necessary to employ a pulsed ion source. This was provided by a medical X-ray set, triggered by the circuit shown in figure 7. A pulse from the decatron unit caused the discharge of a condenser (C1) through a thyratron, and thence, through the primary of the transformer of the X-ray set. The result was a short burst of X-rays through the chamber at a predetermined time, which produced electron tracks. An example of the tracks obtained in this way is

shown/

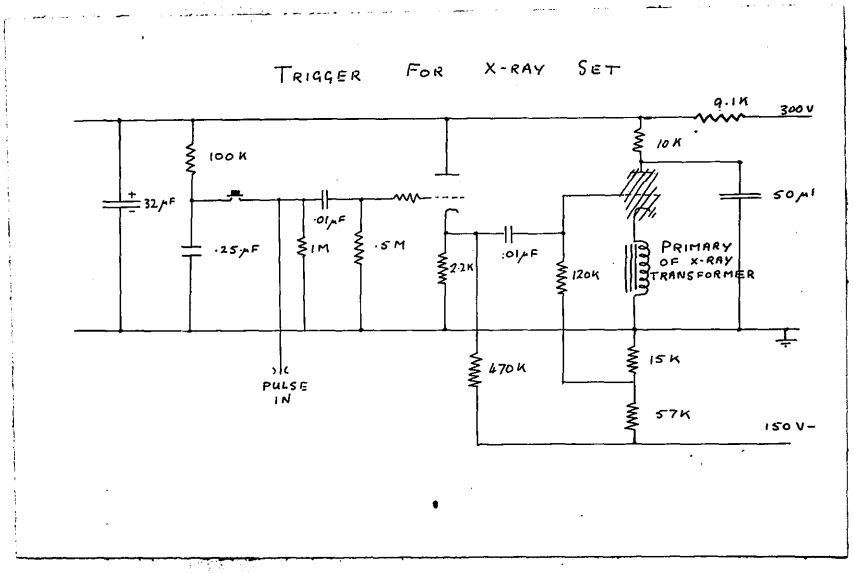

Figure 7

The circuit used to trigger a conventional X-ray set, for timed operation with the cloud chamber.

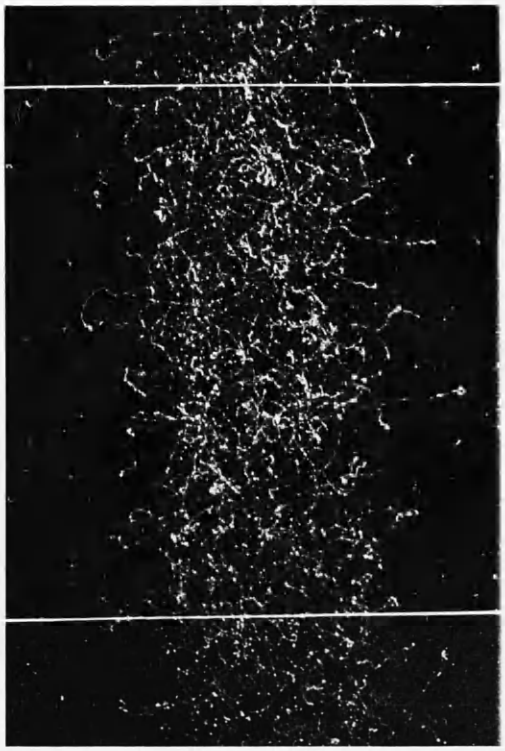

Figure 8

An example of the photographs obtained in testing the cloud chamber with the X-ray set.

shown in figure 8.

(c) The single shot operation of the Cambridge synchrotron: As has already been mentioned, this machine was intended for therapeutic purposes and it was not therefore equipped for timed single shot operation. The circuit shown in figure 9 was designed to synchronise the synchrotron with a pulse from the decatron unit. The synchrotron is fired by two pulses to the gun circuit: the synchronising unit (figure 9) acted as a gate to one of these pulses. When the gate was opened by the decatron, a single pulse was allowed to reach the gun, and the machine fired once. The gate could be adjusted to permit the passage of up to three consecutive pulses, and a switch was provided, to short-circuit the gate, and allow the machine to operate continuously.

---

2. 5 Experimental Operation

A medical X-ray set was adapted to provide a pulsed beam of photons, timed by a pulse from the decatron unit. The expansion ratio of the chamber was varied, and a series of pictures was obtained with values of the machine delay (the time between the chamber expansion and the pulse of X-rays) and the lamp delay (the time between the X-ray pulse and the lamp flash) varying over a wide range at intervals of 20msec. The optimum operating conditions were then determined by a visual examination of these photographs, and these settings were used as a basis for experiments using that cloud chamber.

For experimental work, the chamber was lined up with the synchrotron collimator, and its position was checked by exposing an

X-ray/

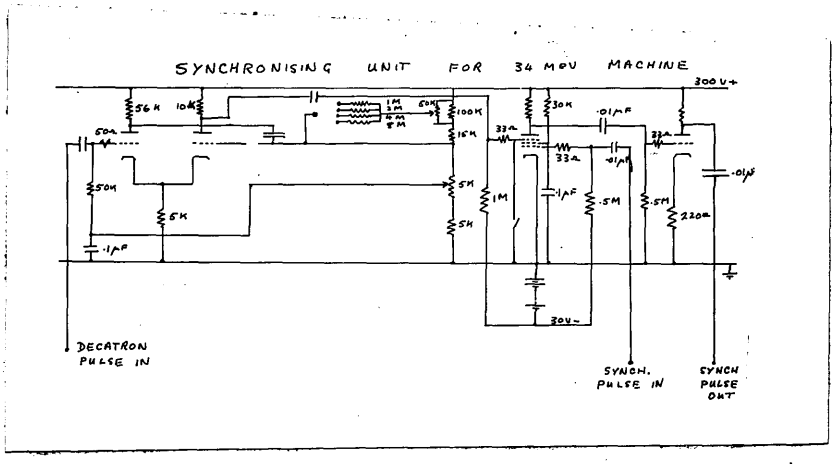

Figure 9

Circuit used to synchronise the operation of the 34MeV machine with the cloud chamber.

X-ray film to the photon beam. The operating conditions were checked by a short series of photographs of the beam passing through the chamber. The cameras were then loaded with 25ft lengths of film, and this film was exposed; each film consisted of about 120 exposures and took about 4hr. On the completion of this set the cameras were removed from the chamber, and reloaded. Throughout the runs, the operation of the chamber was checked in two ways: each expansion was watched visually and on the completion of each film, it was developed, and examined. It was therefore possible to detect immediately any failure of the cloud chamber, or ancillary equipment.

During each experiment, the expanded pressure of the target gas was measured at the beginning and end of each series of exposures, and the machine output was recorded after each exposure. At the end of each film, the parameters of the cloud chamber, and the synchrotron were recorded on the film to which they referred.

CHAPTER 3. The Measurement of Cloud Chamber Tracks

CHAPTER 3 THE MEASUREMENT OF CLOUD CHAMBER TRACKS

3. 1 General Considerations

The analysis of a cloud chamber track involves the measurement of sufficient independent co-ordinates to define the track uniquely in space. Since a track is simply a vector, three quantities are required to define it absolutely (one of magnitude, and two to relate the direction to a fixed axis; if the position of the track in space has any significance, three position co-ordinates are also required). Any analysis system must therefore aim at the measurement of three independent parameters.

In general, the first step is the recording of the track in the cloud chamber. Since one picture of an event can only supply two parameters, (e.g. the difference between the co-ordinates of the end points of the track), at least two photographs of each event must be obtained. These photographs are then examined, and the events of interest are noted; tracks are then measured by one or other of the methods described below.

---

3. 2 Analysis by Reprojection

This is the simplest method of measuring cloud chamber tracks. Events are photographed from several different directions by a set of cameras firmly fixed in a mount. It is convenient to fit a set of reference points to the chamber: this assists the setting of the film in the analysis procedure described below.

After/

After the completion of an experimental run, the cameras are removed from their position above the chamber, and set, in the same relative position, in a frame. Each camera is fitted with a lamp to illuminate the film in it, and project the film image into space below the camera. A flat table, mounted so that it can rotate freely to any desired position, is fixed on a vertical ratchet in the same frame below the cameras: the film images are projected onto this table. In all the ensuing discussions, this will be referred to as the "reprojection system", as opposed to the "chamber system" which comprises the cloud chamber, and the associated cameras in their recording positions.

The analysis of a track now proceeds as follows. The height of the table is adjusted so that the points in the reprojection system corresponding to the reference points in the chamber system lie in its plane. The image of a frame is now projected onto the table, and the position of the film in each camera is adjusted so that the projected images of the reference points co-incide. The track to be analysed is identified, and its images are brought into coincidence on the surface of the table by adjusting its height and orientation. Since the geometries of the reprojection, and chamber systems are now identical, this coincident image is equal in all respects to the track which was originally photographed. Its range and direction can therefore be measured directly.

This method obtains all the required information in a simple and direct manner. It presents this information in a convenient form

and/

and does not waste time in unnecessary measurements (e.g. the position of the track is not generally required, and is not measured unless required). There are several drawbacks however :-

(1) The accuracy of the system is severely limited. It is very difficult to measure ranges with an error of $\sim \pm 1$mm. This is not serious in the case of an event longer than several centimetres, but represents an error of 10% in the range of a track of length 1cm. Further, it is very difficult to orientate a reprojection table accurately so that the images of a short (< 2cm.) track coincide exactly.

(2) The system makes no explicit use of the fact that there are 4"independent" co-ordinates available from two cameras (and six from three) while only three are required to define an event uniquely: it should be possible to use the fourth co-ordinate to check measurements.

(3) The system requires the use of the original cameras for the analysis, and therefore only one operator can work on a set of films at any time. This restricts the speed at which data can be accumulated, but since the reprojection system is inherently rapid in its application, this criticism is not very serious.

---

3. 3 The "Pseudo-reprojection" System

In the course of an investigation of the photo-disintegration of nitrogen (25) it became necessary to measure the range of short tracks accurately. Since the simple reprojection system is not capable/

capable of such measurements, a more accurate method was devised.

The equipment described above was modified slightly (figure 10). The reprojection table was fixed horizontally, and the cameras were used in the analysis as light sources, without any film in their gates. Two additional items were required: a low power microscope, and a track simulator. The microscope eyepiece was fitted with a scale and cross-wire in a goniometer head, and its stage was designed to carry the film to be analysed firmly clamped between two glass plates. The stage could be moved in two mutually perpendicular directions, its motion being measured by vernier scales. The track simulator (figure 11) consisted of a pointer attached to a ball mounted in the centre of a horizontal 360^{o} protractor. A 180^{o} protractor was set perpendicular to the first, with its centre at the same point. The instrument was so designed that the pointer could be set in any desired position, and its orientation could then be conveniently measured with the two protractors.

A cartesian system of co-ordinates was used to describe each track, the origin being on the chamber base directly below the lens of one camera. Grid wires on the base of the cloud chamber were used to define the x- and y- directions of the co-ordinate system and their intersections acted as reference points in the ensuing analysis. For convenience, the chamber was orientated so that the incident beam travelled in the x- direction in the co-ordinate system defined above.

(a) Measurement of co-ordinate.

A film was clamped on the microscope stage, and the eyepiece cross-wires/

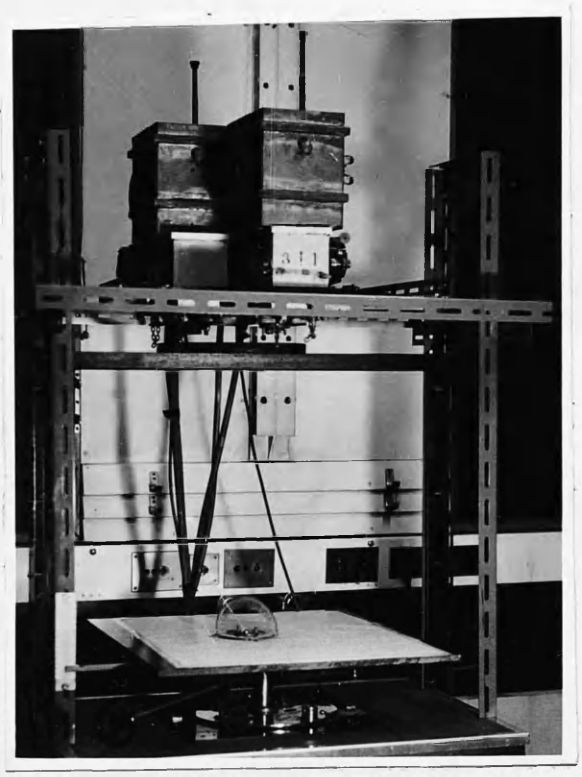

Figure 10

The psuedo-reprojection system.

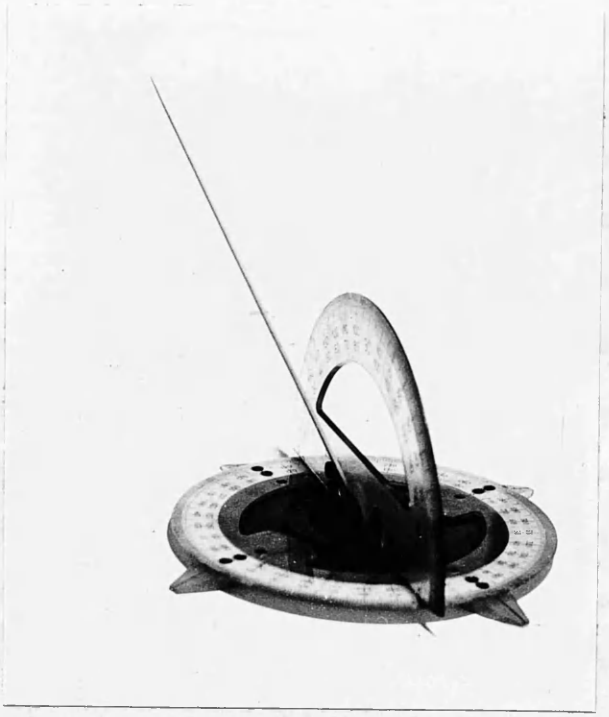

Figure 11.

The track simulator.

cross-wires were focussed first on a reference point, then on the origin and end points of the track under consideration, the vernier scale readings being recorded in each case. The length of the film image of the track and the angle between it and the x- direction were also recorded at this stage, for use later. The film was now removed, and replaced by a second film, and a second photograph of the same track was measured in the same way. The "x"- and "y"- co-ordinates of the track end points on each film, w.r.t. the chosen reference point were now calculated from the difference between the vernier readings of these points. The height of the track end-points in the chamber system is proportional to the difference between corresponding co-ordinates on two films, the constant of proportionality being calculated from the geometry of the chamber system. The z-co-ordinate of the track end points could therefore be calculated. The x- and y- co-ordinates in the chamber system depend on the "x" and "y" co-ordinates on the film, and on the value of z, and could now be calculated from geometrical considerations (figure 12). Thus the position of the origin and end point of the track were obtained, and the range and orientation could be computed. It was, however, considered more accurate, and convenient to obtain them in another way.

(b) Measurement of angles

The angle between the track and the "x"-direction had already been measured. In the reprojection system the reprojection table was set so that the lower end of the track lay in its plane and the track simulator/

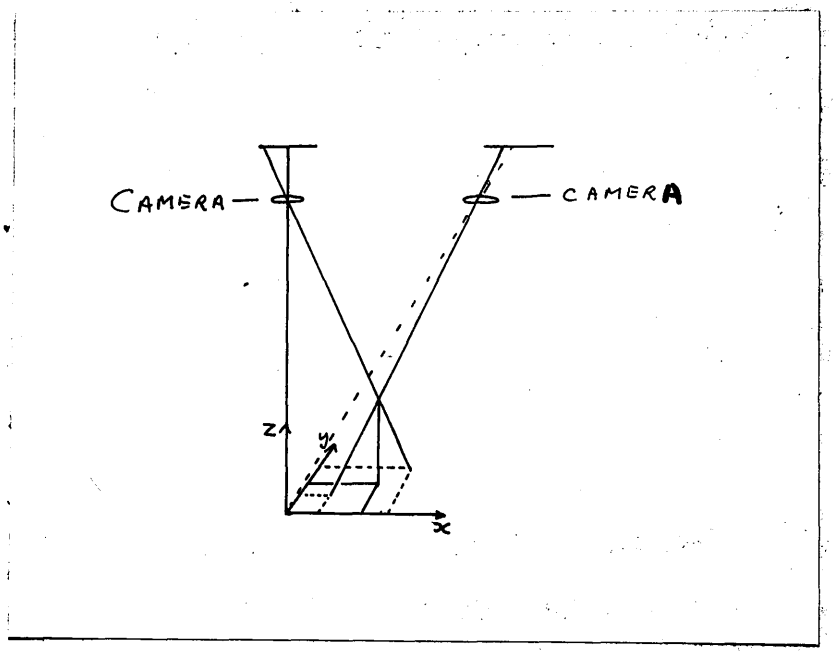

Figure 12

The geometry associated with the calculation of co-ordinates, using the pseudo-reprojection system.

simulator was placed so that its centre coincided with that point and the zero of its horizontal protractor lay in the x- direction. The pointer was now adjusted until the reading indicated by the shadow it cast, in the light from each camera, was equal to the angle already measured on the corresponding film. It can easily (figure 13) be seen that the pointer was then orientated in the reprojection system exactly as the track originally had been in the chamber system. The required spatial angles could therefore be read directly from the horizontal and vertical protractors.

(c) Measurement of lengths.

The method employed used the fact that the ratio of the track length to the length of its image on the film was related, by a geometrical constant, to the ratio of the length of the simulator pointer to the length of its shadow in the light of the corresponding camera, when the pointer was suitably orientated (figure 14). The measurement of the length of a track therefore involved the measurement of the lengths of the film images, and of the shadows cast by the pointer in the light of each camera under the correct conditions.

The geometry associated with the pseudo-reprojection system is fairly simple, but rather tedious, and will not be reproduced in detail here.

This system represents a considerable advance over the simple system in accuracy. It makes the most of the information available - there are several checks which can be applied at certain stages in the process (e.g. the z- co-ordinate can be calculated for each pair of

films/

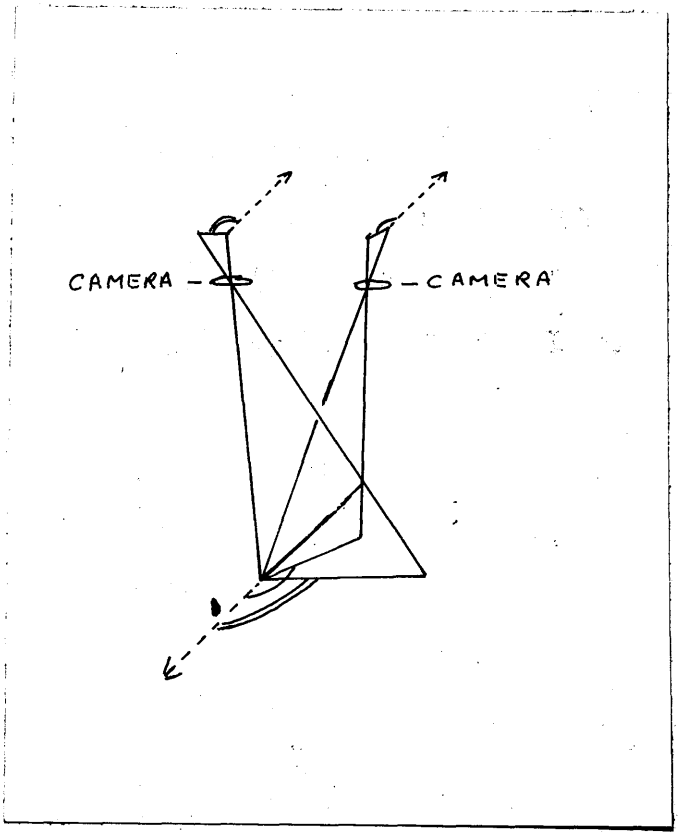

Figure 13

The geometry associated with the measurement of angles by the pseudo-reprojection system.

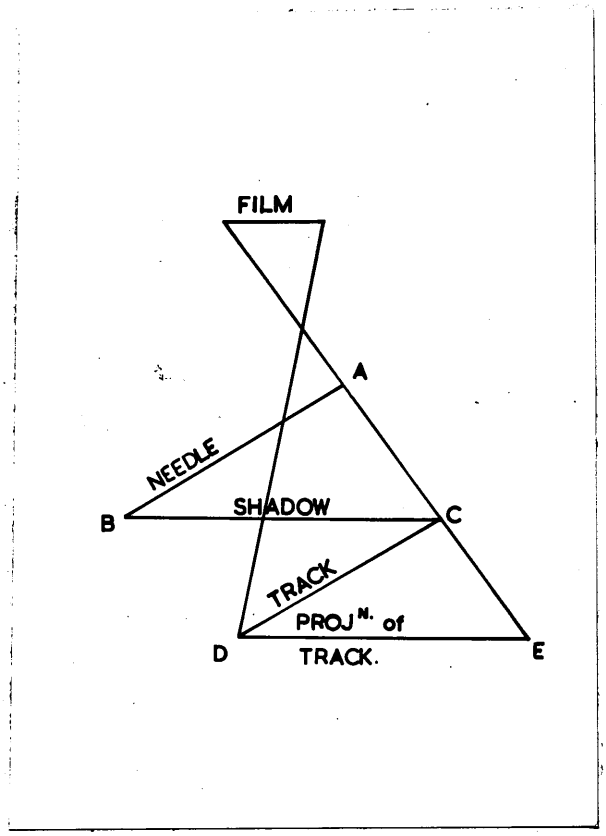

Figure 14

The geometry associated with the calculation of ranges by the pseudo-reprojection system.

films from the difference in the "x"- and "y"- co-ordinates separately, and the range of each track can be measured "independently" for each film). The method is, however, slow in application, and wastes a great deal of time in measuring explicitly the position of the track. A third method was, therefore, devised combining the speed of the simple reprojection method with the accuracy of the pseudo-reprojection system.

---

3. 4 The Microscope-reprojection System

The equipment used for this system was identical to that for the pseudo-reprojection system with the exception of the table, which was replaced with one capable of all the movements of the simple reprojection table (figure 15).

A microscope was used to scan each frame, and the position and appearance of each event observed was sketched and numbered on a diagram of the frame. The length, and angle only of each photographic image were measured, and noted against the reference number of the event concerned. This was repeated for every frame until a set of films had been examined. This set was now inserted in the cameras of the reprojection system and the images of the first frame brought into co-incidence, as in the simple reprojection system. Using the image from one camera, each event on the frame was now identified. The table was kept locked in a horizontal position, and two images of the first event were thrown simultaneously onto it. The lower end of the /

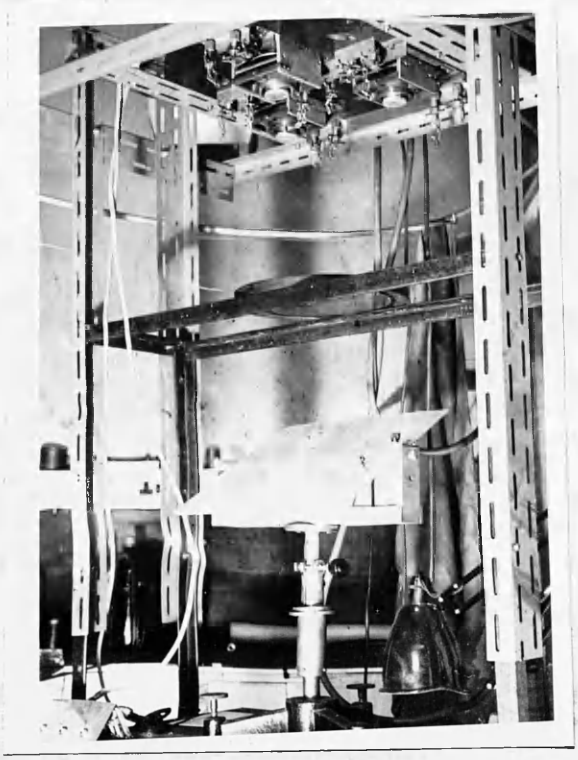

Figure 15

The microscope reprojection system.

the track, in the reprojection system, was found by moving the table vertically until its images co-incided. With the track simulator centred on this point, the spatial angles were measured as in the pseudo-reprojection system. The table was now raised until the upper end of the track lay in its plane, and the track length was measured, again by the method described above for the pseudo-reprojection system.

It has been noted above that the calculation of the lengths depended on the z- co-ordinate of the track under consideration, but this dependence is, in fact, only a second order correction. Although z could be measured easily, using this method, the value obtained would be rather inaccurate, and, in general, the experimental value of z varies only over a small region (the depth of the incident beam). It was therefore considered to be sufficiently accurate to use an average value of z in the calculations.

Long tracks, using this system can be analysed by the simple reprojection system, thus providing another independent check on the values obtained from the microscope measurements. Indeed, in applying this method, it is usual to confine the microscope measurements to short tracks, and the spatial angles of the longer tracks, the ranges and angles of the long tracks being obtained independently from the reprojection system.

---

3. 5 Conclusions

Three systems for the analysis of cloud chamber tracks

have/

have been reported here. The simplest, and most direct is the simple reprojection method, but it suffers from the disadvantages mentioned above - the difficulty in measuring accurately the range and direction of short tracks, and the inefficient use of the available information. The lack of accuracy is due to the fact that the total magnification of a track in the whole system is x1- the introduction of a larger magnification would increase the accuracy correspondingly. This can be done by the use of an optical magnifier, such as a microscope, or a projector, and the required measurements can be obtained directly from such a system by calculation. This method was not discussed, since the calculations involved are such as to render it impracticable without the use of an electronic computer. A track simulator was introduced into the pseudo-reprojection system to eliminate most of these calculations, and obtain the required results in a convenient form. The microscope employed had an effective overall magnification of x4*, so that the error in range measurements was reduced by this factor (to ±1/4mm) in comparison with the simple system. Similarly, the accuracy of the angular measurements was increased, especially for short tracks, and the error in values measured by this method is estimated to be about 3^{o}. The uncertainty in the results is further reduced since the track range is measured independently with each camera, and the spatial angles with each pair of cameras.

Unfortunately/

*The actual magnification of the microscopes was x40, but the recording system reduced the size of a track 10x, giving an overall figure of x4.

Unfortunately, the pseudo-reprojection system is extremely slow in its application - 10 tracks could be analysed by simple reprojection, in the time devoted to 1 using pseudo-reprojection. It was found that most of this time was spent in measuring precisely the position of the track in question, and that the readings obtained from the track simulator were slowly varying functions of its position. It was therefore decided to omit the explicit determination of the track position, and to set the simulator on the end of the track, as determined by simple reprojection. Some time was also saved, by analysing events in large groups, instead of treating them individually as was done in the pseudo-reprojection. As a result, the whole procedure takes only twice as long as the simple system, and since several workers can use the third system simultaneously, while simple reprojection is restricted to one at a time, the speeds are comparable. The accuracy of the third system is vastly superior to the simple system, being comparable with that of the pseudo-reprojection system.

CHAPTER 4. The Reaction $O^{16}(\gamma,p)N^{15}$ at Low Energies

CHAPTER 4 THE REACTION $O^{16}(\gamma,P)N^{15}$ AT LOW ENERGIES

4. 1 Introduction

This chapter is concerned with the reaction $O^{16}(\gamma,p)N^{15}$ at energies a few MeV above the reaction threshold (12.1MeV). The reaction has been studied using nuclear emulsions (26-29), but the results are mainly at fairly high energies. That technique is not suitable for the measurement of low energy protons, because of the uncertainty in the energy required by the proton to traverse the target and reach the emulsion, which must be placed some distance from the photon beam (14). A peak in the cross-section has been observed at about 14.7MeV which lies at the limit of the energy region investigated here.

The reaction was first studied by Spicer (26): he estimated the cross-section at 14.7MeV as 5mb, and found that the angular distribution of the protons from this level was of the form $1+\cos^2\theta$. Wilkinson (77) has explained this distribution by postulating that the 14.7MeV level is excited by E2 absorption of a photon. The work of Stephens et al.(27) and Cohen et al.(28) seems to confirm the existence of the level, but their results are not conclusive. A spectrum with a higher peak energy was used, and the observed low energy proton groups could be due to transitions resulting in the formation of the residual nucleus in an excited state. They observe an isotropic distribution: this may be due to a distribution of the form observed by Spicer - $B(1+\cos^2\theta)$ - together with a distribution of the form $A+B\sin^2\theta$ of low energy protons from the reaction $O^{16}(\gamma,p)N^{15}$ /

$O^{16}(\gamma,p)N^{15}$. Johansson and Forkman also find a peak in the cross-section curve at about 14.7MeV, but obtain a much smaller value for the maximum cross-section than Spicer.

At excitation energies of less than 14MeV, no results are available for the (γ,p) reaction in oxygen, but the cross section can be deduced from the characteristics of the inverse reaction (viz. $N^{15}(p,\gamma)O^{16}$) using the principle of detailed balancing. Bethe (78) has shown that if γ-rays emitted in the reaction $A_Z(p,\gamma)(A+1)_{Z+1}$ are allowed to fall on the nucleus $(A+1)_{Z+1}$, that nucleus can be expected to undergo photo-disintegration with a cross-section given by

$$\sigma_{\gamma,p} = \sigma_{p,\gamma} \frac{(2j+1)(2S+1)}{(2j'+1)(2S'+1)} \left(\frac{\lambda\!\!\!^{-}_{\gamma}}{\lambda\!\!\!^{-}_{p}}\right)^2$$

where j' = angular momentum of the nucleus $(A+1)_{Z+1}$

j and S = the angular momentum of the dissociation products

$(2S'+1)$ = the statistical weight for radiation

(=2, since there are 2 possible directions of polarisation).

$\lambda\!\!\!^{-}_{\gamma}$, $\lambda\!\!\!^{-}_{p}$ = the wavelengths of the incident photon and the emitted proton respectively

$\sigma_{p,\gamma}$ = that part of the capture cross-section which results in the formation of $(A+1)_{Z+1}$ in its ground state.

This method has been applied by Wright et al. to compare the (γ,p) cross-section which they measured in nitrogen with the reaction $C^{13}(p,\gamma)N^{14}$, and satisfactory agreement was obtained (25).

The reaction $N^{15}(p,\gamma)$ was first observed by Schardt Fowler

and/

and Lauritsen (79), in the course of a study of the reactions $N^{15}(p, \alpha)C^{12}$, and $N^{15}(p, \alpha\gamma)C^{12}$. Although the photon detector used was rather insensitive to the energy of the γ-ray, it was found possible to distinguish an energetic component in the radiation spectrum which could only be due to the reaction $N^{15}(p, \gamma)O^{16}$. They found that the maximum cross-section (of $\sim$ 1mb) occurred at a proton energy of about 1.05MeV, which corresponds to an excitation energy in O^{16} of about 13.1MeV, and that the width of the level was about 150keV. The measurements did not extend as far as the 14.7MeV level in oxygen, and suffice only to indicate the part played by a level at 13.1MeV in the (p, γ) reaction, the parameters quoted being little better than orders of magnitude. Kraus (80) considered the same reactions, and assigned the description 1^- to the 13.1MeV level: he estimates the width as 100keV. Wilkinson and Bloom (81) extended measurements of the $N^{15}(p, \gamma)$ reaction to higher energies: they used a thick target, and were not able to study the peak at 1.05MeV - at this energy, they fit their results to those of Schardt. No trace is found of radiation from the level reported at 14.7MeV in the (γ, p) reaction, and, using the principle of detailed balancing, they find that at that energy the (γ, p) cross-section should be about 0.1mb. Bashkin and Carlson (82) examined the radiation from the capture of protons by N^{15}: they find such radiation at a proton energy of 1.05 ± 0.010MeV, and estimate the width of the resonance ss 125 ± 25keV. No other capture radiation, or/

or radiation from the de-excitation of O^{16} by a cascade process amounting to more than 2% of the peak cross-section was observed up to a proton energy of 3.3MeV.

These results, together with the principles of detailed balancing, suggest that the (γ,p) cross-section should show a peak at about 13.1MeV, and none at 14.7MeV. Studies of the (γ,p) reaction, however, show a peak at 14.7MeV, and have not been extended to cover the energy region between the reaction threshold and 14MeV. It was therefore decided to undertake a study of the reaction $O^{16}(\gamma,p)N^{15}$. Protons emitted after the excitation of the 13.1MeV and the 14.7MeV levels have energies of about 1MeV, and 2.6MeV respectively, and can be detected, and measured using a cloud chamber. It was therefore hoped that the part played by the level at 14.7MeV and the cross-section for the reaction at energies between its threshold and the region investigated by emulsion techniques would be determined. The results would also be used to test the principle of detailed balancing for this reaction.

---

4. 2 The Experiments

The cloud chamber, and associated equipment have already been described in chapter 2.

Since it was desired to study reactions resulting in the formation of N^{15} in its ground state, it was decided to use a bremsstrahlung/

bremsstrahlung spectrum with a peak energy of 18MeV. The first excited state of N^{15} lies 17.4MeV above the ground state of O^{16}, and it was felt that the number of photons in the spectrum with energy greater than this would be small. The cloud chamber was operated at an expanded pressure of about 1.3atm: at this pressure, 95% of the 1MeV protons and 50% of the 3MeV protons emitted will remain within the confines of the chamber.

The results obtained gave a measure of the energy and angular distributions of the protons emitted, but the cross-section curve deduced from them was not completely reliable, for two reasons. The stability, and calibration of the peak energy of the synchrotron used (the 23MeV Glasgow machine) were not satisfactory, and no accurate calibration of the output of the machine during the exposure was available. These points could not be checked, since the synchrotron ceased to function satisfactorily soon after the experiment, and has not operated since.

It was therefore decided to repeat the experiment on a smaller scale to confirm the results. The M.R.C. synchrotron, at Cambridge, was used in this second investigation, and was operated at a peak energy of 17.0MeV, to eliminate all possibility of transitions to excited states in N^{15}. The output of the machine was monitored in terms of the ionisation produced by the beam in an ionisation chamber. A pulse from the ionisation chamber was fed into an oscilloscope, and photographed: the photographs were then calibrated by comparing the dose recorded by a 100r victoreen thimble

over/

over a period of 20min with the mean of a randon sample of oscilloscope deflections, the output of the machine being held as constant as possible during the calibration.

---

4. 3 Results

The events obtained in the first experiment were analysed using the pseudo-reprojection method, and the microscope-reprojection method was employed in the second experiment. The ranges thus obtained were converted to the energy of the protons, using a range energy relation based on the data published by Segre' (83). The probability of a proton of a given range stopping within the confines of the chamber was now calculated: this is shown in figure 16. The curve was used to correct the proton energy distribution for the events which left the sensitive volume of the cloud chamber. Some 93 tracks were observed to leave the chamber, and the correction resulted in the addition of 111 events to the distribution. This agreement is reasonable in view of the large correction applied to a few long range events. The corrected proton energy distribution is shown in figure 17.

The energy of the photon responsible for an event was assumed to be given by the formula

$$E \doteq \frac{16}{15} E_p + Q$$ where E_p = the measured proton energy, in MeV.

Q = the reaction threshold energy, in MeV.

More exactly,/

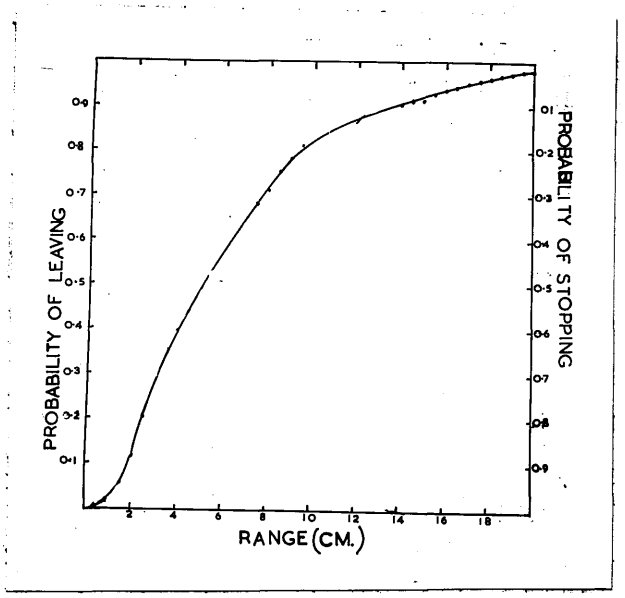

Figure 16

The probability of a particle remaining within the confines of the cloud chamber as a function of its range.

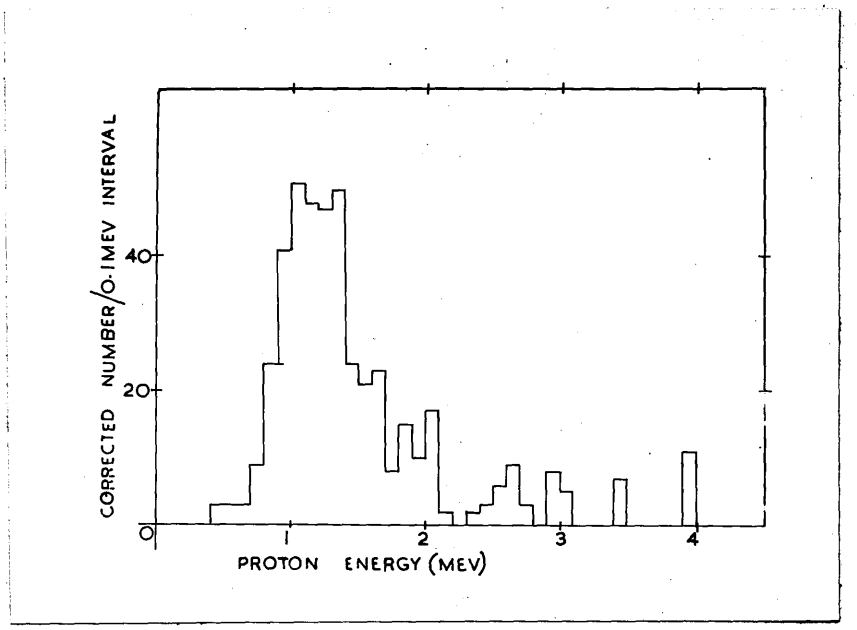

Figure 17

The energy distribution of the protons from the reaction $O^{16}(\gamma, p)N^{15}$.

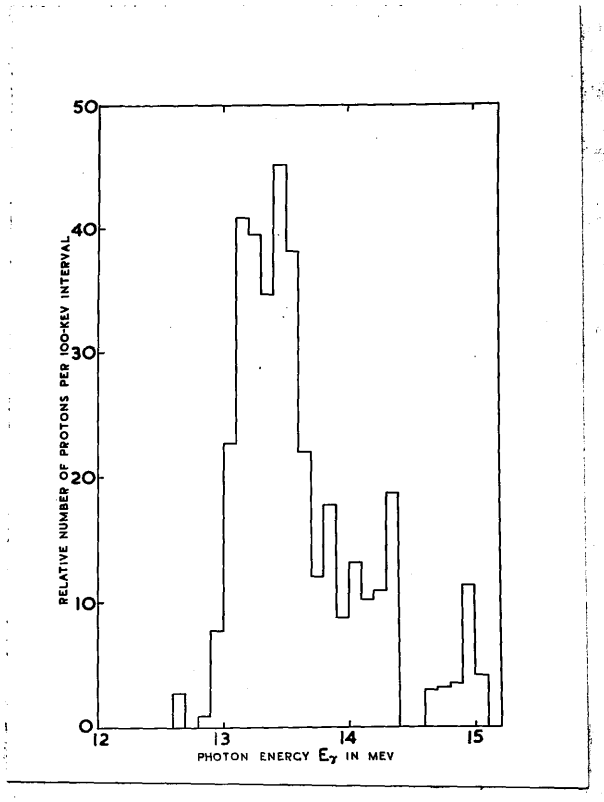

Figure 18

The energy distribution of the photons responsible for the observed (γ,p) reactions.

More exactly,

$$E = E_p + \frac{1}{15} E_p \left(1 - \frac{E^2 \cos^2\theta}{2M_r E_r}\right)$$

where M_r and E_r are the mass and energy of the recoil nucleus, expressed in MeV.

θ ≒ the angle between the proton and the photon beam

The second term, however, amounts to about 1 part in 10,000 and may therefore be neglected. The formula also assumes that there are no transitions to excited states of the residual nucleus, which, in view of the value chosen for the peak energy of the bremsstrahlung spectrum, is reasonable. Equation (1) was used to compute the energy of the photon which corresponded to a given proton energy and the result was plotted in figure 18.

This represents the number of photons absorbed from a bremsstrahlung spectrum, of peak energy 18MeV. The shape of the spectrum (figure 19) was taken from the tables of Katz et al.(12) and used to calculate the cross-section curve (figure 20) from the distribution in figure 18.

The angular distribution of all the observed protons is shown in figure 21. The distribution shows the number of protons emitted per steradian at intervals of 20°. Only events at an angle less than 60° to horizontal were included, and allowance was made for this in calculating the solid angle for each interval.

In all the above distributions, it was found that the results from the separate experiments (at Cambridge and Glasgow) were identical within the statistical limits and they were therefore plotted

together./

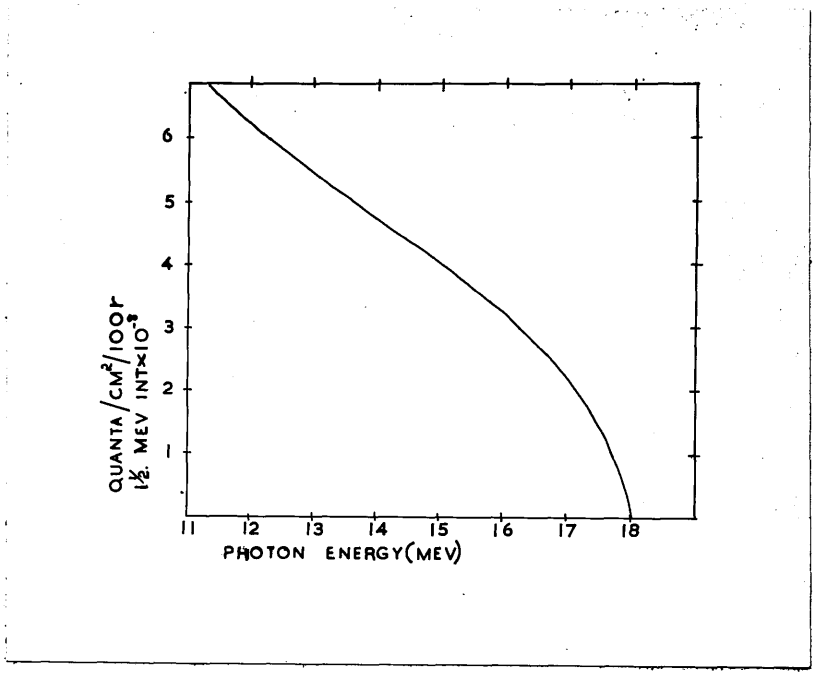

Figure 19

The shape assumed for the bremsstrahlung spectrum, of peak energy 18MeV.

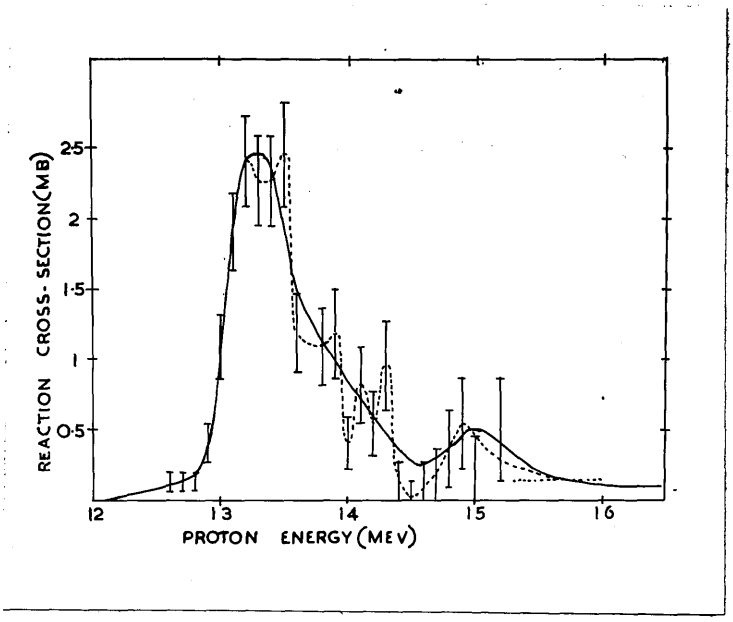

Figure 20

The cross-section curve for the reaction $O^{16}(\gamma,p)N^{15}$.

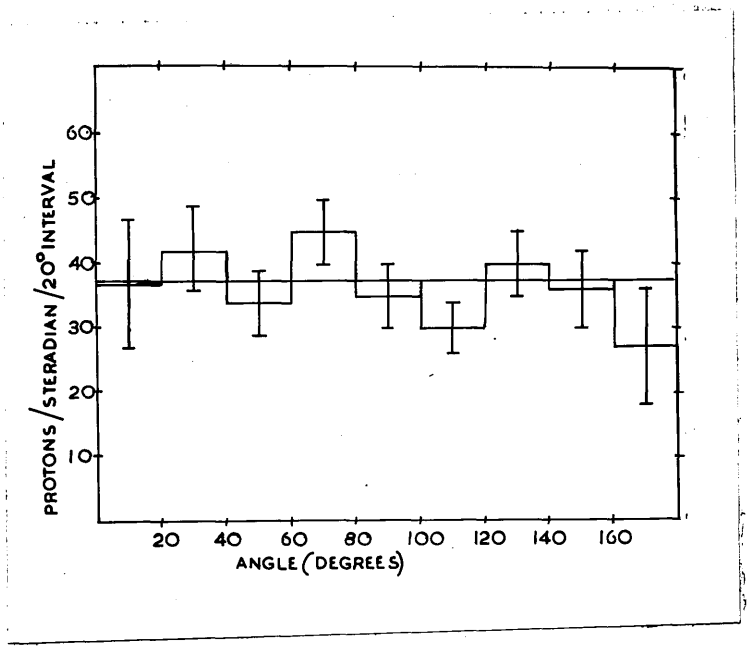

Figure 21

The angular distribution of the protons from the (γ,p) reaction in oxygen.

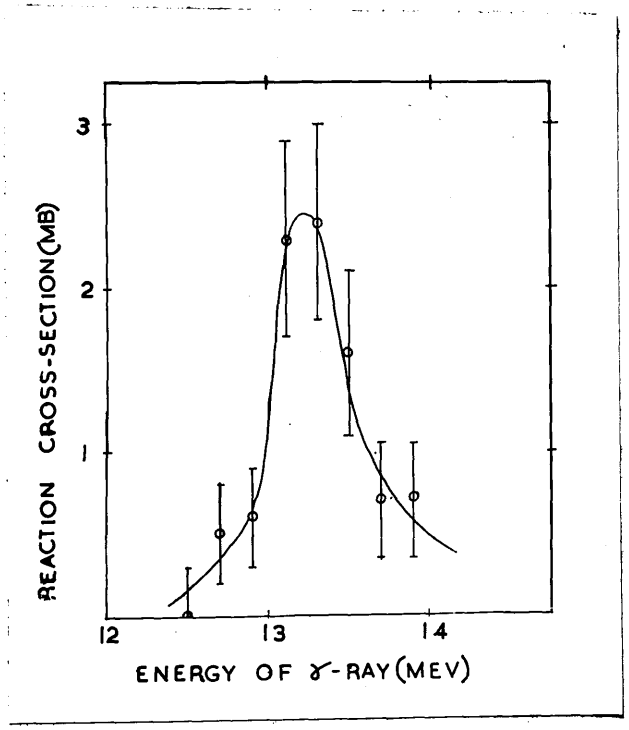

Figure 22

The cross-section curve for the reaction $O^{16}(\gamma, p)N^{15}$ determined from the results of the second experiment.

together. The value of the second experiment lay in its determination of the absolute value of the cross-section: this was calculated using the tables of Katz et al. (12) and the resultant curve is shown in figure 22.

---

4. 4 Discussion

The cross-section curve for the reaction $O^{16}(\gamma,p)N^{15}$ is shown in figure 20: it rises slowly from the reaction threshold to about 12.8 MeV, then sharply to a maximum value of $\sim$ 2.5mb at 13.3MeV. The cross-section then decreases rapidly to a tenth of its maximum value, at about 14.5MeV: a second peak appears in the curve at about 15 MeV, the maximum cross-section here being about .5mb.

The energy resolution of the measurements was good enough to justify plotting the cross-section at intervals of .1MeV, and the resultant curve (dotted) exhibits a much more complex structure than that outlined above. This structure, if real, could be explained by the absorption of photons into levels in O^{16} at about 13.2, 13.5, 13.9,14.3, and 14.9MeV. This hypothesis has been put forward by other workers (84,85) to explain the results for the reaction which are reported here, but it is difficult to reconcile it with the results for the inverse reaction (see introduction to this chapter). Moreover, the observed structure is not statistically significant, since the deviation of the experimental points from the continuous curve is seldom greater than the statistical error of the point. The simpler, continuous curve was therefore preferred in the present work.

The integrated cross-section of the peak centred at 13.3MeV

is/

is about 2.0 ±.4 MeVmb. If it is assumed that the absorption process was E1, then the state excited in O^{16} has spin 1, and, since the ground state of N^{15} has spin 1/2, the emitted proton must have zero angular momentum, and spin 1/2. Substituting these values in the equation for detailed balancing leads to an integrated cross- section for a resonance in the inverse reaction of .16 ± .03 MeVmb. This compares well with the value obtained by Schardt et al. (79) for a resonance at a proton energy of 1.05 MeV: they estimate the integrated cross-section for this resonance to be about .15 MeVmb. The small difference between the energies observed in this experiment and by Schardt et al is probably due to the method used to calculate a range-energy relation for protons in the chamber gas from the curves published by Segre (for protons in air at S.T.P.)

A resonance is also observed at about 15MeV in the present experiment. The cross-section at this energy is considerably less than is suggested by Spicer, and agrees with the value obtained by Johansson. The integrated cross-section for the excitation of the resonance is .35 ± .2MeVmb. This leads to a value for the integrated cross-section in the inverse reaction of 14 ± 7MeV b if the absorption process is assumed to be E1, and of 7 ± 4MeV b if the absorption process is E2. Wilkinson and Bloom (81) have measured the cross-section for the reaction $N^{15}(p,\gamma)O^{16}$ in this energy region. They observe no peak near 15 MeV and find a value for the cross-section there of about 7 μb./

7μb. This agrees satisfactorily with either of the above results, favouring the E2 description slightly. Unfortunately there are insufficient events in this part of the energy distribution to establish the absorption process beyond doubt, either by comparison with the results from the inverse reaction, or by plotting the angular distribution of the emitted protons.

Thus the simple cross-section curve is consistent with the results from the inverse reaction and the principle of detailed balancing. The absorption process in the main resonance (at 13.3MeV) appears to be E1, and the results are unable to establish the process involved in the small resonance.

The shell model picture of a (γ,p) reaction envisages the excitation of a single proton to a higher shell model state. This is followed by the direct emission of that proton, or by the formation of a compound nucleus state in which the energy of the photon is shared among all the nucleons in the nucleus. The protons in the ground state of O^{16} can be described, in shell model notation, by $(1S^{1/2})^2(1P^{3/2})^4(1P^{1/2})^2$. Similarly, the proton configuration in the ground state of N^{15} can be described by $(1S^{1/2})^2(1P^{3/2})^4(1P^{1/2})^1$. A direct reaction resulting in the formation of N^{15} in its ground state must come from an excitation of one of the $1P^{1/2}$ protons in O^{16}, since the ground state of N^{15} is a parent of any such state. Wilkinson (81) has suggested that the level (observed at 13.3MeV in this experiment) is due to the excitation of a 1P proton into a 2S state. The width of the level for proton emission (.8MeV) can be used, with the uncertainty principle,/

principle, to calculate the life of the excited state: the value obtained is 10^{-21} sec, which is of the order of the time taken by a nucleon to traverse the nucleus. It therefore seems unlikely that a compound nucleus state is formed: this suggests that the observed protons are directly emitted. If this is so, the angular distribution of the protons will be in the form predicted by Courant (59). For protons excited from the 1P to the 2S shell, this suggests that the distribution should be isotropic, and this is observed. This is not conclusive, however, since the formation of a compound nucleus state and the subsequent evaporation of a nucleon would also lead to an isotropic distribution.

The second resonance, observed at about 15MeV, appears to have a width of the same order as the first, and may therefore be due to a similar but weaker mechanism . Wilkinson (63) has shown that transitions involving the flip of the spin of a nucleon with respect to its orbital angular momentum are weaker than transitions without spin flip. It may be that the spin of each nucleon is also coupled to the spin of the whole nucleus, and that this causes the 2S states to split. The more probable transition, to the lower 2S state would then account for the main resonance, and a transition to the second 2S state, involving spin flip with respect to the nuclear field would account for the second resonance.

---

4. 5 Conclusions

The experiments described above resulted in the determination

of/

of the cross-section of the reaction O^{16} $(\gamma,p)N^{15}$ at excitation energies between the reaction threshold and 16MeV. The cross-section curve exhibits a broad resonance centred at 13.3MeV, with a maximum cross-section of 2.5 ± 0.4mb, and a width of 800keV. A similar resonance is situated at about 15MeV, with a maximum cross-section of 0.5 ± 0.3mb, and a width of 800keV. These results are consistent with the predictions of the principle of detailed balancing from the inverse reaction (viz. $N^{15}(p,\gamma)O^{16}$) if it is assumed that the interaction is E1 in the 13.3MeV resonance, and either E1 or E2 for the 15MeV resonance. The observed angular distribution is consistent with the direct emission of a proton excited from the 1P shell into the 2S shell, and it is suggested that both resonances result from transitions of this type. The value of the cross-section for the second resonance agrees with the measurements of Johannson and Forkman, and amounts to a tenth of the value obtained by Spicer.

CHAPTER 5. The Disintegration of Nitrogen and Oxygen: The Experiments and Results.

CHAPTER 5 THE DISINTEGRATION OF NITROGEN AND OXYGEN: THE EXPERIMENTS AND RESULTS

This chapter deals with the results of experiments designed to study the disintegration of nitrogen and oxygen, and, in particular, to examine the giant resonance and the cross-section at higher energies.

5. 1 Introduction

In the introduction to this thesis, it was pointed out that the disintegration of light nuclei had not been exhaustively studied, and that the results available were not sufficiently comprehensive to make a detailed comparison with theoretical predictions. It was therefore decided to investigate the reactions induced by radiation in some light nuclei using a cloud chamber. The elements nitrogen and oxygen were chosen: in their natural form, these elements are more than 90% isotopically pure.

Considerable interest is attached to the photo-disintegration of nitrogen 14 and oxygen 16. The ground state configurations of protons and neutrons in N^{14} are identical according to the shell model, each lacking one nucleon to complete the 1P shell. The possible E1 transitions are therefore $1P \rightarrow 2S$, $1P \rightarrow 1D$, and $1S \rightarrow 1P$, and different angular distributions are predicted for nucleons emitted directly as a result of eachof these processes. Measurements of the angular distributions should be capable of identifying the important transitions. Oxygen 16 is a doubly magic nucleus, and is therefore of particular interest from/

from the shell model stand point. The shell model would predict some differences between the energy and angular distributions of the nucleons emitted by O^{16} and N^{14} - in particular, since the 1P shell is filled, 1S-1P transitions are not possible. The collective model, on the other hand, takes no account of magic number effects, and would therefore expect similar results from both elements.

The (γ,pn) reaction also deserves some study. In N^{14}, its threshold lies at 12.5MeV, which is only slightly greater than the (γ,p) and (γ,n) thresholds (7.5MeV, and 10.5MeV respectively). There will therefore be considerable competition between these reactions in the energy region of the giant resonance. In the case of O^{16}, the threshold is at a much higher energy (23MeV), and this reaction will therefore be less important relative to the (γ,p) and (γ,n) reactions in the giant resonance region.

Considerable interest has centred recently on Levinger's quasi-deuteron model, and on the limit of its applicability. Wilkinson (63) suggests that the limit will lie at a few tens of MeV, which might mean that the model is valid in the region of the giant resonance. This hypothesis can be tested by measurements of the recoil nuclei from the (γ,pn) reaction, and, in particular, of the angular distribution of these recoils with respect to the direction of the emitted proton. The distributions can be measured for both N^{14} and O^{16}, and a comparison of the results, in view of the difference of the thresholds, may throw further light on the (γ,pn) process.

For these reasons, and with these ends in view, a study of the recoil/

recoil nuclei from the (γ,p), (γ,n), and (γ,pn) reactions in nitrogen and oxygen was undertaken.

5.1.1 The Disintegration of Nitrogen

The (γ,p) reaction in nitrogen has been studied by several workers. The cross-section for the process has been measured at low energies using nuclear emulsions (88) and a cloud chamber (25). The cloud chamber experiment was extended to higher energies by measurements of the recoil nuclei, but the statistics are poor, and the pressure of the chamber was too high to permit accurate measurements. Using other techniques, it is not possible to distinguish the protons from the (γ,p) and (γ,pn) reactions because of the proximity of their thresholds. The energy and angular distributions of the photo-protons have been measured (89), using spectra with peak energies of 30MeV and 70MeV. Three energy groups of protons are reported, and the angular distributions of the protons belonging to each group are discussed. No significant difference is observed in the distributions caused by the two spectra. These protons will be due to both the (γ,p) and the (γ,pn) reaction. Johansson (90), and Cortini (91) have also studied the distributions.

The (γ,n) reaction has been studied by an activation technique (86) up to an energy of 25MeV. The results show the giant resonance at about 24MeV, and a smaller peak at a lower energy. The neutron yield has also been measured as a function of the peak energy of the photon spectrum (87). The cross-section derived in this way/

way differs from that determined by activation, since neutrons from the (γ,pn) reaction were also detected.

The (γ,pn) reaction has not been studied explicitly, but a comparison of the cross-section for photo-neutron production with the cross-section for the (γ,n) reaction determined by activation indicates that the (γ,pn) cross-section is large, and that it exhibits the giant resonance.

Other reactions have been examined, and their cross-section was found to be small. The emission of an α-particle or a deuteron is forbidden by isotopic spin selection rules (92) at low energies, and the cross-section for these processes has been observed to be small at energies below 23MeV (25). The (γ,2n) reaction has been studied by an activation technique (93), and the cross-section was found to be very small. Reactions involving the emission of more than two charged fragments have also been observed (25), and the cross-section for such a process was estimated as being an order of magnitude less than the (γ,p) cross-section, up to a photon energy of 23MeV.

5.1.2 The Disintegration of Oxygen

As in the case of nitrogen, several reactions have been observed and studied.

The reaction $O^{16}(\gamma,n)O^{15}$ has been investigated extensively by the activation method (12,32a,66,86,95,96). The cross-section curve shows the familiar giant resonance shape, and in the later experiments (12, 32a) breaks in the activation curve have been observed/

observed which are interpreted as fine structure in the giant resonance.

The (γ,p) reaction has been studied using nuclear emulsion techniques (26-29.97,98). Most of the results refer to excitation energies less than 25MeV. Since the (γ,pn) reaction threshold lies at 23MeV, it is reasonable to suppose that very few of the observed protons are due to this reaction, and the results can be interpreted unambiguously. Several energy groups of protons are observed, and these are attributed to reactions involving excited states of oxygen 16 and nitrogen 15. Livesey (98) used spectra with peak energies of 30MeV, 35MeV, and 70MeV, but since the energetic protons did not stop within the emulsion, the cross-section curve above a photon energy of about 30MeV was not measured. Livesey also examines the angular distributions of the protons from four energy groups, and fits curves of the form

$$A + B\sin^2\theta$$

to the low energy groups, and

$$A + B\sin^2\theta\ (1 + p\cos\theta)^2$$

to the distribution for protons of energy greater than 10.5MeV.

Reactions involving the emission of an α-particle or a deuteron are forbidden at energies below about 25MeV by isotopic spin selection rules (92). The (γ,α) and the (γ,4α) reactions have been investigated, using nuclear emulsions (14), and the cross-sections were found to be small (about 0.1mb). The (γ,d) and (γ,pn) reactions/

reactions have not been investigated, and studies of photo-protons have been confined to particles which could only be attributed to the (γ,p) reaction.

5.2 The Experiments

The cloud chamber was set in the path of the beam from the 340MeV Glasgow synchrotron and filled to an expanded pressure of about 0.5atm with gas of commercial purity. This pressure was chosen as the lowest pressure at which the operation of a conventional cloud chamber was practicable. A photon spectrum with a peak energy of 200MeV was chosen for the experiment with nitrogen, so that the number of reactions involving mesons would be small, and such processes were not considered in the identification of the events. A few photographs were also taken of the disintegration of nitrogen, using a spectrum with a peak energy of 340MeV, and no significant difference was observed between these films and the results reported below: accordingly, they were not completely analysed. In the case of oxygen, only a short time was available for the exposure of the films, and the machine was operated at its peak energy (340MeV) in order to obtain the maximum possible number of events.

The beam output was monitored in terms of the movement of a ballistic meter, which was connected to an ionisation chamber. Unfortunately, it was not found possible to calibrate this meter absolutely with any accuracy, and the record therefore only provides a relative measure of the strength of each synchrotron beam pulse.

A/

A total of 1800 photographs were taken, 1500 of the disintegration of nitrogen, and about 300 of events in oxygen. On the nitrogen films, 2000 events were analysed, and 700 events were obtained from the oxygen films. The microscope-reprojection system was employed for the analysis. Curves relating the range and energy of the recoil nuclei (O^{15}, N^{15}, N^{14}, N^{13}, C^{13}, C^{12} - see Appendix 1) in air at STP were derived using a method developed by Papineau (99). The measured ranges were converted into an equivalent air range by multiplication by a factor which took into account the electron density and the expanded pressure of the chamber gas.

5.3 The Classification of the Observed Events

Each photograph was examined with a microscope, and all events were recorded. They were then measured, and classified as follows :-

(1) Stars : This class included all events involving the emission of two or more charged particles and a recoil. In general, most of the fragments from stars left the sensitive volume of the cloud chamber, and it was not possible to study the events in this group in detail.

(2) Single recoil tracks : these result from reactions of the type (γ,n), (γ,2n), etc.

(3) Flags : Such events consisted of a fragment and a recoil/

recoil. The group is subdivided into

(a) Events involving the emission of an α-particle. The tracks of α-particles were distinguished from those of protons by their density. The group includes events due to the (γ, α) and the $(\gamma, \alpha n)$ reactions. It was found possible to identify some of the events positively with the (γ, α) reaction since both fragments stopped within the chamber, and could be measured.

(b) Collinear flags : events in which the fragment and recoil appear almost collinear. These were provisionally identified with the (γ, p) reaction, and on this assumption, a value was estimated for the angle between the fragment and the recoil. Only events with a measured value which agreed with this, within the limits of the experimental error were finally accepted in this group, the remainder being placed in class (c). Events due to reactions of the type (γ, p) and (γ, d) belong to this group.

(c) Non-collinear flags : in this group, the angle between the fragment and the recoil is such that, to conserve momentum, an uncharged fragment must also have been emitted. Events in this group can be ascribed to reactions of the type (γ, pn), (γ, dn), $(\gamma, p2n)$ etc.

Some typical photographs are shown in Appendix 2.

5.4 Results - General

Three reactions have been submitted to particular study, viz. the (γ, p), (γ, n), and (γ, pn) reactions. It is assumed that the single recoils (group 2) can be attributed to the (γ, n) reaction, with/

with very few (γ,2n) events. Measurements have shown that the cross-section for the second reaction is small in the case of N^{14} (93), and the assumption therefore appears reasonable.

Group 3(b) (collinear flags) was assumed to contain a preponderance of (γ,p) events. It was found quite impossible to distinguish the tracks of protons from those of deuterons, but the number of deuterons is expected to be small from considerations of isotopic spin (92). This has been observed, in the case of nitrogen, using a photon spectrum with a peak energy of 23MeV (25).

Possible reactions involving deuterons were also ignored in identifying the non-collinear flags (group 3c), and these were all attributed to the (γ,pn) reactions.

With these assumptions it was possible to assess the relative importance of each reaction in the disintegration of N^{14} and O^{16}.

Table 2

Nitrogen

Type of Event	Reaction	Number	Relative Number
(1) Star	"3 prong" "4 prong"	477) 321)	1.51
(2) Single recoil	$N^{14}(\gamma,n)N^{13}$	627	1.18
(3)a α-particle flags	$N^{14}(\gamma,\alpha)B^{10}$ $N^{14}(\gamma,\alpha n)$ etc.	28	0.05
(3)b Collinear flags	$N^{14}(\gamma,p)C^{13}$	528	1.00
(3)c Non-collinear flags	$N^{14}(\gamma,pn)C^{12}$	786	1.49

Oxygen/

Oxygen

Type of Event	Reaction	Number	Relative Number
(1) Star	3 prongs	94)	1.16
	4 or more prongs	78)	
(2) Single recoil	$O^{16}(\gamma,n)N^{15}$	288	1.95
(3)a α-particle flags	$O^{16}(\gamma,\alpha)C^{12}$ $(\gamma,\alpha n)$	10	0.07
(3)b Collinear flags	$O^{16}(\gamma,p)N^{14}$	148	1.00
(3)c Non-collinear flags	$O^{16}(\gamma,pn)N^{14}$	214	1.45

No account of the shape of the bremsstrahlung spectrum has been taken at this stage, and because of this, the results may be slightly misleading. A number of events may be due to the absorption of low energy photons into excited states of the target nuclei. Reactions of this type will be given a much greater weight because of the relatively large number of photons in this part of the spectrum. On the other hand, if the cross-section for each reaction varies with energy in a similar manner, the above figures may be taken as the relative integrated cross-sections for the indicated reactions.

5.5 The Disintegration of Nitrogen

5.5.1 The Reaction $N^{14}(\gamma,p)C^{13}$

The energy distribution of the recoil nuclei attributed to this reaction is shown in figure 23. The error due to range measurements was small, but that due to straggling was much larger, and could amount to about 0.2MeV at the peak of the distribution (94).

It/

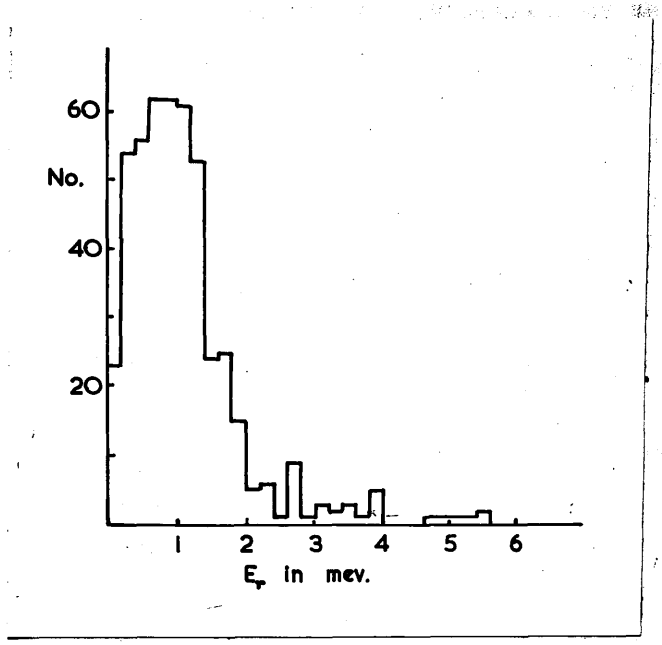

Figure 23

The energy distribution of the recoils from the reaction $N^{14}(\gamma, p)C^{13}$.

It was therefore decided to plot the number of events at intervals of 0.2MeV.

The energy of the emitted protons was calculated from the energy and direction of the recoil nucleus. By an application of the principle of conservation of momentum to the system, resolving the momenta along the direction of the emitted proton, and neglecting second order terms, it can be shown that the proton energy is given by the equation

$$(E_p)^{1/2} = \left(\frac{M_r}{M} E_r\right)^{1/2} - (Q + E_r)(2M_p)^{-1/2}\cos\theta$$

where

E_p and E_r, are the energies of the proton and recoil (in MeV)

M_p and M_r, are the rest mass energies of the proton and recoil (in MeV)

Q is the reaction threshold (in MeV)

θ is the angle between the emitted proton and the photon beam direction.

This formula was applied to each event, and a histogram of the energy distribution of the emitted protons was prepared (Fig 24)

The kinematics of the reaction are such that three independent equations can be derived to relate the energy and momentum of the incident photon, the emitted proton, and the recoil. Since only three parameters are unknown (the energy of the photon, the energy of the proton, and the state of excitation of the residual nucleus), it would appear that the problem can be solved exactly. Unfortunately, the solution depends critically upon the angle between the proton and the recoil, which varies by less than 15^o for most

(γ, p)/

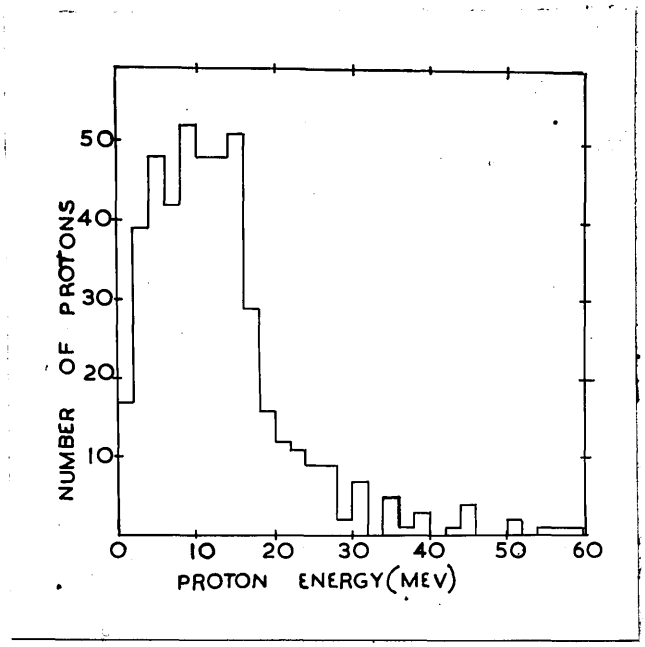

Figure 24

The energy distribution of the protons from the reaction $N^{14}(\gamma, p)C^{13}$.

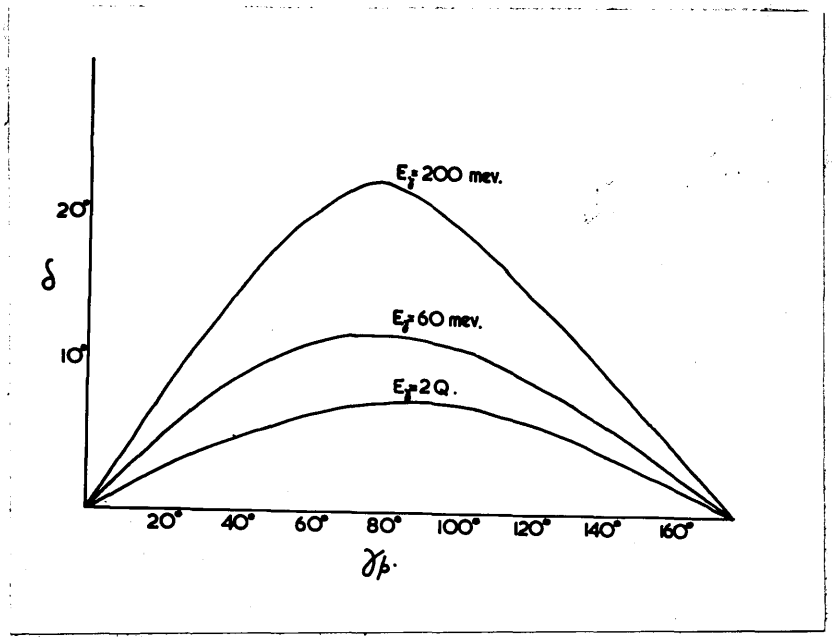

Figure 25

The variation of the angle between the emitted proton and the recoil from (γ ,p) events, as a function of the angle between the proton and the photon beam, and of the photon energy.

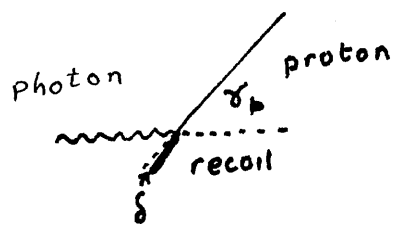

(γ,p) reactions* (figure 25). It is not possible to measure this angle with the required degree of precision, and it was therefore decided to treat it as an unknown quantity, and assume at this stage that the excitation energy of the residual nucleus was zero. On this basis, the energy of the photon responsible for each event was calculated from the equation

$$E_t = E_r + E_p + Q, \quad \text{where} \quad Q = 7.5\text{MeV}$$

with the obvious significance of the symbols. The resultant histogram is shown in figure 26.

The angular distribution of all the protons from the (γ,p) reaction, with respect to the direction of the photon beam is shown in figure 27. The curve

$$27 + 28\sin^2\theta$$

was fitted to this distribution, using the method of leastsquares. The number of particles emitted per steradian per angular interval has been plotted in this distribution, and in all other angular distributions, unless the contrary is specifically stated.

Figure 28 shows the angular distributions of protons of different energies. For this purpose, the protons were divided into three energy groups: protons of energy less than 12MeV - the experimental points are plotted with a cross within a circle - protons of energy between 12MeV and 22MeV, marked with a large spot, and protons of energy greater than 22MeV, marked with a dot within a circle. Curves were fitted/

*i.e for photon energies between 2Q and the peak photon energy (200MeV); larger variations are possible if absorption energies just above the reaction threshold are considered, but in such cases, the recoil range is too short to measure the angle accurately.

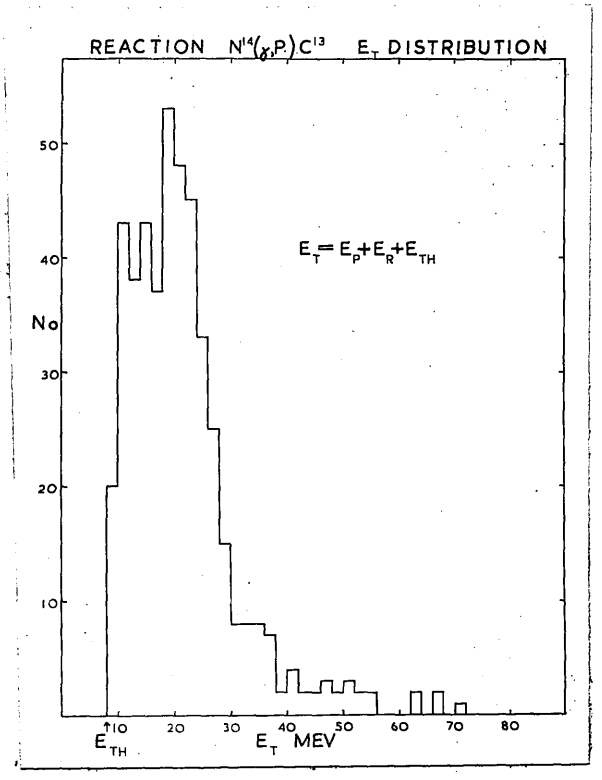

Figure 26.

The energy distribution of the photons inferred from the recoil energy distribution, on the assumption that all reactions resulted in the formation of C^{13} in its ground state.

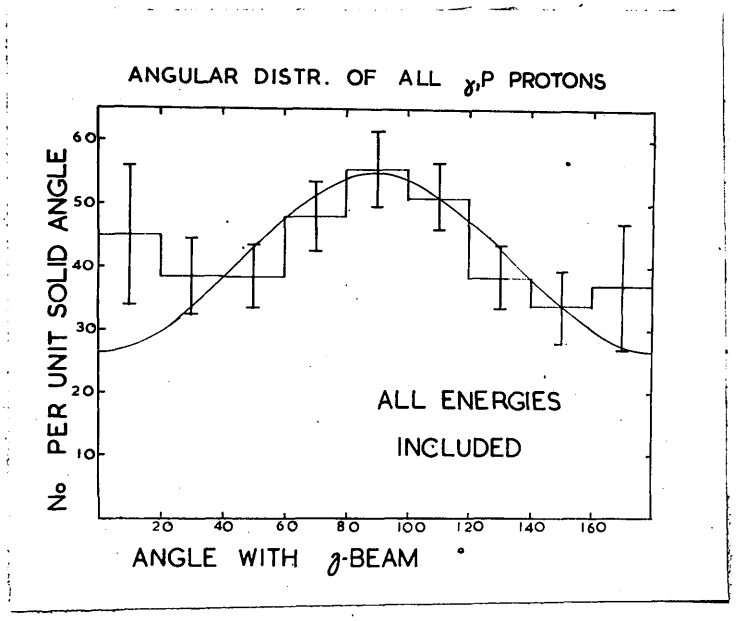

Figure 27

The angular distribution of all the protons from the (γ ,p) reaction.

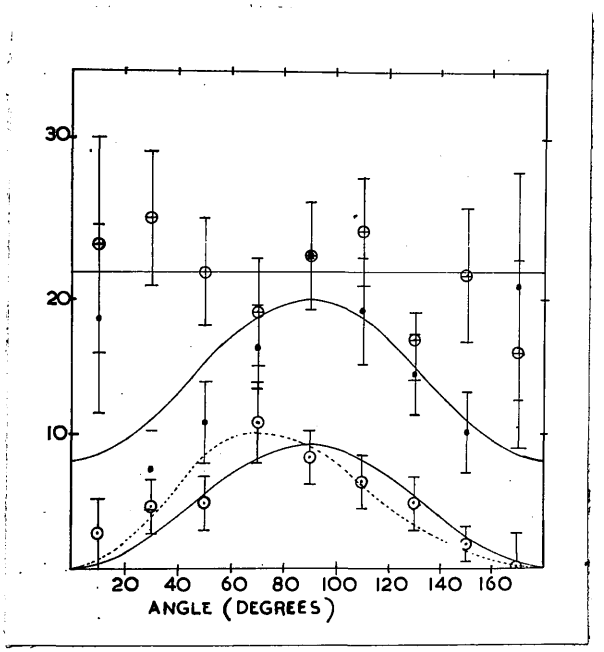

Figure 28

The angular distributions of protons from (γ,p) reactions in nitrogen:

(1) protons of energy less than 12MeV. The distribution is fitted with the line

$$f(\theta) = 22$$

and the experimental points are plotted with a cross within a circle.

(2) protons of energy between 12MeV and 20MeV. The distribution is fitted with the curve

$$f(\theta) = 8 + 12\sin^2\theta$$

and the experimental points are plotted with a large spot.

(3) protons of energy greater than 20MeV. The distributions is fitted with the curves

$$f(\theta) = 9\sin^2\theta, \quad \text{and } f(\theta) = 9\sin^2\theta(1 - 0.35\cos\theta)^2$$

and the experimental points are marked with a dot within a circle.

fitted to each distribution: the distribution of the low energy group was isotropic (line 1 in the figure), the second group fitted the curve (line 2)

$$8 + 12\sin^2\theta$$

and the angular distribution of the fast protons took the form (line 3)

$$9\sin^2\theta \qquad \text{or} \qquad 9\sin^2\theta\,(1 + .35\cos\theta)^2$$

5.5.2 The reaction $N^{14}(\gamma,n)$

The energy distribution of the recoils from events attributed to this reaction is shown in figure 29, the energy resolution being similar to that obtained in the measurement of the recoils from the (γ,p) reaction. Further interpretation of these results is difficult, since the emitted neutron could not be detected, and it was seldom obvious which end of the recoil track corresponded to the origin of the event. It was therefore impossible to calculate exactly the energy of the emitted neutron, or of the photon responsible for the reaction.

For the same reason, the measured angular distributions were ambiguous: since the direction of the recoil was doubtful, each measured angle (θ_m) was related to the angle (θ) between the recoil track and the direction of the photon beam by the equation

$$\theta_m = \theta \pm n\pi/2, \quad \text{where} \quad n = 0, \text{ or } 1.$$

It was therefore decided to plot the acute angle between the recoil and the direction of the photon beam. The angular distribution of all the recoils attributed to the (γ,n) reaction is shown in figure 30.

This/

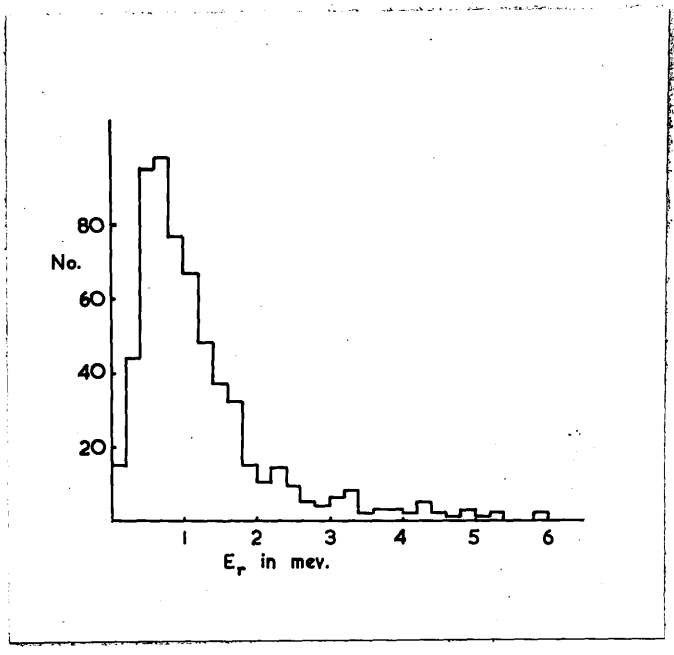

Figure 29

The energy distribution of the recoils from the reaction $N^{14}(\gamma, n)N^{13}$.

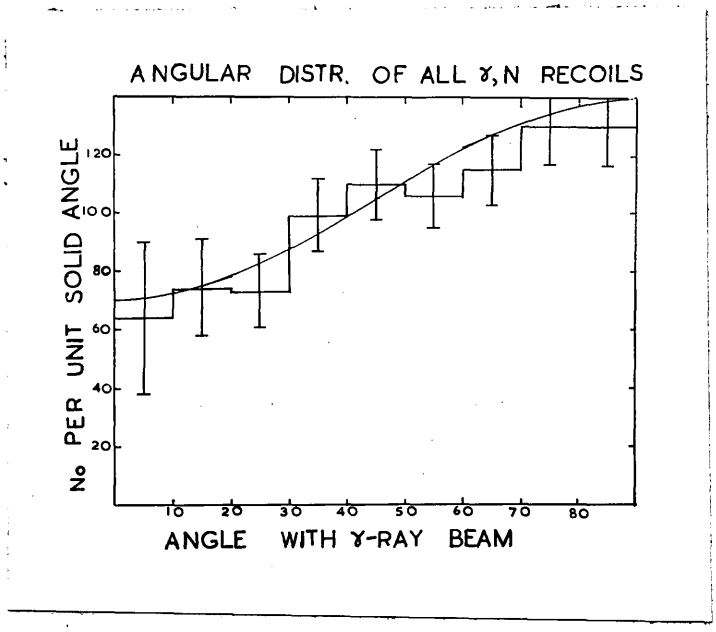

Figure 30

The angular distribution of all the recoils (neutrons) from (γ,n) events. The curve $70(1+\sin^2\theta)$ has been fitted to the distribution.

This has been fitted with the curve

$$70 + 70\sin^2\theta$$

As in the case of the (γ,p) reaction, distributions were plotted of recoils belonging to each of three energy groups. The low energy group, including recoils of energy less than 1MeV, was fitted with the curve (line 1 in figure 31)

$$40(1 + \sin^2\theta),$$

and the experimental points are marked with a cross within a circle. The second energy group was comprised of recoils with an energy between 1MeV and 2 MeV: the experimental points are plotted with a large spot, and line 2,

$$15 + 25\sin^2\theta$$

has been fitted to the distribution. The distribution of recoils from reactions resulting in the emission of a fast neutron (recoil energy greater than 2MeV) is indicated by the points marked by a dot within a circle: the distribution was fitted with the curve (line 3)

$$25\sin^2\theta.$$

If it is assumed that the neutrons are emitted symmetrically about 90°, which seems reasonable from a comparison with the corresponding results for protons, then the distributions in figures 30 and 31 may be taken as the angular distributions of the emitted neutrons, and may be extrapolated to 180°. The three recoil energy groups will then correspond to neutrons of energy less than 13MeV, with an energy which lies between 13MeV and 26MeV, and with energy greater than 26MeV respectively./

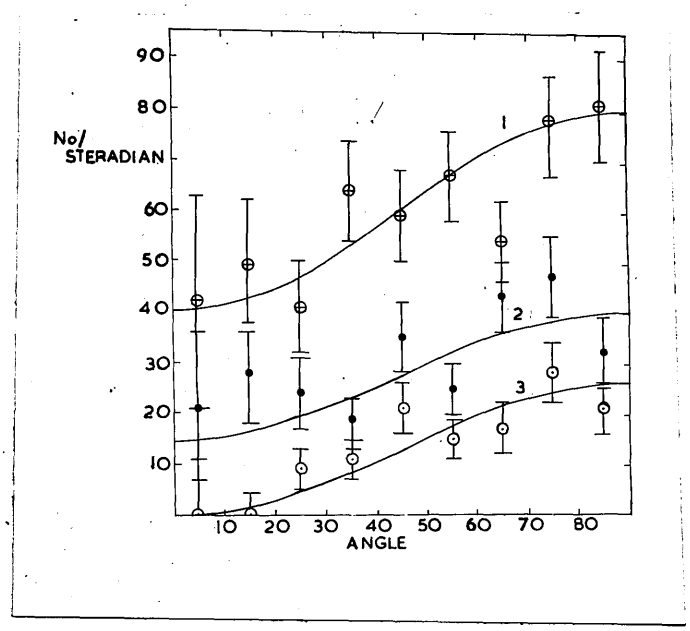

Figure 31

The angular distributions of recoils (neutrons) from (γ,n) reactions :

(1) Recoils of energy less than 1MeV ($E_n < 13$MeV). The distribution is fitted with the curve

$$f(\theta) = 40(1 + \sin^2\theta)$$

and the experimental points are plotted with a cross within a circle.

(2) Recoils of energy between 1MeV and 2MeV ($E_n \gg 13$MeV , $E_n < 26$MeV). The distribution is fitted with the curve

$$f(\theta) = 15 + 25\sin^2\theta$$

and the experimental points are plotted with a large spot.

(3) Recoils of energy greater than 2MeV ($E_n \gg 26$MeV). The distribution is fitted with the curve

$$f(\theta) = 25\sin^2\theta$$

and the experimental points are plotted with a dot within a circle.

respectively. These energies are, of course, only approximate values, calculated from a simple momentum balance.

5.5.3 The reaction $N^{14}(\gamma,pn)C^{12}$

The observed (γ,pn) events can be conveniently separated into two groups :-

(a) events involving the emission of a slow proton which remains within the confines of the cloud chamber;

(b) events from which the proton left the cloud chamber.

In the first group, it is possible to solve the kinematical equations exactly. For the purposes of the calculation, it can be assumed that the proton, neutron and recoil are coplanar - this amounts to neglecting the effect of the momentum of the photon. Two equations can then be derived connecting the momentum of the three particles, and since only the neutron energy (or momentum) and its direction are unknown, these equations can be solved. The energy of the photon can then be calculated, on the assumption that the residual nucleus is left in its ground state, from the sum of the kinetic energies of the recoil, neutron, and proton, together with the Q-value (12.5MeV) of the reaction. Unfortunately, only 30 events fall into this group: the energy and angular distributions relating to these events are shown in figure 32. Figure 32a shows the distribution of the energies inferred for the photons which caused the reactions: the histogram in figure 32b shows the angular distribution of the recoil with respect to the emitted proton, and that in figure 32c shows the direction/

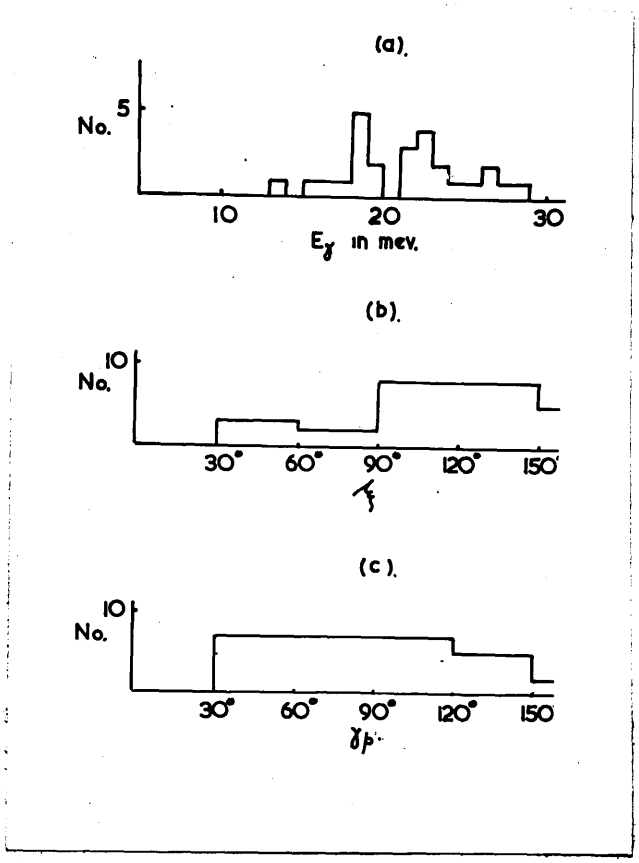

Figure 32

The distributions of (γ,pn) events in nitrogen involving the emission of a slow proton which remained within the cloud chamber.

(a) the energy of the photon responsible which caused the reaction, on the assumption that the residual nucleus is left in its ground state.

(b) The angular distribution of the emitted protons with respect to the direction of the recoil nucleus.

(c) The angular distributions of the emitted protons with respect to the direction of the photon beam.

direction of the proton with respect to the incident photon beam.

In the second group, since the proton leaves the sensitive part of the cloud chamber, it is not possible to measure its range, and its energy is therefore also unknown. This means that there are two independent equations involving three unknown quantities, which cannot therefore be calculated. The energy distribution of all the recoils from the (γ,pn) reaction is shown in figure 33. The form of the distribution is similar to that of the corresponding distributions for the (γ,p) and (γ,n) reactions, but the peak occurs at a much lower energy.

Various angular distributions were compiled from measurements of the events attributed to the (γ,pn) reaction. Figure 34 shows the distribution of the recoils (continuous histogram) and of the protons (dotted histogram), with respect to the direction of the incident photon beam. The figure shows the similarity of these distributions. In figure 35, the distribution of the emitted protons with respect to the direction of the recoil nucleus has been plotted. There are sufficient events to justify plotting this histogram at intervals of 10^{o}, and the distribution shows the observed number of protons per 10^{o} interval, and not the number emitted per steradian.

---

5. 6 The Disintegration of Oxygen

This study was not intended to provide results as comprehensive as those obtained from the experiment with nitrogen. The number of photographs/

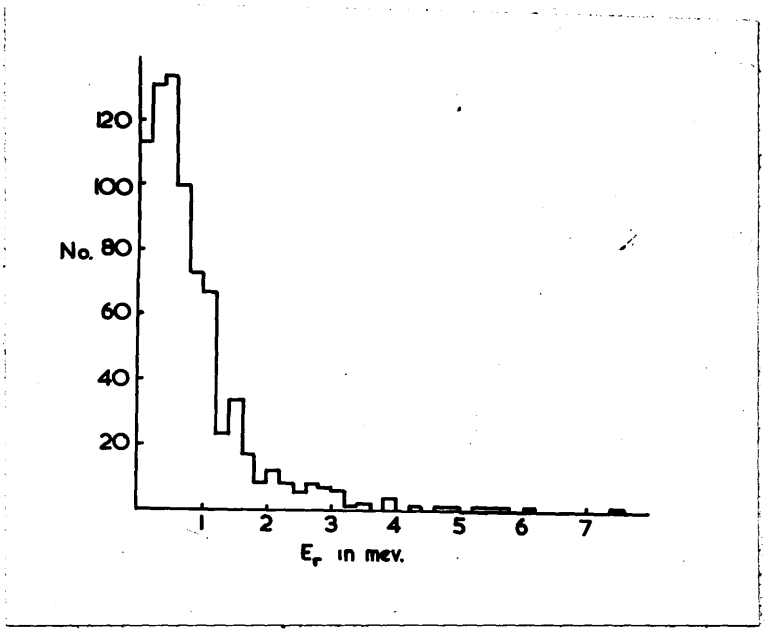

Figure 33

The energy distribution of the recoils from the reaction $N^{14}(\gamma, pn)C^{12}$.

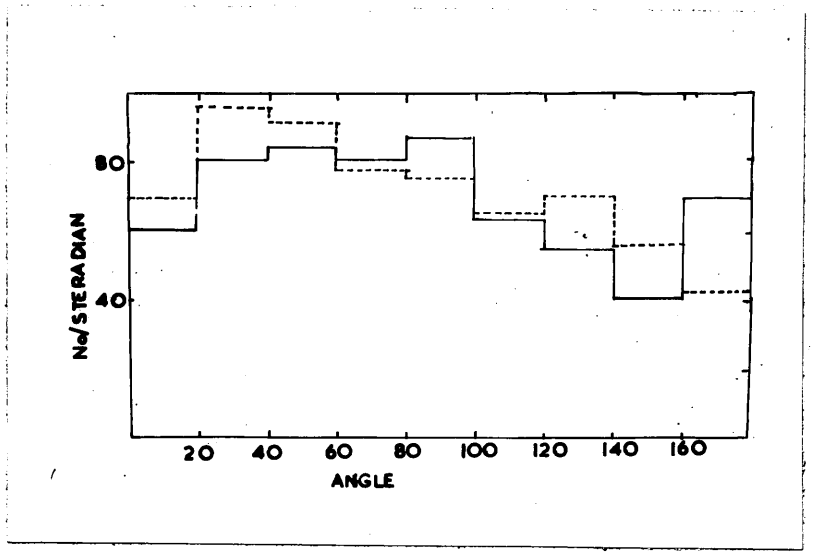

Figure 34

The angular distributions of the protons and recoils from (γ,pn) events in nitrogen with respect to the direction of the photon beam.

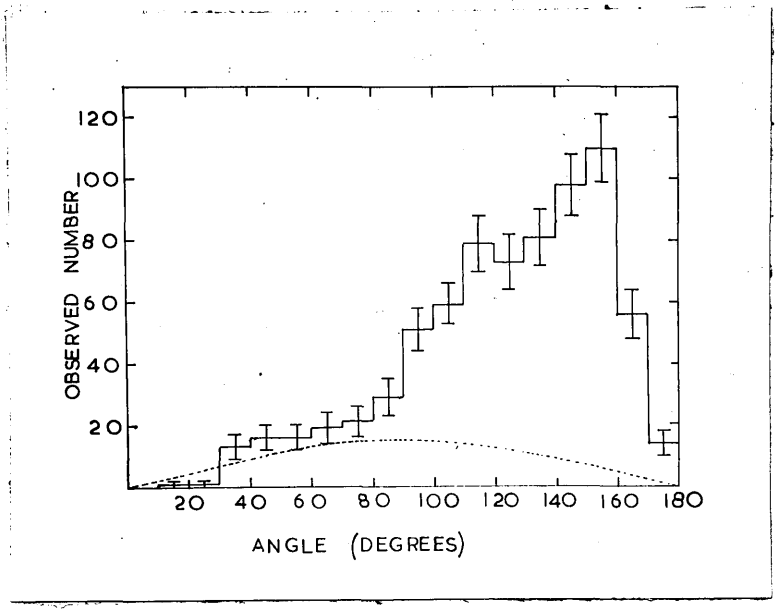

Figure 35

The angular distribution of the protons from (γ,pn) events in nitrogen with respect to the direction of the recoil nucleus.

photographs taken was considerably smaller, and from these about 700 useful events were obtained. The statistics of the histograms which were compiled are therefore inferior in comparison with the nitrogen results, but are sufficiently good for some conclusions to be drawn.

5.6.1 The Reaction $O^{16}(\gamma,p)N^{15}$

The energy distribution of the recoils attributed to this reaction is shown in figure 36. The energy resolution was again estimated to be about 0.2MeV, and the histogram was therefore plotted at intervals of 0.2MeV.

The energy of the protons emitted from each reaction was now calculated from the energy and direction of the recoil nucleus. The principle of conservation of momentum was applied, as in the case of the corresponding reaction in nitrogen. The energy distribution of the emitted protons is shown in figure 37.

On the assumption that the residual nucleus is left in its ground state, it was now possible to calculate the energy of the photon responsible for each reaction: the resultant histogram is shown in figure 38. Since a large number of transitions will result in the formation of N^{15} in an excited state, the low energy part of this distribution has little significance. On the other hand, at higher energies, above the giant resonance, the excitation energy of the residual nucleus is small compared with the energy of the emitted particle, and the distribution in this region will therefore reflect the variation of the cross-section for the reaction.

The angular distribution of all the protons from events attributed/

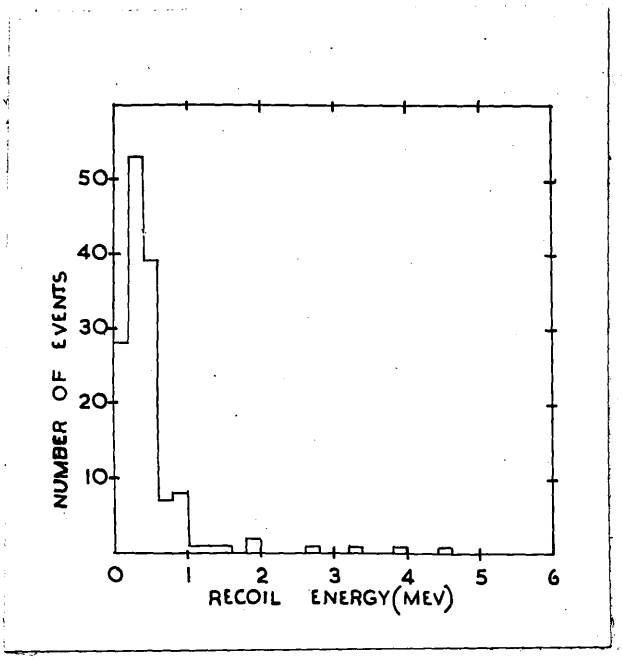

Figure 36

The energy distribution of the recoils from the reaction $O^{16}(\gamma,p)N^{15}$.

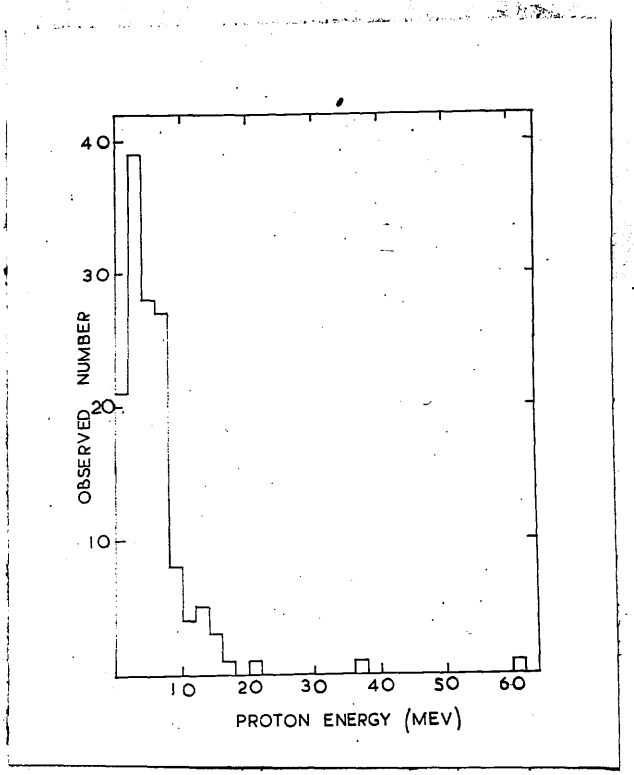

Figure 37

The energy distribution of the photons from the reaction $O^{16}(\gamma, p)N^{15}$.

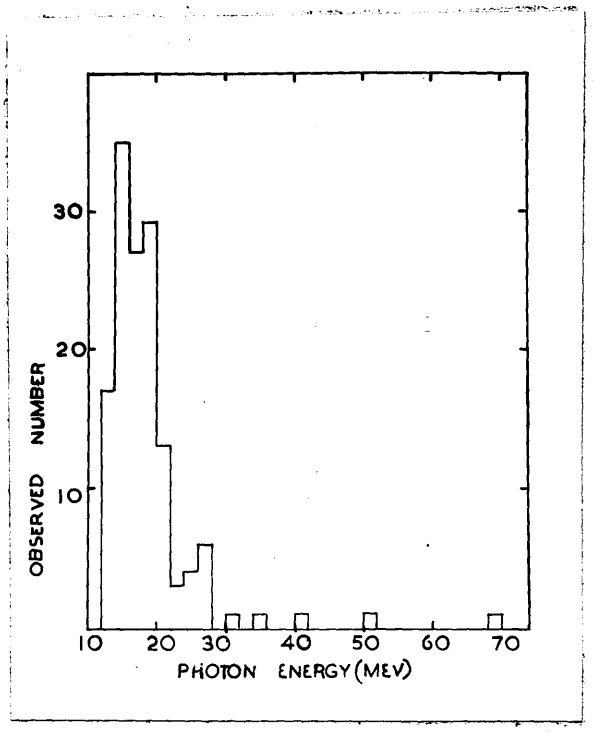

Figure 38

The energy distribution of the photons absorbed in the reaction $O^{16}(\gamma,p)N^{15}$, calculated on the assumption that the residual nucleus was left in its ground state.

attributed to the (γ,p) reaction is shown in figure 39. In this case, there were insufficient events to justify the plotting of the angular distributions of protons of different energies. The distribution of all protons has been fitted to the curve

$$7 + 8\sin^2\theta$$

and this curve is shown in figure 39.

5.6.2 The reaction $O^{16}(\gamma,n)N^{15}$

The energy distribution of the recoils from events assigned to this reaction is shown in figure 40. As in the case of nitrogen the direction of the recoils is ambiguous. Further interpretation of the results was therefore difficult, and the calculation of the energy of the neutron, or that of the incident photon was impossible.

The measurements of the angles again yielded two possible values, and the acute angle between the recoil and the photon beam was plotted. The angular distribution of all the recoils which were assigned to the (γ,n) reaction is shown in figure 41. The distribution has been fitted with the curve

$$30 + 33\sin^2\theta.$$

Since the observed number of (γ,n) events was considerably greater than the number of (γ,p) events, it was possible to plot the angular distributions in two energy regions. The regions selected included recoils of energy less than, and greater than 0.7MeV. These distributions are shown in figure 42: the experimental points referring to recoils of energy less than 0.7MeV are plotted with a

cross/

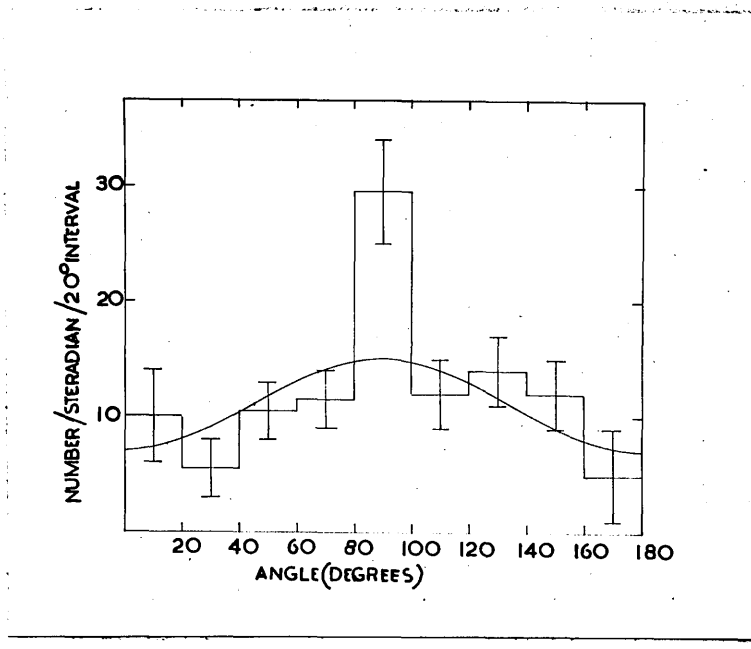

Figure 39

The angular distribution of all protons assigned to the (γ,p) reaction in oxygen.

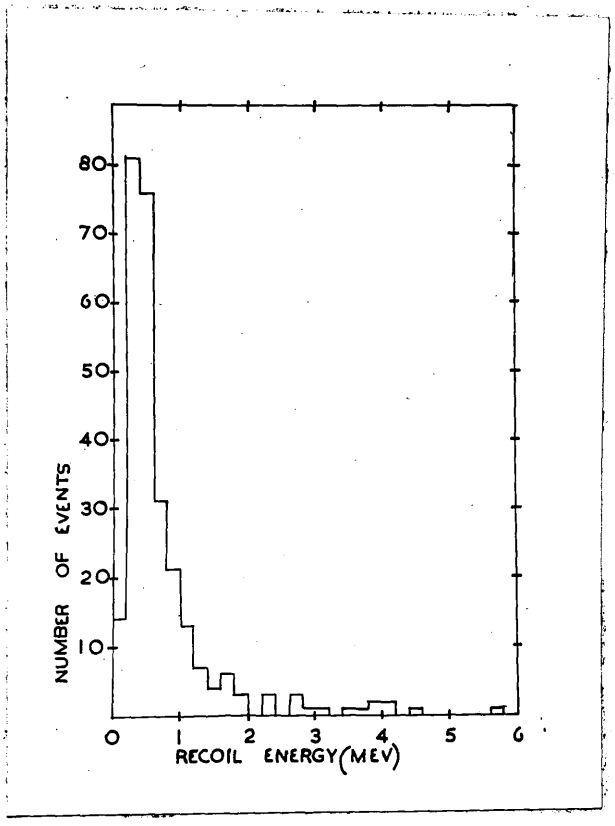

Figure 40

The energy distribution of all recoils from the reaction $O^{16}(\gamma, n)O^{15}$.

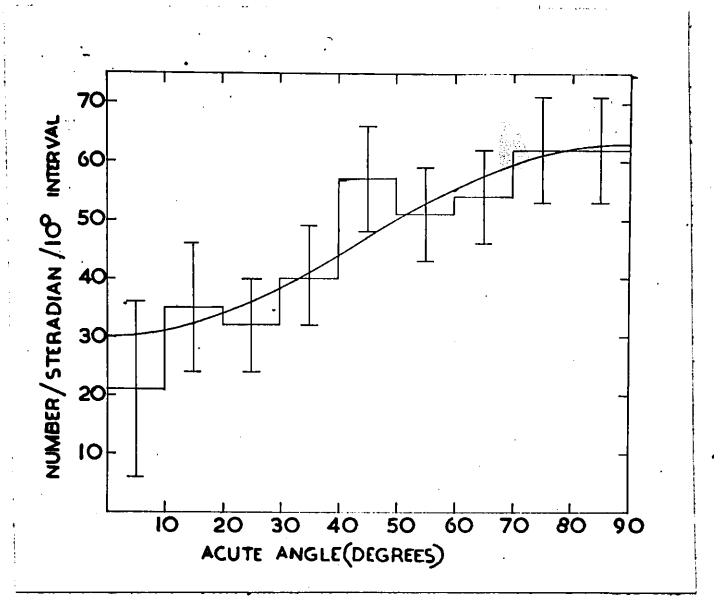

Figure 41

The angular distribution of all recoils (neutrons) from (γ,n) reactions in oxygen.

cross, and those referring to recoils of energy greater than 0.7MeV are plotted with a large spot. The distributions have been fitted with the curves

(1) $23 + 23\sin^2\theta$ and (2) $11 + 5\sin^2\theta$

respectively.

As in the case of nitrogen, these distributions can be taken as the angular distributions of the emitted neutrons, if they are symmetric about 90°. In this case, the two distributions in figure 42 will refer to neutrons of energy less than, and greater than 12MeV.

5.6.3 The Reaction $O^{16}(\gamma,pn)N^{14}$

In this case, the number of events involving the emission of a slow proton which remained within the confines of the chamber (only 6 events were observed) did not justify the plotting of a set of histograms.

The energy distribution of the recoils from (γ,pn) events is shown in figure 43. As in the case of nitrogen, the form of the distribution is similar to those resulting from the emission of a single nucleon, but the peak occurs at a lower energy.

The angular distributions compiled from measurements of the (γ,pn) reaction in oxygen are shown in figures 44, and 45. Figure 44 shows the distribution of the recoils (continuous histogram) and the protons (dotted histogram) with respect to the direction of the photon beam. The angular distribution of the emitted protons with respect to the direction of the recoil nucleus is shown in figure 45: the/

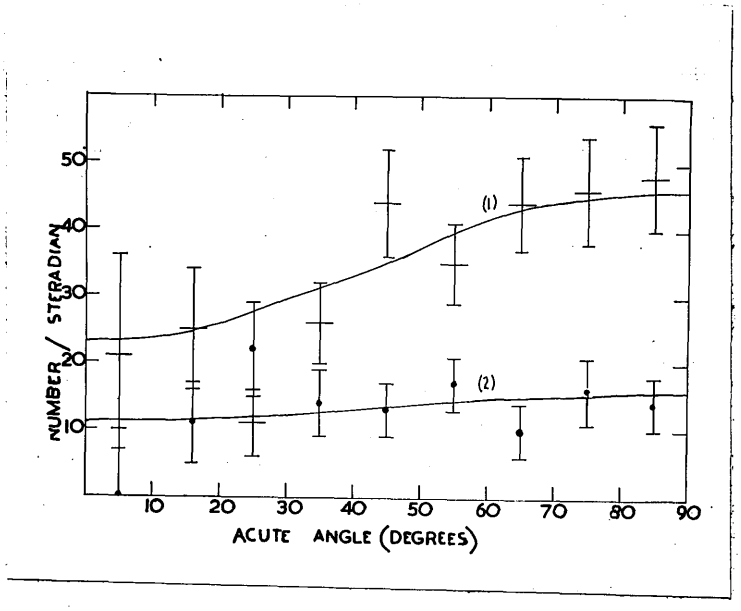

Figure 42

The angular distributions of recoils (neutrons) from (γ,n) reaction in oxygen.

(1) the distribution of recoils of energy less than 0.7MeV ($E_n < 11$MeV). The curve

$$23(1 + \sin^2\theta)$$

has been fitted to the distribution, and the experimental points are plotted with a cross

(2) The distribution of recoils of energy greater than 0.7MeV ($E_n \gtrsim 11$MeV). The curve

$$11 + 5\sin^2\theta$$

has been fitted to the distribution and the experimental points are marked with a large spot.

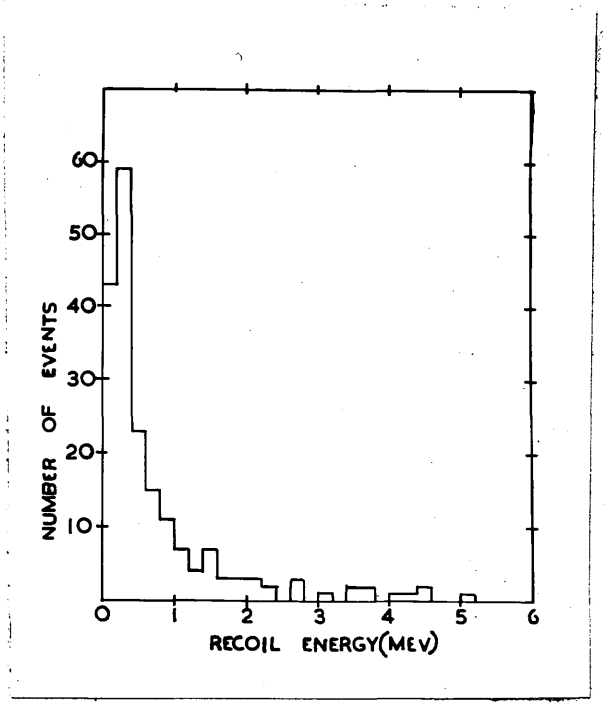

Figure 43

The energy distribution of the recoils from the reaction $O^{16}(\gamma,pn)N^{14}$.

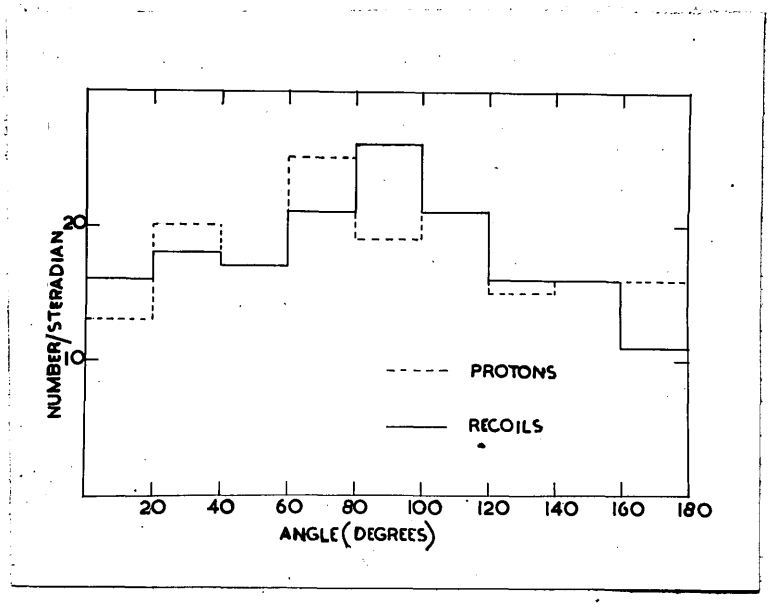

Figure 44

The angular distributions of protons and recoils from (γ,pn) reactions in oxygen with respect to the direction of the photon beam.

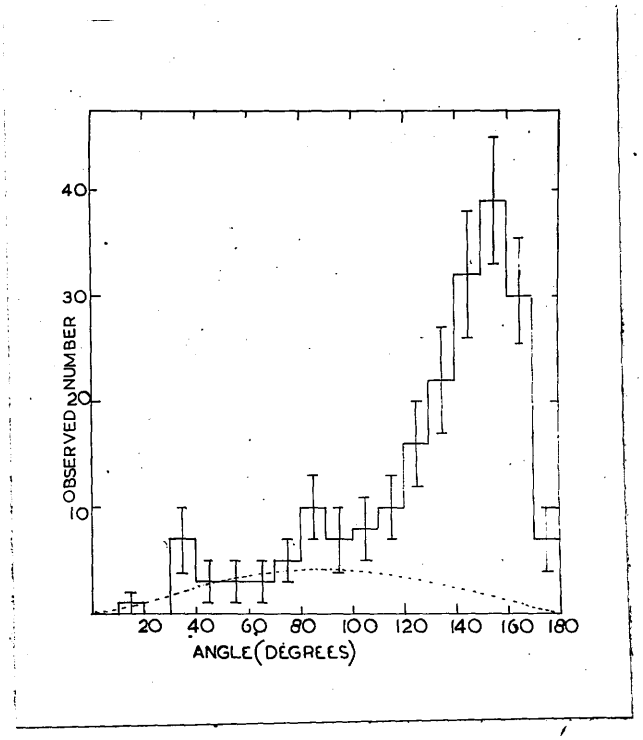

Figure 45

The angular distribution of the emitted protons from (γ,pn) reactions in oxygen with respect to the direction of the nuclei.

the observed number of protons per 20^{o} interval has been plotted in this case.

5.7 Summary

The results of the experiments on the photo-disintegration of nitrogen and oxygen have just been described. They may be summarised as follows :-

(1) The integrated cross-section forthe (γ,p), (γ,n), and (γ,pn) reactions (table 2) are all of the same order of magnitude, but the relative values of the cross-section differ for the two nuclei.

(2) The recoil energy distributions from the (γ,p) (figure 23) and (γ,n) (figure 29) reactions in nitrogen take the form of a broad peak with a tail extending to higher energies. The peak of the (γ,p) histogram is broader than that referring to the (γ,n) events, and there is some evidence of structure in the other energy distributions associated with the (γ,p) reaction (figures 24, 25). In the case of oxygen, the distributions resemble each other (figures 36,41) again taking the form of a broad peak. The high energy tail of the distributions is much less pronounced than in the corresponding distributions from nitrogen.

(3) The angular distributions of the nucleons from the (γ,p) and (γ,n) reactions can all be fitted by curves of the form

$$A + B \sin^2\theta$$

For/

For the total angular distributions (figures 27, 30, 39, 41)

$$B/A = 1 \pm 0.2.$$

In nitrogen, the value of B/A tends to increase with the energy of the particles considered (figures 28, 31), but the angular distribution of the fast neutrons from oxygen is almost isotropic (figure 42). There is some sign of assymmetry in the distribution of the fast protons from nitrogen, and the peak at 70-80^{o} in the corresponding neutron angular distribution may be due to a similar effect.

(4) The energy distributions of the recoils from (γ,pn) events (figures 33, 43) is similar to the distributions of recoils from reactions resulting in the emission of a single nucleon, but the peak occurs at a lower energy, and the distribution is somewhat narrower.

(5) The angular distributions of the recoils and protons from (γ,pn) events with respect to the direction of the photon beam (figures 34, 44) are similar, and almost isotropic, but show a tendency towards forward angles. The distributions of the emitted protons with respect to the direction of the recoil nucleus shows a marked preference for angles greater than 90^{o}, and the distributions are peaked at about 150^{o} - 160^{o}.

(6) The energy distribution calculated from the (γ,pn) events from which the protons did not leave the cloud chamber (figure 32a) shows two peaks, at 18MeV and 22MeV, which may not be statistically significant. The distribution shows that the cross-section for this type/

type of event reaches a maximum at about 20MeV: this behaviour may, or may not be typical of the (γ,pn) reaction.

The angular distributions associated with these events show the same general trends as those referring to all the (γ,pn) events. In the case of the distribution of the protons with respect to the direction of the recoil nucleus, the tendency towards angles greated than 90^{o} is not quite as marked, and the peak appears to occur at a smaller angle (about 120^{o}).

CHAPTER 6. Discussion

CHAPTER 6 DISCUSSION

6.1 The Relative Importance of Reactions

In the introduction to chapter 5, it was indicated that the (γ,p), (γ,n) and (γ,pn) reactions were expected to account for a large part of the photo-nuclear cross-section in light elements. Measurements have shown that the cross-section curves for these reactions have similar general characteristics (25, 29, 87), but it has been observed that the cross-sections for the (γ,p) reactions are appreciably below the threshold of the (γ,n) reactions (25, and chapter 4 of this thesis). The figures in table 2 may therefore be taken as a measure of the relative cross-sections of each reaction, with the proviso that those quoted for the (γ,p) reactions are upper limits. With this reservation, the results in table 2 indicate that the integrated cross-sections for the (γ,p), (γ,n) and (γ,pn) reactions are of the same order of magnitude, while the integrated cross-section for reactions involving the emission of a single α-particle is considerably smaller.

In oxygen and nitrogen, the cross-section for the emission of a proton is not negligible in comparison with that for the emission of a neutron. From considerations of the charge independence of nuclear forces, and the fact that O^{16} and N^{14} are self mirrored nuclei, it might be expected that the cross-sections would be identical, but this picture must be modified slightly to take into account the effect of the coulomb barrier. In heavy nuclei, this enhances the (γ,n) cross-section/

section at the expense of the (γ,p) reaction, but in light nuclei, the barrier is small, of the order of a few MeV, and the (γ,n) cross-section is only slightly greater than that of the (γ,p) reaction. This can be clearly seen in table 2.

The integrated cross-sections for the (γ,pn) reactions are also of the same order of magnitude. In the case of the nucleus N^{14}, the ratio of the cross-sections of the (γ,p) and (γ,pn) reactions have been observed using bremsstrahlung spectra with peak energies 19MeV, 21MeV, and 23MeV to be 3:1, 3:2, and 3:3 respectively (25). In table 2, the relative numbers of (γ,p) and (γ,pn) events is 1:1.5, which is somewhat larger than the earlier values. It therefore appears that the (γ,pn) reaction cross-section is increasing to a maximum in a manner similar to the (γ,p) cross-section, but that the maximum occurs at an energy greater than 23MeV. The peak of the cross-section must also lie at a higher energy than the peak in the (γ,p) cross-section, since if the variation were identical, the ratio of events would not depend on the peak energy of the spectrum. In the case of oxygen, there are no previous measurements of the (γ,pn) cross-section for comparison, but since the threshold for the reaction lies at 23MeV, it can be deduced that the cross-section is large at greater energies. The observed result would be consistent with a variation of the cross-section similar to that suggested above for the (γ,pn) reaction in nitrogen.

The cross-section for the emission of an α-particle from both N^{14} and O^{16} appears to be small. This is consistent with the arguments,/

arguments, based on isotopic spin selection rules, advanced by Goldhaber and Teller, and others (92). For E1 transitions in self-mirrored nuclei, the change in isotopic spin (T) is ± 1, and this means that the E1 absorption of radiation by N^{14} or O^{16} must excite a T = 1 state. Since the isotopic spin of an α-particle (or a deuteron) is zero, the emission of such a fragment will leave the residual nucleus (B^{10} or C^{12}) in a T = 1 state. Thus for a (γ,α) reaction to occur, the excitation energy must be sufficient to leave the residual nucleus in such a state - i.e. an excitation energy of about 25MeV is required. At energies greater than this, the photon absorption cross-section is small, and the reactions should therefore have a small relative probability, as is observed.

The number of stars observed is relatively large, being of the same order as the number of events attributed to each of the other reactions. The cross-section for such events has been observed to be small (in the case of N^{14} - 25) at energies less than 23MeV, and the present result therefore indicates that the cross-section must be large at greater energies, especially since the number of photons in this part of the spectrum is small. These events may result from a (γ,α) reaction, leaving the residual nucleus in an excited (T = 1) state which decays by the emission of a further charged fragment. About 60% of the nitrogen stars consisted of three fragments, and could be due to reactions of this type - the reactions $N^{14}(\gamma, \alpha p)Be^{9}$, and $N^{14}(\gamma, \alpha\alpha)Li^{6}$ have been observed at lower energies, and would account for the events observed. The remaining 40% of the nitrogen stars

consisted/

consisted of events involving four charged fragments which could be due to a different type of reaction. At high excitation energies, the reaction $N^{14}(\gamma, 3\alpha pn)$ has been observed (100), and this would account for these events. This type of reaction, involving the emission of a fast proton and neutron, is predicted by Levinger's quasi-deuteron model. The relative number of stars in oxygen is rather smaller, and the percentage of three and four pronged events is slightly different. The $(\gamma,4\alpha)$ reaction has been observed (14), and will account for a number of the four pronged events. Since no other data is available on the disintegration of oxygen into many fragments, a more detailed analysis of the results is not possible. Since most of the fragments from the stars generally left the confines of the chamber, it was not possible to study these events in detail, or to identify the reactions positively.

The above discussion has referred to the relative cross-sections of the reaction for each nucleus. A comparison of these relative cross-sections also leads to some interesting conclusions. The relative cross-sections for the (γ,p), (γ,n) and (γ,pn) reactions in nitrogen and oxygen are respectively

1.0 : 1.2 : 1.5 and 1.0 : 2.0 : 1.5.

Thus in nitrogen, the cross-sections of the single nucleon reactions are comparable, while that of the (γ,pn) reaction is 50% greater; in the case of oxygen, the (γ,n) reaction is 100% more probable than the (γ,p) reaction, and the (γ,pn) reaction is rather less favoured.

This/

This is probably due to the low threshold of the (γ,pn) reaction in nitrogen. In general terms, the photo-nuclear process can be envisaged as follows :- the absorption of a photon will result either in the direct ejection of a nucleon, or in the excitation of a compound nucleus state. The excited state then decays by the emission of one or more particles, or by radiation, the former process being more probable if it is energetically possible.

For nitrogen, the threshold for the (γ,pn) reaction lies a few MeV above the thresholds for the emission of a single nucleon, and it follows that if the absorption of a photon does not result in the direct ejection of a nucleon, the evaporation of two particles will be probable. In the case of oxygen, the threshold of the (γ,pn) reaction lies at a much greater energy, (23MeV), and the evaporation of a single nucleon will therefore account for a large part of the photo-nuclear cross-section. Further, in an evaporation process, such as this, the emission of low energy particles is probable, and, the coulomb barrier will therefore have an appreciable effect in suppressing the emission of a proton in favour of the emission of a neutron. The (γ,n) cross-section will therefore be enhanced relative to the (γ,p), and (γ,pn) reactions, as is observed.

The results in table 2 have been discussed in the above pages. They indicate that the (γ,p), (γ,n) and (γ,pn) reactions are all important in the photo-disintegration of light nuclei, while the (γ,α) reaction is relatively unimportant in the energy region of the giant resonance./

resonance. At greater energies the cross-section for reactions involving the emission of more than two charged fragments appears to be large, and it is suggested that these reactions may be attributed to two types of process: one involving the emission of an α-particle followed by a second fragment, and the other involving the disintegration of the whole nucleus in a "quasi-deuteron" type of process. The relative cross-sections for the (γ,p), (γ,n) and (γ,pn) reactions in nitrogen and oxygen indicate the type of process which is responsible for each reaction. The single nucleon reactions in nitrogen appear to be due mainly to a direct emission process; the formation of a compound nucleus state will generally result in a (γ,pn) reaction. On the other hand, in oxygen, the excitation of a compound nucleus state can result in the evaporation of either a proton or a neutron, with a preference for the latter, and the (γ,pn) reaction cannot become important at energies less than 23MeV.

6.2 The Photo-production of a Single Nucleon

6.2.1 The Energy Distribution

The energy distribution of the protons from events identified with the reaction $N^{14}(\gamma,p)C^{13}$ (figure 24) shows peaks centred at about 14MeV, 9 MeV, and 5MeV. This agrees with the measurements of Livesey (89). These may be interpreted as follows (see figure 46) :-

(1) The energetic group is due to the absorption of a photon, by N^{14}, in the energy region of the giant resonance, followed by the emission of a proton leaving the residual nucleus (C^{13}) in its ground state./

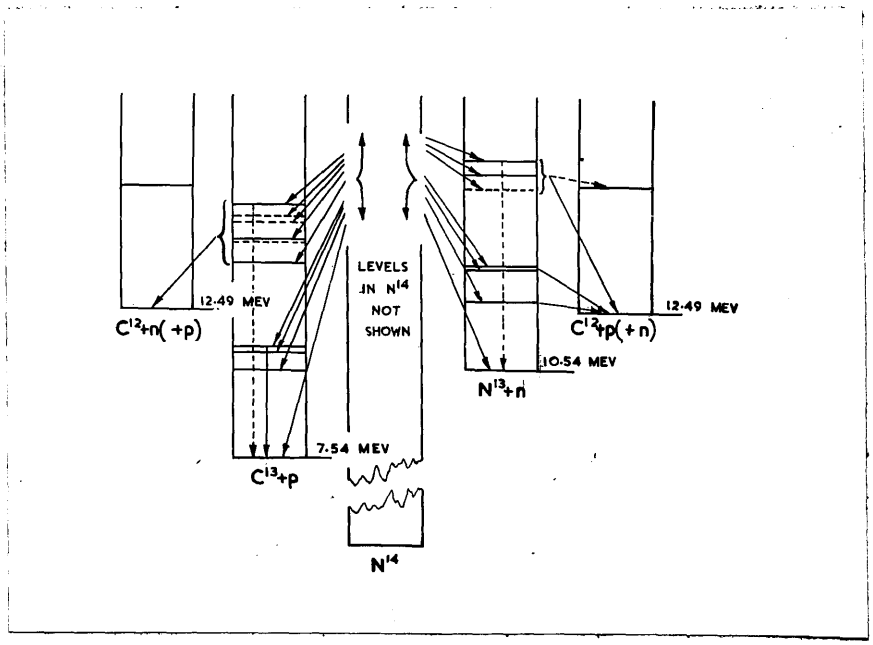

Figure 46

The photo-disintegration of nitrogen.

state.

(2) The group centred at about 9MeV may also be attributed to giant resonance transitions resulting in the emission of a proton, but leaving the carbon nucleus in an excited state some 4MeV above its ground state (there are suitable energy levels in C^{13} at 3.1MeV, 3.7MeV, and 3.9MeV). This group is about the same size as the energetic group, indicating that these processes are equally likely.

(3) The low energy protons may be due to three types of processes. There is a possibility of a giant resonance transition resulting in the emission of a proton and leaving the residual nucleus in a higher excited state. The probability of such a state de-exciting by the emission of radiation cannot be large, since the state must be above the threshold for the emission of a neutron and would therefore tend to decay in this way. Secondly, there is a chance that some (γ,pn) reactions have been mis-identified as (γ,p) events: from a study of the angular distributions referring to the (γ,pn) reaction, an upper limit of 40 events of this type was set, and if the recoil energy distribution of these events resembles that of the (γ,pn) reaction, this would only account for about 20% of the group. Finally, the events may be due to the absorption of a low energy photon, forming an excited state of N^{14} which decays, by the emission of a proton, to the ground state, or a low lying excited state of carbon 13. It is believed that reactions of this type produce most of the slow protons which were observed.

If the above interpretation is correct, it is possible to synthesise the cross-section curve for the (γ,p) reaction from the distribution/

distribution in figure 26. Figure 26 shows E_t, the total kinetic energy of all the particles together with the threshold energy of the reaction. This will be equal to the energy of the incident photon only if the residual nucleus is left in its ground state: if the residual nucleus is excited, its energy must be added to the value shown in figure 26 to obtain the photon energy.

To obtain the cross-section, it was assumed that events with E_t greater than 40MeV resulted in the formation of C^{13} in its ground state. The number of events in each box of the histogram of energy E MeV was then subtracted from the distribution at an energy (E - 3.5)MeV. Since it is believed that reactions resulting in the ground state of C^{13} and in its first excited state are equally probable, the distribution obtained in this way represents the cross-section for the formation of C^{13} in its ground state (under radiation from a bremsstrahlung spectrum of peak energy 200MeV). The cross-section curve for the (γ,p) reaction was now obtained by adding the subtracted events to this distribution at an energy 3.5MeV greater than the box from which they were subtracted and correcting the resultant points for the shape of the bremsstrahlung spectrum. For the above processes, a histogram plotted at intervals of 1MeV was employed, and the subtraction and additions were performed by operating with half the events from an interval on the intervals of energy 3MeV and 4MeV less or greater. It was assumed that the energy distribution of the photons in the bremsstrahlung spectrum was given by

$$N(E)\,dE = \frac{k}{E}\,dE$$

and the distribution was corrected accordingly. The resultant cross-

section/

section curve is shown in figure 47.

In the case of the reaction $N^{14}(\gamma,n)N^{15}$, the recoil energy distribution takes a much simpler shape. In Figure 46 it will be seen that the first excited state of nitrogen 13 lies above the threshold for the emission of a proton. If the nitrogen nucleus were formed in this state, and the state de-excited by the emission of a photon, there would be a number of low energy recoils in the distribution. Since these are not observed, it is reasonable to suppose that the formation of the state tends to result in the emission of a proton, and the reaction is then of the (γ,pn) type. No correction is therefore required for the effect of transitions to excited states in nitrogen 13 in a calculation of the cross-section for the (γ,n) reaction.

On the other hand, since the direction of the recoil nucleus is ambiguous, there are two possible values for the energy of the neutron emitted in each reaction. Rather than perform a calculation for each event, it was decided to compute the distribution statistically. It was assumed that the angular distribution of the emitted neutrons was symmetric about 90^{o}, and that the distribution in each box of the histogram was identical with the angular distribution of all the (γ,n) recoils. The overlap of one unit in each energy interval of the histogram into the neighbouring intervals was calculated using the observed angular distribution, and the formula quoted in section 5.5.1. The photon energy corresponding to each of the calculated points was deduced from the equation

$$E_{\gamma} = 14E_r + Q$$

where Q = reaction threshold, 10.5MeV

and/

and the resultant curve was corrected for the shape of the photon spectrum, as for the (γ,p) reaction. The cross-section curve obtained is also shown in figure 47.

In both the above cases, it was not possible to estimate the absolute value of the cross-section for the reactions since no calibration of the synchroton monitor was available. The cross-section for the (γ,n) reaction has been measured up to an energy of about 25MeV (86), and this result is shown in figure 47 by a broken line. The peak cross-section for the (γ,n) reaction from the present experiment has beennormalised to this result.

It should perhaps be indicated that this cross-section curve bears out the interpretation of the low energy (γ,p) events. The integrated cross-section for the (γ,p) reaction below the threshold of the (γ,n) reaction, at 10.5MeV, has been measured (25) and found to be about 2.6MeVmb. The observed cross-section for the emission of a low energy proton is of this order, the energy spread being easily accounted for by the poorness of the resolution in this energy region. The width observed for the giant resonance in the (γ,n) cross-section curve is rather larger than that obtained by the activation technique: this is probably due mainly to comparitively poor energy resolution of the present experiments. This factor becomes much less important at greater energies, where the resolution is better, and the cross-section varies only slowly with energy. In this region, the curves will follow closely the true cross-section for the reaction.

The energy distribution of the recoils from the (γ,p) and (γ,n) reactions in oxygen (figures 36, 40) are rather different from

those/

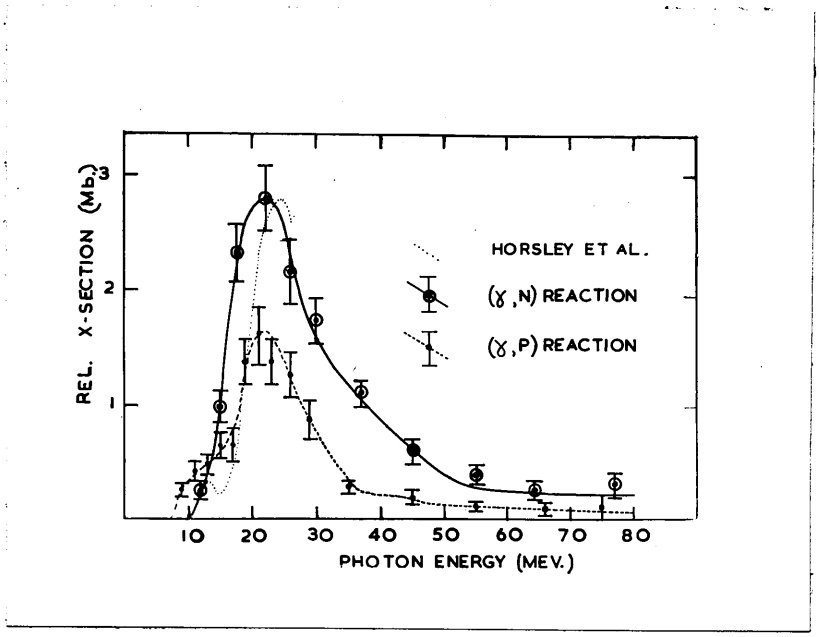

Figure 47

The cross-section for the reactions $N^{14}(\gamma,p)C^{13}$ and $N^{14}(\gamma,n)N^{13}$ as a function of the photon energy.

those obtained in the case of nitrogen. The distributions are much broader, and their peaks occur at lower energies. This is consistent with the disintegration process suggested earlier in this chapter. The absorption of a photon may result in the direct ejection of a nucleon, or in the excitation of a compound nucleus state. In the case of nitrogen, the compound nucleus can decay by the emission of a low energy proton and neutron, but from oxygen, because of the high threshold of the (γ,pn) reaction, only one nucleon will be emitted. Since this type of process favours the emission of low energy fragments, the residual nucleus will often be left in an excited state, and the spectrum of emitted nucleons will contain a corresponding number of slow particles. The recoil energy distribution will therefore be complex in its structure, due to the part played by a large number of compound nucleus levels, in both O^{16} and O^{15} or N^{15}, in the reactions. The energy resolution of the present technique is insufficient to detect the individual groups in the distribution due to the operation of each level. The process is too complex for the cross-section curve to be deduced by a method similar to that used for the (γ,p) reaction in nitrogen.

At greater energies, the excitation energy of the residual nucleus will be small compared with the kinetic energy of the fragments emitted in the reactions. The energy of the photon causing the reactions can then be taken as the sum of the kinetic energies and the threshold energy for the reaction. This quantity is shown in figure 38 for the (γ,p) reaction, and the variation of the relative cross-section

for/

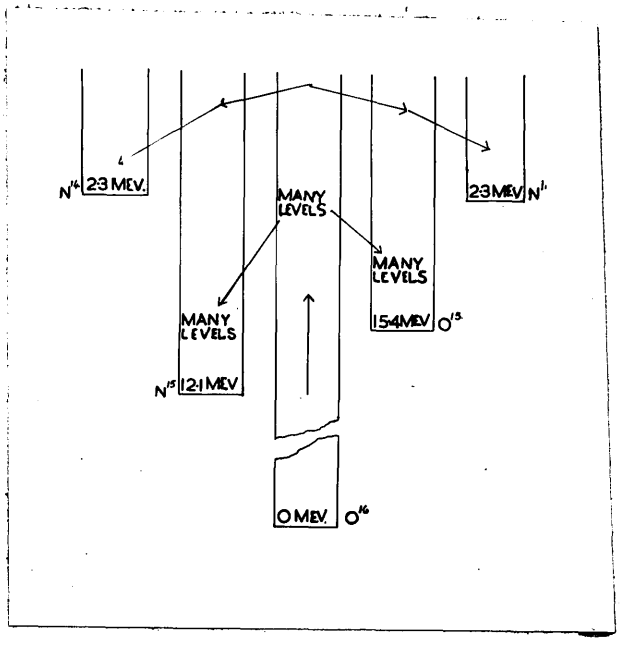

Figure 48

The photo-disintegration of oxygen.

for that reaction with energy is therefore shown in this figure at energies greater than about 30MeV. The relative cross-section curve for the (γ,n) reaction has not been calculated, since in addition to the difficulties mentioned above, there is the complication introduced by the ambiguity in the recoil direction. The curve may be obtained approximately from the recoil energy distribution using the relation

$$E_{\gamma} = 16E_r + 15.6\text{MeV}$$

to calculate the photon energy corresponding to a measured recoil energy, and correcting the result for the shape of the photon spectrum.

6.2.2 Angular Distributions

The observed angular distributions are of the form

$$A + B\sin^2\theta$$

In order to explain the relative number of events, it was suggested that the (γ,p) and (γ,n) reactions in nitrogen were due mainly to the direct emission of a nucleon while in oxygen a number of these events were due to an evaporation process. These processes each lead to certain forms for the angular distributions.

The evaporation of a nucleon can lead to non-isotropic forms of angular distribution, but calculations show that the most probable distribution following an El absorption process in nitrogen or oxygen is, in fact, isotropic (101). The angular distributions of the directly emitted particles is of the form

$$A + B\sin^2\theta$$

where A and B depend on the initial and final states of the nucleons involved/

involved in the reaction (see page 12).

The angular distribution of the directly emitted nucleons can be predicted from considerations of the shell model transitions involved. The ground state configuration of nitrogen 14 can be expressed in shell model notation, as

$$(1S^{1/2})^2(1P^{3/2})^4(1P^{1/2})^1$$

The possible E1 shell model transitions are therefore from the 1P to the 1D or 2S shells, and from the 1S to the 1P shell. These transitions, and the relative strengths of each are shown in table 3.

Table 3

Transition			Square of Overlap Integral	Relative Contribution	Multiplicity	Relative Strength
1P → 2S :	$1+\frac{1}{2}$	$0+\frac{1}{2}$	0.092	2/3	4x2	0.49
	$1-\frac{1}{2}$	$0+\frac{1}{2}$		1/3	1x2	0.06
1P → 1D	$1+\frac{1}{2}$	$2+\frac{1}{2}$	0.38	6/5	4x6	10.9
	$1+\frac{1}{2}$	$2-\frac{1}{2}$		2/15	4x4	0.81
	$1-\frac{1}{2}$	$2-\frac{1}{2}$		2/3	1x4	1.01
1S → 1P :	$0+\frac{1}{2}$	$1+\frac{1}{2}$	0.28	2/3	2x0	0.00
	$0+\frac{1}{2}$	$1-\frac{1}{2}$		1/3	2x1	0.19

The square of the overlap integral (D), and the relative contribution of each transition are taken from the tables published by Wilkinson; the/

the multiplicity was calculated as the product of the number of nucleons in each initial state and the number of possible final states. The relative strength of each transition was then computed as the product of D, the relative contribution and the multiplicity of the transition.

The angular distribution of directly emitted nucleons following one of these transitions can be calculated from the relations published by Courant (see page 12). These are shown in table 4:

Table 4

Transition	Form of Distribution $A + B\sin^2\theta$
1P → 2S	$2 + 0\sin^2\theta$
1P → 1D	$2 + 3\sin^2\theta$
1S → 2P	$0 + 1\sin^2\theta$

The angular distribution of all nucleons directly emitted from nitrogen will be given by the sum of the individual distributions, weighted according to the relative strengths of each transition :

$$2 \times 0.55 + (2 + 3\sin^2\theta) \times 12.72 + \sin^2\theta \times 0.19$$

$$\text{i.e. } 26.5 + 38.4\sin^2\theta \text{ or } 2 + 3\sin^2\theta$$

In the case of oxygen, the ground state configuration of

the/

the nucleons is

$$(1S^{1/2})^2(1P^{3/2})^4(1P^{1/2})^2$$

and the above arguments will therefore apply equally to oxygen, with the exception of the transitions involving the $1P^{1/2}$ states. The strength of the transitions of nucleons in these states will be doubled, and the $1S \rightarrow 1P$ transition will no longer be allowed, since the 1P shell is filled in oxygen. This leads to a distribution of the form

$$2 \times 0.61 + (2+3\sin^2\theta) \times 13.83$$

$$\text{i.e. } 29.9 + 41.5\sin^2\theta, \quad \text{or} \quad 2 + 3\sin^2\theta$$

The observed angular distributions are all of the form

$$A + B\sin^2\theta, \qquad \text{where} \quad \frac{B}{A} = 1 \pm .2$$

The discrepancy between this result and the predicted value indicates that the distribution must include a number of evaporated nucleons. If the distribution of such nucleons is isotropic, then the results indicate a ratio of direct to evaporated particles of $2 \pm .4 : 1$, in the single nucleon reactions.

The photo-nuclear process has been described as the absorption of a photon by a nucleon in the nucleus, followed by the direct emission of that nucleon, or by the formation of a compound nucleus state in which all the energy of the photon is shared among all the nucleons. The relative probability of the processes can be estimated from the present measurements. Assuming that all the observed (γ,pn) events were due to an evaporated process, the ratio of direct photo-disintegrations to reactions of the evaporation type

is/

is 0.7 ± 0.14 in nitrogen, and 0.8 ± 0.2 in oxygen.

Wilkinson has estimated this ratio, using a description of the photo-nuclear process similar to that mentioned above (63, see page 16):

$$C = \frac{2kP\ (\hbar^2/mR)}{2W}$$ with the significance of the symbols as on page 16.

If W is taken as 8MeV, and R is assumed to be given by the equation

$$R = 1.2A^{1/3},$$

this expression reduces to

$$C = 1.1P.$$

The values of P for protons with $L = 0$ and $L = 2$ are about 0.8 and 0.4 respectively and the corresponding figures for neutrons will be larger, on account of the lack of the coulomb barrier. Thus, since D-wave emission accounts for most of the photo-nuclear cross-section, the ratio of direct to evaporation processes is of the order of 0.6. The agreement with the experimental value is good, in view of the fact that the theoretical figure is little better than an order of magnitude guess at the true ratio.

The description of the process is further confirmed by the angular distributions in different energy regions. For nitrogen, the distribution of the low energy protons is isotropic, that of the protons of energy between 12MeV and 20MeV fits a curve of the form

$$8 + 12 \sin^2\theta$$

and the energetic protons, of energy greater than 20MeV, fit a distribution/

distribution of the form

$$\sin^2\theta.$$

The first group includes the low energy protons, and will be mainly due to an evaporation process, giving an isotropic distribution. The second group includes many of the giant resonance transitions, and will be due mainly to the direct emission of a proton from the D-shell (table 3), leading to a distribution of the form

$$2 + 3\sin^2\theta$$

which is observed. The angular distribution of the fast protons indicates that the transition of the type $1S \rightarrow 1P$ must be largely responsible for these events.

In the case of the (γ,n) reaction in nitrogen, the low energy distribution is of the form

$$1 + \sin^2\theta$$

which indicates that a number of the transitions are due to an evaporation process. The giant resonance group again gives a distribution of the form

$$2 + 3\sin^2\theta$$

and the angular distribution of the fast neutrons fits a curve of the form

$$\sin^2\theta.$$

This indicates the similarity of the (γ,p) and (γ,n) reaction in nitrogen. The fact that the evaporation process does not dominate the low energy group of neutrons is probably due to the proximity of the/

the (γ,pn) and (γ,n) thresholds, but this does not affect the general argument.

In oxygen, the statistics were not sufficiently good to justify plotting the angular distributions of different energy groups of protons. This fact in itself is worthy of some comment: in nitrogen, about 10% of the (γ,p) reactions could be attributed to an interaction by a photon of energy greater than 30MeV, but in oxygen, out of 150 (γ,p) events, only 4 are due to energetic photons.

In the case of the (γ,n) reaction, the position is slightly better, and it was possible to plot the distributions of neutrons of energy less and greater than 0.7MeV. The low energy distribution is of the form

$$23 + 22\sin^2\theta$$

which, since the predominant transition is that from the 1P to the 1D shell, indicates a large percentage of reactions due to an evaporation process. The distribution of energetic recoils, on the other hand is almost isotropic, being of the form

$$11 + 5\sin^2\theta.$$

This is again consistent with the picture presented by the shell model of the photo-disintegration process: in the case of nitrogen, the transition from the 1S to the 1P shell accounted for the high energy particles, but in oxygen, this transition is not possible, and the contribution of high energy reactions to the (γ,p) and (γ,n) cross-section is therefore much smaller, and the angular distributions no longer show the strong anisotropy associated with the direct emission of nucleons following transitions from the 1S to the 1P shell.

So/

So far, the above discussion has been confined to E1 interactions of radiation with nuclear matter. In the case of the distributions of energetic nucleons from nitrogen, there is some evidence of asymetry about 90^{o}. This can be explained by a small percentage of E2 absorption. The distribution of the energetic protons has been fitted with the curve

$$9.2 \sin^2\theta,$$

but agrees better with a curve of the form

$$9.2 \sin^2\theta \, (1 + 0.35\cos\theta)^2$$

which is shown in figure 28 by the dotted curve. This distribution can be accounted for by the interference of emission from about 2.5% quadrupole transitions with the dipole reactions (see page 16).

Thus the angular distributions of the nucleons from nitrogen and oxygen are consistent with the shell model description of the photo-nuclear process. The form of the total distributions confirms the arguments regarding direct and evaporation processes of disintegration which were advanced to explain the relative number of events in nitrogen and oxygen. The ratio of reactions of the direct and evaporation type is in good agreement with the value predicted by Wilkinson. The angular distributions of nucleons of different energies indicate the mechanisms responsible for each energy group: the low energy nucleons can largely be accounted for by the evaporation process, the direct emission of a nucleon following a transition of the type $1P \rightarrow 1D$ accounts for the giant resonance. At greater energies, in nitrogen, transitions from the 1S to the 1P shell are important but in oxygen, these transitions are

not/

not possible, and the relative cross-section for the emission of a fast nucleon is smaller: the distribution of the energetic neutrons is almost isotropic.

6.3 The Photo-production of Two Nucleons

6.3.1 General

The emission by a nucleus of two nucleons can usefully be envisaged in three ways :

(1) The process may take place in three stages: an initial interaction of a photon with one nucleon, followed by the sharing by that nucleon of its energy with the remainder of the nucleus. This leads to the formation of a compound nucleus state: if the excitation energy of the state is sufficient, it may de-excite by the evaporation of two fragments.

(2) The reaction may be a two stage process: the initial interaction of a photon with a single nucleon, followed by a collision between two nucleons. The kinetics of the collision may be such that both nucleons then have sufficient energy to escape from the nucleus. This is sometimes known as a "knock-on" process and is, in fact, a special case of the first type of process.

(3) The reaction may occur in a single stage: Levinger has described the photo-nuclear process at high energies in terms of the quasi-deuteron model. The photon is regarded as interacting with a small sub-unit of the nucleus, consisting of a proton and neutron.

The/

The photon shatters this unit, and both particles are ejected directly without further interaction- the remainder of the nucleus merely acts as a spectator to the process.

The evaporation and knock-on processes will lead to a form of the cross-section curve resembling that observed for the single nucleon reactions, since the interaction of the photon is similar. The detailed shape of the curve will be determined by the probability of each process relative to the direct emission of a nucleon, and by the threshold for the (γ,pn) reaction. This matter has been considered in the discussion of the Relative Importance of Reactions, and it was indicated that the results were in general agreement with the hypothesis (see section 6.1). The discussion dealt with the evaporation process, but the arguments will apply equally to the knock-on process. A more detailed determination of the reaction cross-section from the experimental data is not possible, since, in general, the protons from the disintegration left the sensitive volume of the cloud chamber. In the case of nitrogen, some 30 events involved the emission of a slow proton which remained within the chamber - the results relating to these events will be discussed at a later stage, and it will be shown that they lead to a cross section curve of the expected shape.

6.3.2 Recoil Energy Distribution

From a statistical stand-point, it is reasonable to suppose that the momentum distribution of the protons neutrons and recoils are identical, if the process is of the evaporation type. The most probable recoil momentum corresponds to an energy of about 0.4MeV, in the case of nitrogen/

nitrogen (figure 33), and leads to a value of about 5MeV for the most probable nucleon energy. Thus the most probable value for the total kinetic energy of the emitted fragments is $\sim$10.4MeV, and this corresponds to a photon energy of 23MeV, which is close to the value obtained for the peak in the cross-section for the (γ,p) and (γ,n) reactions in nitrogen. In the case of oxygen, the energy distribution of the recoils from the (γ,pn) reaction (figure 43) contains a large number of low energy events, and an accurate estimate of the energy of the peak in the distribution is therefore difficult, but it can be said that the most probable photon energy will be of the order of a few MeV. The recoil energy distributions are thus consistent with the evaporation picture of the (γ,pn) reaction.

The knock-on process will be expected, in the first instance, to lead to a distribution of the same form as the recoil energy distributions of single nucleon reactions. This will be modified slightly by the knocking out of the second nucleon- the recoil nucleus acts as a spectator in this process, and the effect of the removal of the nucleon will be the subtraction of the momentum in the nucleus of that nucleon from the recoil momentum. This means that the peak in the energy distribution will lie at a lower energy, as is observed.

6.2.3 Angular Distribution

The angular distribution of the protons and recoils from (γ,pn) reactions are, within the statistical limits, identical, and are almost isotropic. The assumption of a statistical mode of emission leads/

leads to a similar treatment for the proton and recoil and therefore predicts similar distributions. The formation of a compound nucleus implies the creation of a relatively long lived entity, which "forgets" the manner in which it was created - this means that there should be no preferred direction, and that the angular distribution of the emitted fragments with respect to any direction in the centre of mass system should be isotropic, as is observed. The knock-on picture of the process will also tend to give an isotropic distribution, since the angular distribution of the direct protons and neutrons will be "smeared out" by their interaction with the second nucleon. The distribution will depend on the direction of the primary particle, the impact parameter, and the momentum state of the secondary particle before the interaction. The competition of these effects will probably lead to an isotropic distribution.

The angular distribution of the emitted protons with respect to the recoils from the (γ,pn) reactions shows a marked preference for angles greater than 90^{o} (figures 35, 45). The distribution to be expected from the evaporation of one nucleon followed by a second can be calculated for any value of the ratio of the momenta of the emitted particles, if it is assumed that the neutrons are isotropically distributed with respect to the protons. Some typical distributions (not normalised) are shown in figure 49. It will be seen that, if all values of the ratio of the momenta are equally probable, the sum of distributions/

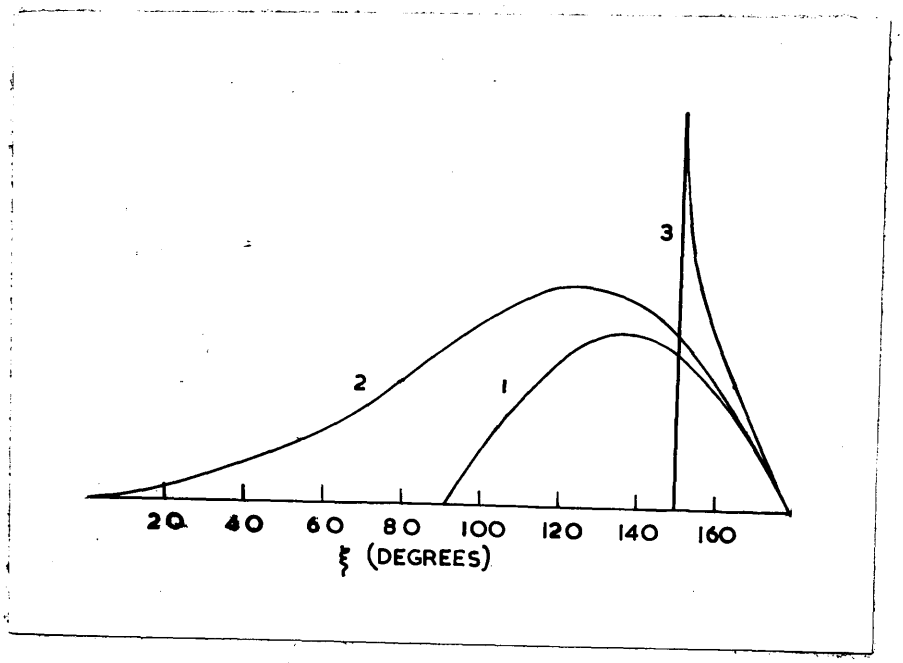

Figure 49

Forms of the angular distribution of the angle between the proton and recoil from (γ,pn) reactions which might be predicted by a statistical model.

(1) This curve is calculated for the emission of a proton and neutron of equal momentum

(2) This is calculated for the emission of a neutron with 10x momentum of the emitted proton.

(3) This is calculated for the emission of a neutron with 1/10 of the momentum of the emitted proton.

distributions of this type would lead to a result similar to that obtained in the present experiment. In fact, the process will tend further to favour the angles greater than 90^{o}, since the momentum ratios leading to angles less than 90^{o} involve the emission of a slow proton and a fast neutron, which will be rather less probable than the emission of a fast proton and a slow neutron because of the effect of the coulomb barrier.

The knock-on process will also strongly favour angles greater than 90^{o}. An angle less than 90^{o} in this picture of the process requires that the secondary nucleon has an energy greater than the primary particle. This is improbable, since the primary nucleon has sufficient energy to escape from the nucleus, while the secondary nucleon is in a bound state.

The events involving an angle less than 90^{o} might possibly be explained by some other mechanism, such as the quasi-deuteron process. The quasi-deuteron model assumes that a close proton neutron conjugation can exist in the nucleus for a relatively long time. The (γ,pn) interaction is then regarded as an interaction between the incident photon and such a pair of nucleons, resulting in the direct emission of both from the nucleus. Since the remainder of the nucleus takes no part in the interaction, the energy and direction of the recoil nucleus will depend only on the state of the quasi-deuteron just before the interaction. The model therefore predicts that all the angular distributions of the recoil nuclei will be isotropic (i.e. that the observed distribution will be of a form proportional to $\sin\theta$) and that the momentum distribution of the recoils will indicate the state of

the/

the quasi-deuterons in the nucleus. It has already been indicated that a number of the stars could be accounted for by a process of this type. Other work (100) has shown that of the events resulting in the emission of a proton of energy about 100MeV from nitrogen 70% are stars, and 30% are due to (γ,pn) reactions - at this energy, the process can largely be accounted for by the quasi-deuteron model. If all the 4-pronged stars observed in nitrogen are due to reactions of the quasi-deuteron type, then the number of (γ,pn) events to be attributed to this type of process will be $\sim$100. An isotropic distribution of 100 events is shown in figure 35 - the curve is proportional to sinθ, since this distribution shows the observed number of protons per 10° interval. It will be seen that this will account for a large number of the events resulting in an angle less than 90°, and in view of the crudity of the calculation, the agreement is remarkable. In the case of oxygen it was not possible to identify the observed stars, and a similar comparison would therefore be valueless. From an examination of the angular distribution of the protons with respect to the recoils, an upper limit of about 50 was set to the number of quasi-deuteron transitions, and the curve in figure 45 shows an isotropic distribution of 50 events: the agreement with the observed distribution at angles less than 90° is again good. If this in fact represents the number of quasi-deuteron reactions in oxygen, then the percentage of such processes (about 30%) is considerably greater than the value estimated for nitrogen (10%). This discrepancy can easily be accounted for by the relatively high threshold of the (γ,pn) reaction in oxygen, which will suppress the evaporation/

evaporation part of the (γ,pn) cross-section. The quasi-deuteron model is therefore capable of accounting for some of the features of the (γ,pn) reaction, but is in fact not applicable to most of the events observed, since the energy of the photon involved is small, and an interaction with a single nucleon is then much more probable.

6.3.4 Reactions Involving the Emission of a Slow Proton

Thirty events were observed from which the proton did not leave the sensitive volume of the cloud chamber, and the distributions referring to these events have some interesting features. The distribution of the sum of the total kinetic energy of the reaction products and the threshold energy for the reaction (figure32a) exhibits peaks at 18MeV and 23MeV. The statistics are naturally poor, but taking the distribution as it stands, the peaks can be accounted for as being due to giant resonance transitions resulting in the formation of carbon 12 in an excited state (some 5MeV above the ground state) and in its ground state respectively. If this interpretation is correct, the distribution indicates an energy for the peak in the cross-section curve which is consistent with the results of the single nucleon reactions and earlier arguments in this section.

The angular distributions of the protons from these events (figure 32b, and c) are similar in form to the distributions obtained from all the (γ,pn) events, but the statistics are much poorer. In the case of the distribution of the angle between the proton and recoil, there is some indication of a slight difference from the more general distribution. The peak of the distribution occurs at about 120^{o},

instead/

instead of 145°. These events will be mainly due to reactions resulting in the emission of a neutron of energy much greater than that of the proton and the distribution should therefore resemble curve 2 in figure 49, which shows the distribution expected for a fast neutron and a slow proton from the evaporation model. The peak of this curve is at 120°, in good agreement with the experimental value.

6.3.5. Summary

The results obtained from measurements of the (γ,pn) reaction in nitrogen and oxygen are consistent with two types of process - the evaporation of two nucleons, or a special case of the first type of process, the sharing by collision of the energy of the incident photon between two nucleons which both escape from the nucleus. The results for events from which the protons do not leave the chamber seem to favour the former process. The cross-section for the reaction appears to vary with energy in a manner rather similar to the variation of the cross-sections for the single nucleon reactions, and this is confirmed,if the process is of the evaporation type, by the energy distribution of the recoils from the events attributed to the (γ,pn) reaction, and in any case by the energy calculated from the distribution associated with events from which the proton did not leave the chamber. The quasi-deuteron model might account for about 10% of the observed events in nitrogen, and 30% in oxygen and the observed angular distribution is consistent with a number of quasi-deuteron type events estimated from measurements

of/

of high energy protons in the case of nitrogen. It therefore appears that the (γ,pn) reaction is due to an evaporation process at low energies, or possibly a knock-on type of reaction, and that the quasi-deuteron model can account for the reaction at greater energies. The results give no indication of the energy at which the second type of process becomes important, but the results would be consistent with a value of several tens of MeV, as suggested by Wilkinson (63).

6.4 Conclusion

In the introduction to this thesis, several models for the photo-disintegration process were discussed, and it was indicated that the properties of the giant resonance in medium and heavy nuclei could be accounted for by two models, the collective model and the shell model. In the case of light nuclei, the disintegration process tends to involve a single nucleon, rather than the nucleus as a whole, and the shell model is therefore better equipped to describe the process. The collective model can account for the properties of nuclear matter in mass, but fails to describe the behaviour of a single nucleon in detail.

The results of the experiments described in this thesis indicate that the photo-nuclear process in light nuclei can be described well by the shell model, in the region of its applicability. The photo-process is regarded as occurring in three stages: the initial absorption of a photon and the formation of a compound state, secondly the formation of the compound nucleus state, and finally the decay of this state by the emission of one or more particles.

In/

In the first stage, the interaction of the photon is with a single nucleon in a shell model state. The nucleon is excited into a higher shell model state, and may be emitted directly, without further interaction. This state can be regarded as a compound system, consisting of the core of nucleons, compounded with a nucleon in an orbit. The interactions of the nucleon are described by cloudy crystal ball wave potentials (see page 13 of Introduction), and this leads to a value for the relative probability of a nucleon escaping without further interaction. The observed angular distributions indicate that, in nitrogen and oxygen, the experimental value for this quantity is in good agreement with the figure estimated by Wilkinson, and the distributions are consistent with the predictions of the model.

If the nucleon does not escape, it will interact with the remainder of the nucleus. This interaction may take the form of a collision with a second nucleon which results in the sharing of the energy, and the emission of both nucleons. It has been shown that the results obtained for the (γ,pn) reaction can be accounted for by a process of this type. Eventually, if no particles escape, the energy of the incident photon will be shared among all the nucleons, forming a compound nucleus state. In this state, the nucleons will take some form of collective motion, and the collective model might describe the system. This state would be attained rapidly in a heavy nucleus, where there are a large number of nucleons, and the chance of a particle escaping without interaction is small. On the other hand,/

hand, in light nuclei it has been shown that the relative probability of direct emission is large, and the collective model will therefore fail to describe the photo-nuclear process.

The compound nucleus state has a fairly long life, and therefore has no memory of the manner in which it was created. Eventually, the third stage of the photo-nuclear process is reached, and a particle, in the course of its random movement in the nucleus, obtains sufficient energy to "boil off" from the nuclear surface. This method of decay has two consequences: because of the long life of the compound nucleus state, the angular distribution of the emitted particles will tend to be isotropic with respect to any direction fixed in the centre of mass system, and the evaporation method of decay will favour the emission of low energy fragments. The experimental measurements for the (γ,p), (γ,n) and (γ,pn) reactions are consistent with both these predictions. Furthermore, if the excitation energy is sufficient, the description would suggest that the emission of two low energy fragments would be preferred rather than the emission of a single energetic particle, and the experimental measurements again appear to bear this out.

At greater energies, the disintegration of the nucleus becomes more complex, involving in a large number of cases the emission of several charged fragments. In this energy region, the precise analysis of the reaction characteristics was not attempted, since the reactions generally resulted in the emission of some particles which did not remain within the confines of the cloud chamber, and could not therefore/

therefore be measured. From the number of events observed, however, it was deduced that the cross-sections for the reactions was appreciable, and it was suggested that they might be due either to a cascade process commencing with the emission of an α-particle, or to a reaction of the quasi-deuteron type.

Other workers have measured the relative number of (γ,pn) events and stars resulting in the emission of a 100MeV proton from nitrogen. From a comparison of their result with the present work, it was estimated that about 10% of the observed (γ,pn) events in nitrogen were due to a reaction of the quasi-deuteron type. A corresponding figure of 30% was suggested for oxygen, and both these figures are consistent with the measured angular distributions.

In the case of nitrogen, it was found possible to calculate the relative cross-sections for the (γ,p) and (γ,n) reactions from the energy distributions of the recoils from these reactions. These curves are shown in figure 47. The results are normalised to the peak value of the (γ,n) cross-section obtained by an activation technique.

The results obtained in the experiments described in this thesis may be summed up briefly as follows :-

(1) In the disintegration of nitrogen and oxygen, three reactions are responsible for the photo-nuclear cross-section in the energy region of the giant resonance - the (γ,p), (γ,n) and (γ,pn) reactions. The cross-sections for the reactions $N^{14}(\gamma,p)C^{13}$ and $N^{14}(\gamma,n)N^{13}$ are shown/

shown in figure 47.

(2) At greater energies, the cross-section for the emission of several fragments becomes appreciable. The results indicate that this rise in the cross-section is due in part to the fact that as the excitation energy increases, isotopic spin selection rules cease to forbid the emission of α-particles. Other reactions in this energy region may be accounted for by the quasi-deuteron model.

(3) The photo-nuclear process in light nuclei is satisfactorily described by the shell model. The predictions of the shell model regarding the angular distributions of the emitted nucleons, and the relative number of direct and evaporation reactions are all in good agreement with the experimental results. The results for the (γ,pn) reaction are also consistent with this description of the process, but it was not found possible to determine the parts played by the evaporation and knock-on processes in the reaction. The results from events involving the emission of a slow proton seemed to favour the evaporation description, but the statistics of these distributions are not sufficiently good to be beyond all doubt.

APPENDIX

APPENDIX 1: RANGE ENERGY RELATIONS FOR RECOIL NUCLEI

In the experiments described in this thesis, the characteristics of several reactions were studied in terms of measurements of the recoil nuclei from them. It was therefore necessary to derive range energy relations for these nuclei in the energy range 0 - 10MeV under the conditions in which they were observed. Little work has been published on this subject: the experimental data is listed in the following section, and in the second section, several methods of deriving relations are discussed.

A. 1. Experimental Results

(1) Boron: In the course of an investigation of the reaction $N^{14}(n, \alpha)B^{11}$ in a cloud chamber, it was found possible to derive a range energy relation for the boron recoils, up to an energy of about 7MeV, which correspond to a range of 11mm in air at STP (102).

(2) Carbon: The range of carbon 12 recoils has been studied in a cloud chamber by measurements of elastic collisions with α-particles (103, 104). Some difference was detected between relations derived from measurements of recoils in light and heavy gases (104).

The range-energy relations for C^{13} have also been measured by the technique used in the study of Boron - in this case, the recoils from the reaction $O^{16}(n,\alpha)C^{13}$ were measured (102).

(3) Nitrogen: The range energy relations for nitrogen in air at STP have been derived by a study of elastic collisions with α-particles (105).

(4) Oxygen:/

(4) Oxygen: Relations referring to oxygen nuclei have been obtained, again by the elastic collision technique (105).

(5) Fluorine: Range energy relations for fluorine 19 recoils have been obtained by a study of the elastic collisions of α-particle in a helium - carbon tetra-fluoroide mixture (103). The results were reduced to equivalent air ranges.

(6) Neon: The relations for neon nuclei have been dervied, again by a study of the elastic collisions of α-particles (110).

These results are satisfactory as far as they go. Lillie's results provide useful relations for boron and carbon, but for other nuclei, the experimental data extends only to energies of a few MeV, which was not high enough for the experiments which were undertaken. Possible theoretical methods of calculating the relations, or of extending the existing relations were therefore studied. The experimental results are detailed in table A1, at the end of this appendix.

A.2 Theoretical Approaches

The theoretical approaches are based on the assumption that a relation of the form

$$-\frac{dE}{dX} = Z_e^2 F(v) \qquad (1)$$

where Z_e is the effective charge of the ion, and

F(v) is a simple function of the ion velocity,

generally assumed to be given by

$$F(v) = kv^{-n}, \text{ where K is a constant}$$

The problem is then reduced to that of estimating n and the effective charge on the ion.

The/

The effective charge of an ion at low velocities is not a constant, but is constantly altering as electrons are captured, or escape from their orbits. In calculations, it is usual to assume that an electron will be captured if the ion velocity is less than the velocity of the electron in its orbit, and more precisely, that the ratio of the electron orbital velocity to the ion velocity at which capture occurs is constant. This has been used to derive range energy relations for recoil nuclei (106). The results agreed reasonably at low energies with the experimental data then available, but at greater energies, the range of an ion is badly underestimated, and the results obtained disagree with the relations obtained by Lillie for carbon and boron.

Livesey (107) derived relations for light nuclei (Z less than 10) from the range energy relations for protons and α-particles. He used the formula in equation 1, and chose a value of n of 1.34, which he derived from a study of the published data. The effective charge of the nuclei was calculated from considerations of the velocity of the electrons in their orbits. His results agree reasonably with the low energy data, but again, as the energy of the ion increases, the agreement worsens.

The most recent work in this field is that of Papineau (99). He calculates the range of ions of energy 10MeV to 200MeV in air and several other media. His method is based on the equation

$$R_m(E) = \frac{M}{M} \left(\frac{Z}{Z_o} \right)^2 \quad R_{m_o} \left(\frac{M}{M} oE \right) \qquad (2)$$

This equation holds for protons and α-particles, under conditions

when/

when the particles are completely stripped of their electrons, and it is therefore reasonable to expect that the equation will still hold for heavy ions, if the range intervals are sufficiently short for the average charge to be regarded as a constant. Papineau plots the ratio of the effective charge to the maximum possible charge for the ion (Z) against the ion velocity divided by $Z^{2/3}$ for nitrogen oxygen and neon, and shows that the results all lie close to one curve. He therefore assumes that this curve may be taken as a measure of the effective charge on every ion with Z between 2 and 10. The range energy relations for these nuclei were then calculated from relations for α-particles, using the values for the effective charges of these particles published by Allison and Warshaw (108). The results agreed well with the publisheddata for energetic ions, but Papineau's curves could not be extrapolated to cover the energy range required in the present experiments (0 - 10MeV). His method was therefore applied to the calculation of the curves in that range, but it was found that the results did not agree well with the data for boron and carbon published by Lillie. It was therefore decided to investigate the method further in an attempt to achieve agreement.

A.3. The Calculation of the Range Energy Relations

Experimental relations are available for the nuclei boron 11, carbon 12, carbon 13, nitrogen 14, oxygen 16, fluorine 19, and neon 20. These relations were used to calculate the effective charge on each ion as/

as a function of its velocity, using equation (2), and the results were plotted in a manner similar to that employed by Papineau: the curve obtained differed slightly from that of Papineau in the energy region considered (see figure A1). The range energy curves for slow protons and α-particles published by Bethe (109), and the proton charge velocity relations of Allison and Warshaw, (108), together with their values for the charge on α-particles, as far as they went, and thereafter, the values of Papineau for the α-particles charge were used. (99). It will be seen that the calculated values all lie near a smooth curve, and it was assumed that this curve could be used to obtain the effective charge on ions.

The range energy relations for the required nuclei were now calculated. Papineau's method was used to estimate the change in range for each energy interval: in table A3, the calculated values are compared with the experimental results, and it will be seen that the agreement improves as the energy increases. The calculated intervals were therefore used to extrapolate the experimental curves over the required energy range. The agreement obtained in this way with the experimental results of Lillie is good, and the curves (figure A2) derived were used in the experiments on the disintegration of nitrogen and oxygen described in chapters 5 and 6 of this thesis.

EXPERIMENTAL DATA

Table A1

Proton (109

Range (cm)	0.1	0.2	0.3	0.4	0.6	0.8	1.0	0.2	1.4	1.6	1.8	2.0	2.2	2.4	2.6	2.8	3.0
Energy (MeV)		.135	.205	.275	.394	.50	.58	.66	.73	.80	.86	.92	.98	1.03	1.08	1.14	1.19

α-particle (109

Range (cm)	0.05	0.1	0.15	0.2	0.3	0.4	0.5	0.6	0.7	0.8	0.9	1.0	1.2	1.4	1.6	1.8	2.0
Energy (MeV)	.05	.11	.18	.28	.51	.75	.99	1.21	1.43	1.63	1.82	2.00	2.34	2.65	2.93	3.20	3.45

Boron 11 (102)

Range (cm)	0.1	0.2	0.3	0.4	0.5	0.6	0.7	0.8	0.9	1.0	1.1
Energy (MeV)	0.3	0.8	1.3	1.95	2.7	3.4	4.0	4.7	5.4	6.2	6.8

Carbon 12 (103, 104)

Range (cm)	0.1	0.2	0.3	0.4	0.5	0.6	
Energy (MeV)	-	0.97	1.63	2.39	3.14	3.78	- Feather
	0.25	0.71	1.47	2.19	2.88	3.45)	
	0.25	0.83	-	2.47	3.54	5.19)	- Wrenshall

Carbon 13 (102)/

Table A1 (contd)

Carbon 13 (102)

Range (cm)	0.1	0.2	0.3	0.4	0.5	0.6	0.7	0.8	0.9	1.0	1.1
Energy (MeV)	0.2	0.65	1.2	1.9	2.7	3.4	4.2	5.0	5.8	6.6	7.1

Nitrogen 14 (105

Range (mm)	0.5	1.28	2.10	2.92	3.72	4.54	5.35
Energy (MeV)	0.07	0.29	0.65	1.16	1.81	2.61	3.55

Oxygen 16 (105)

Range (mm)	0.5	1.40	2.30	3.17	4.07	4.94	5.8
Energy (MeV)	0.08	0.33	0.75	1.32	2.06	2.98	4.0

Fluorine 19 (103)

Range (cm)	0.1	0.2	0.3	0.4	0.5	0.6
Energy (MeV)	0.17	0.52	1.07	1.74	2.65	3.65

Neon 20 (110)

Range (cm)	0.05	0.10	0.65	0.20	0.25	0.30	0.35	0.40	0.45	0.50	0.55	0.60	0.65	0.70
Energy (MeV)	0.08	0.22	0.33	0.52	0.62	0.87	1.02	1.39	1.61	1.98	2.34	2.72	3.12	3.54

Table A2 Effective charges of particles, as a function of their energy.

Proton (108)

Energy (keV)	20	30	40	50	60	70	80	90	100	110	120	130
Eff.charge (exp.)	.404	.500	.545									
(theor.)	.	.530	.582	.643	.674	.723	.764	.800	.831	.860	.883	.902

α-particle (108)

Energy (keV)	100	120	140	160	180	200	220	240	260	280	300	320	340	360	380	400	420
φ_1	50	43	38	34	28	26	23	21	19	17	15	14	13	12	11	95	8
φ_2	50	57	62	66	69	71	73	74	75	75	76	75	74	73	72	71	70
φ_3					2.5	3	3.5	5	6.5	8	9.5	11	13	15	17	19	21

	440	460	480
φ_1	7	6.5	5.5
φ_2	69	68	66
φ_3	24	26	29

φ_i is the percentage of ions with charge i.

Table A2 (contd) Values of the effective charge on ions calculated from Range-energy relations in table A1.

E/A		.025	.05	.10	.15	.20	.25	.30	.35	.40	.45	.50
q_{eff} proton		.50	.63	.83	.94	1.00	1.00					
α		.50	.77	1.33	1.4	1.6	1.8	1.82	1.91	1.92	1.92	1.93
B^{11}	0.6	1.4	2.1	2.6	3.1	3.3	3.3	3.4	3.5	3.7	3.8	
	0.6	1.08	1.88	2.1	2.6	3.0	3.2	3.3	3.5	3.6	3.9	
C^{12}	0.6	1.7	2.2	2.6	3.0	3.2	3.3	3.4				
	0.4	1.3	1.8	2.4	2.6	3.0	3.2	3.5				
C^{13}	0.5	2.1	2.2	2.5	3.0	3.4	3.4	3.6	3.8	4.0	4.2	
	0.4	1.2	1.7	2.3	2.7	3.2	3.3	3.7	3.8	3.9	4.3	
N^{14}	0.6	1.5	2.3	2.9	3.6	4.3	4.2					
	0.4	1.2	1.8	2.6	3.1	4.3	4.5					
O^{16}	0.6	1.6	2.2	2.8	3.9	4.3	4.1					
	0.4	1.3	1.8	2.7	3.2	4.0	4.1					
F^{19}	0.6	1.5	2.2	3.0	3.7							
	0.4	1.2	1.7	2.8	3.2							
Ne^{20}	0.6	1.3	2.1	2.8	3.2							
	0.4	0.8	1.7	2.5	2.7							

In each case, 1st figure is calculated from the proton range and charge, and 2nd from α-particle data.

E/A	.55	.60	.65
$q_{eff.proton}$	1.94	1.95	1.96
B^{11}	4.2	4.5	4.9
(cont)	4.2	4.2	4.8
C^{12}			
C^{13}	4.5	4.8	
(cont)	4.5	4.5	

Table A3 Calculated Range-energy relations for Boron, Carbon, Nitrogen & Oxygen. For Boron and Carbon, the calculated ranges (R_c) are compared with Lillie's results (R_m) and for nitrogen and oxygen, the low energy experimental results are extrapolated using Papineau's method.

Proton	Energy	.025	.05	.10	.15	.20	.25	.30	.35	.40	.45	.50	.55	.60	.65
	Range	.062	.094	.158	.222	.294	.366	.440	.522	.612	.706	.808	.920	1.05	1.18
	Δ R	.032	.064	.064	.072	.072	.074	.082	.090	.094	.102	.112	.128	.130	
	Mean q	.25	.57	.73	.89	.97	1.00	1.00	1.00	1.00	1.00	1.00	1.00	1.00	1.00
Boron 11	Mean q	.5	1.2	1.85	2.34	2.70	2.94	3.17	3.33	3.50	3.67	3.80	3.94	4.03	4.13
	Δ R	.17	.079	.110	.102	.103	.092	.081	.082	.081	.077	.078	.079	.086	.084
	R_c		.174	.270	.352	.453	.522	.591	.673	.754	.831	.909	.988	1.074	1.158
	R_m	.095	.16	.25	.35	.43	.51	.59	.675	.755	.835	.91	.98		
	E(MeV)	.28	.55	1.10	1.65	2.20	2.75	3.30	3.85	4.40	4.95	5.50	6.05	6.60	7.15
Carbon 12	Mean q	.48	1.32	2.00	2.62	3.06	3.30	3.48	3.78	3.96	4.13	4.27	4.44	4.56	4.68
	Δ R	.202	.090	.103	.089	.087	.079	.069	.069	.069	.066	.067	.068	.074	.071
	R_c		.226	.302	.375	.461	.534	.601	.670	.739	.805	.872	.940	1.014	1.085
	R_m	.136	.199	.286	.374	.455	.532	.613	.688	.761	.836	.902	.970	1.040	
	E	.30	.60	1.20	1.80	2.40	3.00	3.60	4.20	4.80	5.40	6.00	6.60	7.20	7.80
Carbon 13	R_m	.147	.215	.310	.405	.493	.577	.663	.744	.824	.905	.978	1.049	1.123	
	E	.33	.65	1.30	1.95	2.60	3.25	3.90	4.55	5.20	5.85	6.50	7.15	7.80	8.45
Nitrogen 14	q	.46	1.34	2.09	2.80	3.22	3.61	3.85	4.10	4.33	4.48	4.69	4.83	4.97	5.12
	Δ R	.25	.081	.110	.090	.091	.078	.070	.068	.067	.065	.065	.067	.073	.070
	Range	.148	.224	.320	.401	.472	.529	.609	.677	.744	.799	.864	.931	1.004	1.074
	Energy	.35	.70	1.4	2.1	2.8	3.5	4.2	4.9	5.6	6.3	7.0	7.7	8.4	9.1
Nitrogen 13	Range	.137	.208	.297	.372	.438	.491	.556	.629	.690	.742	.802	.864	.932	.987
	Energy	.33	.65	1.30	1.95	2.60	3.25	3.90	4.55	5.20	5.85	6.50	7.15	7.80	8.45
Nitrogen15	Range	.159	.240	.358	.430	.505	.566	.652	.725	.796	.855	.925	.997	1.078	1.152
	Energy	.38	.75	1.5	2.25	3.0	3.75	4.5	5.25	6.0	6.75	7.5	8.25	9.0	9.75
Oxygen 15	q	.48	1.36	2.10	2.88	3.44	3.79	4.14	4.40	4.64	4.82	5.02	5.20	5.36	5.62
	Δ R	.269	.84	.116	.086	.086	.075	.065	.063	.063	.061	.061	.062	.067	.062
	Range	.158	.235	.331	.415	.481	.542	.607	.670	.733	.794	.855	.917	.984	1.046
	Energy	.38	.75	1.50	2.25	3.00	3.75	4.5	5.25	6.00	6.75	7.50	8.25	9.00	9.75

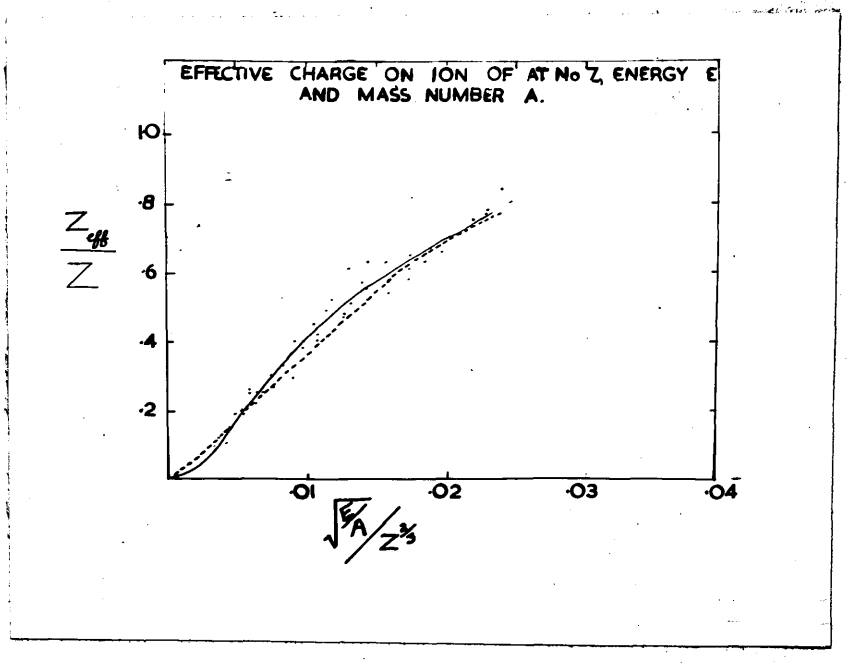

Figure A1.

The effective charge (Z_{eff}) on an ion of atomic number Z, mass number A, and energy E.

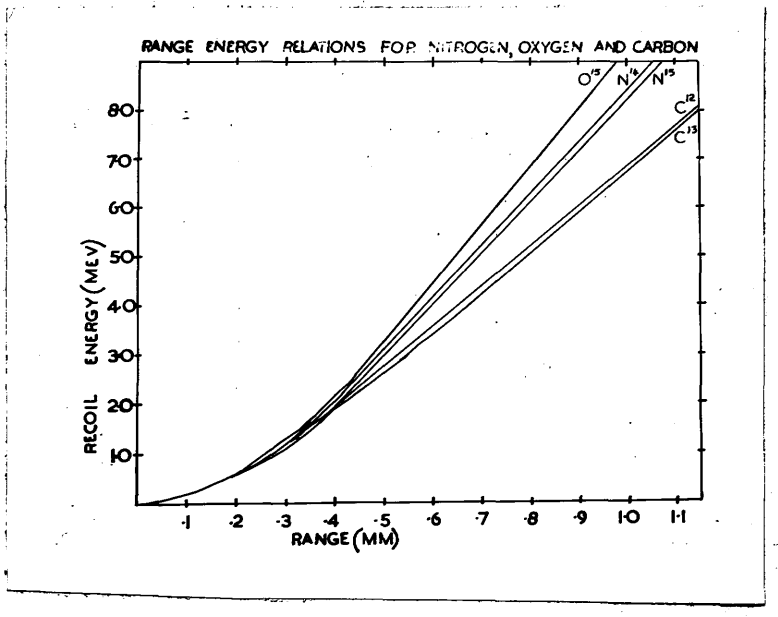

Figure A2

The Energy of carbon, oxygen and nitrogen ions as a function of their range.

APPENDIX 2

In the following pages are shown some examples of the cloud chamber photograph obtained in the course of experiments. The pictures show that it is possible to pick out the track of a heavy particle from the back-ground caused by electrons from the photon beam. It should perhaps be pointed out that a print, because of the relatively short range of tones possible on printing paper, can only give a poor reproduction of the negative used for measurement: it is much easier to pick out the dense black of a track in a negative, than to distinguish the pure white in a print. Figure A3 shows a (γ,p) event, of the type discussed in chapter 4, and Figure A4, A5, A6, are typical of the photographs obtained of disintegrations of nitrogen and oxygen in the work described in chapter 5.

Figure A3

This photograph shows a proton of energy about 1MeV from a low energy (γ,p) reaction in oxygen, of the type discussed in chapter 4.

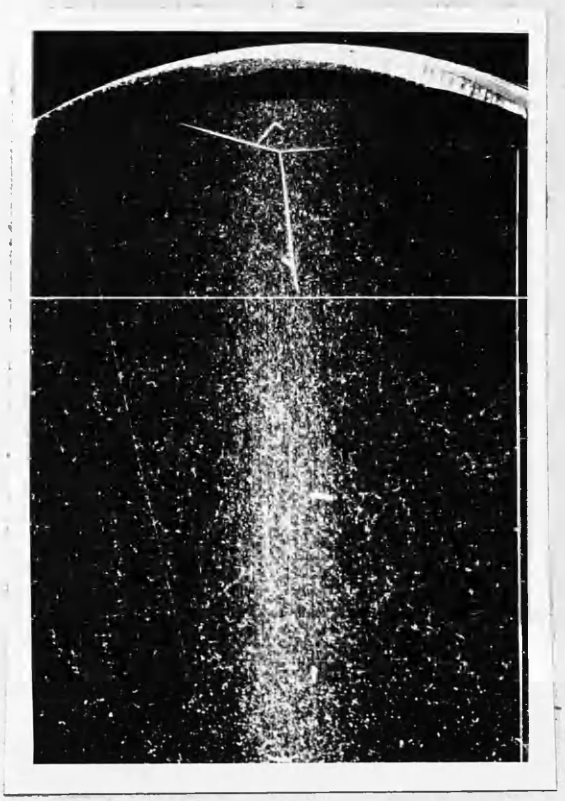

Figure A4

A single recoil track, from a (γ,n) reaction in nitrogen can clearly be seen. There are also a 3 pronged star, a non collinear flag (with a steep proton track), and a second single recoil.

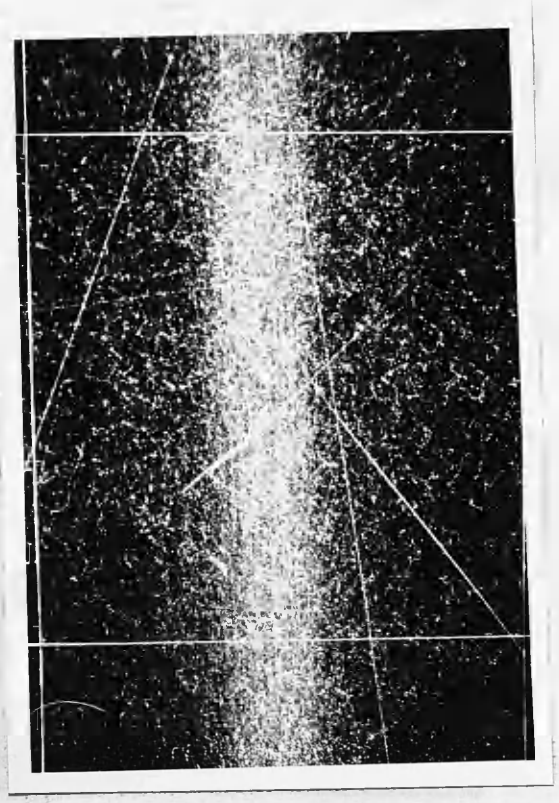

Figure A5

A collinear flag is visible in the core of the photon beam. Also in the picture are a 4 pronged star, a non-collinear flag and a single recoil.

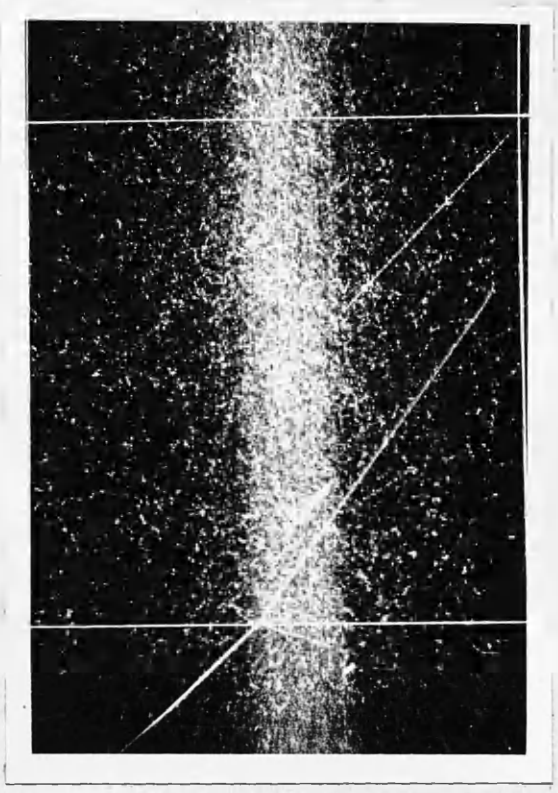

Figure A6

The picture shows a non-collinear flag near the edge of the photon beam. Two three-pronged stars can also be distinguished easily.

REFERENCES

REFERENCES

(1) Chadwick, J. and Goldhaber, M. Nature 134, 237 - 1934

(2) Szilard, L. & Chalmers, T.A. Nature 134, 494 - 1934

(3) Bethe, W. and Gentner, W. Zeit.f.Phys. 106, 236 - 1937

(4) Kerst, D.W. Phys.Rev. 60, 47 - 1941

(5) Huber, O Leinhard, O
Scherrer, P and Waffler, H. Helv.Phys.Acta. 17, 139 - 1944

(6) Baldwin, G.C. and
Klaiber, G.S. Phys.Rev. 70, 289 - 1946

(7) Baldwin, G.C. and
Klaiber, G.S. Phys.Rev. 73,1156 - 1948

(8) Weinstock, E. and Halpern, J. Phys.Rev. 94,1651 - 1954

(9) Weil, J.W., McDaniel, B.D., Phys.Rev. 92, 391 - 1953
Goldemberg, J. Phys.Rev. 93,1426L -1954

(10) Dixon, D. Private Communication

(11) Katz, L. and Cameron, A.G.W. Can.J.Phys. 29, 518 - 1951

(12) Katz, L., Haslam, R.N.H., Horsley, R.J.,
Cameron, A.G.W., and
Montalbetti, R. Phys.Rev. 95, 464 - 1954

(13) Halpern, J., Mann, A.K.,
Nathans, R. Rev.Sci.Inst. 23, 678 - 1952

(14) Titterton, E.W. Prog.Nuc.Phys. 4, 1 - 1955

(15) Reid, J.M., Swinbank, P.
and Atkinson, J.R. Physica. 22,1142A- 1956

(16) Toms, M.E., & Stephens, W.E. Phys.Rev. 92, 362 - 1953

(17) Montalbetti, R., Katz, L.
and Goldemberg, J. Phys.Rev. 91, 659 - 1953

(18) Okamoto, K. Phys.Rev. 110, 143 - 1958
Prog.The.Phys. 15, 75 - 1956

(19) Ferrero, F., Malvano, R.
Tribuon, C. Nuo.Cim. 6, 385 - 1957

Spicer, B.M. N.B.S. Photo nuclear Conf. paper B1- 1958

Fuller, E.G. N.B.S. Photo nuclear Conf. paper B2- 1958

(20) Carver, I.H. and Turchinez, W. N.B.S. Photo nuclear Conf. Paper S7 - 1958

(21) Kerst, D.W. and Price, G.A. Phys.Rev. 79, 725 - 1950

(22) Terwilliger, K.M., Jones, L.W. and Jarmie, W.M. Phys.Rev. 82, 820 - 1951

(23) Levinger, J.S. and Bethe, H.A. Phys.Rev. 85, 577 - 1955

(24) de Sabbata, V. Suppl. to Nuo.Cim. Ser. 10, 243 - 1957

(25) Wright, I.F., Morrison, D.R.O., Reid, J.M., and Atkinson, J.R.A. Proc.Phys.Soc. 59, 77 - 1956

(26) Spicer, B.M. Phys.Rev. 99, 33 - 1955

(27) Stephens, W.E., Mann, A.K., Patton, B.J., & Winhold, E.J. Phys.Rev. 96, 939 - 1955

Stephens, W.E. Physica. 22,1143A-1956

(28) Cohen, L., Mann, A.K., Patton, B.J., Winhold, E.J. Phys.Rev. 104, 108 - 1956

(29) Johansson, S.A.E. & Forkman, B. Phys.Rev. 99,1031L- 1955

Johansson, S.A.E. Physica. 22,1144A- 1956

Johansson, S.A.E. and Forkman,B. Ark.f.Phys. 12, 359 - 1957

(30) Katz, L., Haslam, R.N.H., Horsley, R.J., Cameron, A.G.W., and Montalbetti, R. Phys.Rev. 95, 464 - 1954

(31) Penfold, A.S. Proc. of Photo nuclear Conf. at "Case Institute of Technology"

(32) Katz, L. N.B.S. Photo nuclear Conf., Paper B8 - 1958

(33) de Sabbata, V. Suppl. to Nuo.Cim. Ser.10, 11, 225 - 1959

(34) Dixon, W.R. Can.J.Phys. 33, 785 - 1955

(35) Feld, B.T., Godbole, R.D., Odian, A., Scherb, F., Stein, P.C., Wattenburg, A. Phys.Rev. 94,1000- 1954

Levinthal, C., Silverman A. Phys.Rev. 82, 822 - 1951

Keck, J.C. Phys.Rev. 85, 410 - 1952

(36) Odian, A., Stein, P.C., Wattenberg, A. — Phys.Rev. 95, 576 - 1954

Odian, A., Stein, P.C., Wattenberg, A. and Feld, B.T. — Phys.Rev. 102, 837 - 1956

(37) Lalovic, B., Reid, J.M. and Turnbull, R. — Private Communication.

(38) Goward, F.K. and Wilkins, J.J. — Proc.Roy.Soc.A. 212, 357 - 1953

Millar, C.H. and Cameron, A.C.W. — Phys.Rev. 78, 76 - 1950; Can.J.Phys. 31, 723 - 1953

(39) Devons, S. — Excited States of Nuclei, P.92

(40) Bethe, H.A. and Longmire, C. — Phys.Rev. 77, 647 - 1950

Levinger, J.S. — Phys.Rev. 77, 970 - 1950

de Sabbata, V. — Nuo.Cim. 6, 368 - 1949

(41) Levinger, J.S. and Bethe, H.A. — Phys.Rev. 78, 115 - 1950

(42) Bethe, H.A. — Rev.Mod.Phys. 9, 87-90 - 1937

(43) Feenberg, E. — Phys.Rev. 49, 1328 - 1936

Siegert, A.J.F. — Phys.Rev. 52, 787 - 1937

(44) Levinger, J.S. and Kent, D.C. — Phys.Rev. 95, 418 - 1954

(45) Levinger, J.S. — Phys.Rev. 97, 122 - 1955

(46) Goldhaber, M. and Teller, E. — Phys.Rev. 74, 1046 - 1948

(47) Steinwedel, H. & Jensen, J.H.D. — Zeits.f.Naturfor 5a, 413 - 1950

(48) Danos, P. — Ann.d.Phys. 10, 265 - 1952

(49) Sagane, R. — Phys.Rev. 83, 175 - 1951; 84, 587 - 1951

(50) Danos, M. & Steinwedel, H. — Zeits.f.Naturfor 6a, 217 - 1951

(51) de Sabbata, V. & Sugie, A. — N.C. 3, 16 - 1956

(52) Businaro, V.L. & Gullone, S. — N.C. 1, 1285 - 1955

(53) Schiff, L.I. — P.R. 73, 1311 - 1948

(54) Danos, M. Bull Am.Phys.Soc.II, 1, 135 - 1956
Nucl.Phys. 5, 23 - 1958

(55) Weisskopf, V.F., and Ewing, D.H. Phys.Rev. 57, 472 - 1940

(56) Wolfenstein, L. Phys.Rev. 82, 690 - 1951

(57) Burkhardt, J.L. Phys.Rev. 91, 420 - 1953

(58) Byerly, P.R., Jr., and Stephens, W.E. Phys.Rev. 83, 54 - 1951

(59) Courant, E.D. Phys.Rev. 82, 703 - 1950

(60) Curtis, N.W., Hornbostel, J., Lee, D.W., Salant, E.O. Phys.Rev. 77, 290 - 1950

(61) Levinthal, C. & Silverman, A. Phys.Rev. 82, 822 - 1951

(62) Wilkinson, D.H. Proc. of Glasgow Conf. on Nuc. & Meson Phys.161 - 1954

(63) Wilkinson, D.H., Physica 22, 1039 - 1956

(64) Weisskopf, V. Phys.Rev. 96, 668 - 1954

(65) Lane, A.M. & Wilkinson, D.H. Phys.Rev. 97, 499 - 1955

(66) Penfold, A.S. & Spicer, B.M. Phys.Rev. 100, 1377 - 1955

(67) Rand, S. Phys.Rev. 107, 208 - 1957

(68) Wilkinson, D.H. Phil.Mag., Ser.8 3, 567 - 1958

(69) Toms, M.E. & Stephens, W.E. Phys.Rev. 108, 77 - 1957

(70) Mann, A.K., Stephens, W.E. and Wilkinson, D.H. Phys.Rev. 97, 1184 - 1955

(71) Lejkia, E., Osokina, R. and Ratner, B. Suppl. Nuo.Cim. 3, 105 - 1956

(72) Eichler, J., and Weidenmuller, H.A. Private Communication.

(73) Levinger, J.S. P.R. 84, 53 - 1951

(74) Dedrick, K.G. P.R. 100, 58 - 1955

(75) Brink, D.M. Nuc. Phys. 4, 215 - 1957

(76) Atkinson, J.R., McFarlane, W. Reid, J.M. and Swinbank, P. — Nuc.Instruments 1, 152 - 1957

(77) Wilkinson, D.H. — Phys.Rev. 99, 1347 - 1955

(78) Bethe, H.A. — Rev.Mod.Phys. 9, Section 14

(79) Schardt, A., Fowler, W.A. and Lauritsen, C.C. — Phys.Rev. 86, 527 - 1952

(80) Kraus, A.A., Jr., — 94, 975 - 1954

(81) Wilkinson, D.H. & Bloom, S.D. — Phys.Rev. 105, 683 - 1957

(82) Bashkin, S. and Carlson, R.R. — Phys.Rev. 106, 261 - 1957

(83) Bethe, H.A., Ashkin, J. — Experimental Nucl.Phys.I P.182 - 1953

(84) Crawford, I.G. — Thesis Sub. to Glasgow Univ.

(85) Preston, I.M.H.P. — Thesis Sub. to Glasgow Univ.

(86) Horsley, R.J., Haslam, R.N.H., Johns, H.E. — Can.J.Phys.30, 159 - 1952

Ferguson, G.A. Halpern, J., Nathans, R. — Phys.Rev. 84, 856 - 1951

(87) Yergin, P.F. — Phys.Rev. 95, 776 - 1954

(88) Spicer, B.M. — Aus.J.Phys. 6, 391 - 1953

(89) Livesey, S.L. — Can.J.Phys. 35, 987 - 1957

(90) Johansson, S.A.E. — N.B.S. Photo nuclear conf. Paper A.10 - 1958

(91) Certini, G.,Milone, M., Rinzivillo, R. and Tribuno, A. — Nuc. Cim. 9, 188 - 1958

(92) Burcham, W.E. — Prog.Nuc.Phys.4, 171 - 1955

Goldhaber, G. & Teller, E. — Phys.Rev. 74, 1046 - 1948

Radicatti, L.A. — Proc.Phys.Soc.A66, 139 - 1953

(93) Panofsky, W.K.H. and Reagan, D. — Phys.Rev. 87, 543 - 1952

(94) D.R.O. Morrison, Thesis - Glasgow Univ.1958

(95) Montalbetti, R., Katz, L. Can.J.Phys. 31, 798 - 1953

(96) Spicer, B.M. Aus.J.Phys. 10, 326 - 1957

(97) Milone, C. and Ricamo, R. Nuo.Cim. 5, 1338 - 1957

Milone, C., Milone-Tamburino, S., Rinzivillo, R., Rubbiro, A., and Tribuno, C. Nuo.Cim. 7, 729 - 1958

(98) Livesey, S.L. Can.J.Phys. 34, 1022 - 1956

(99) Papineau, A. Compte Rendu 242, 2933 - 1956
C.E.A. 543 - 1950

(100) Reid, J., Lalovic, B., and Turnbull, R. Private Communication

(101) Balfour, D. Thesis

(102) Lillie, A.B. Phys.Rev. 87, 716 - 1952

(103) Feather, N. Proc.Roy.Soc. A141, 194 - 1935

(104) Wrenshal, G.A. Phys.Rev. 57, 1095 - 1940

(105) Blackett, P.M.S. Proc.Roy.Soc. 107, 349 - 1926

Blackett, P.M.S. and Lees Proc.Roy.Soc. 134, 658 - 1933

(106) Knipp, J. and Teller,E. Phys.Rev. 59, 659 - 1941

(107) Livesey, S.L. Can.J.Phys. 34, 215 - 1956

(108) Allison, S.K. and Warshaw, S.D. Rev.Mod.Phys. 25, 779 - 1953

(109) Bethe, H.A. Rev.Mod.Phys. No.2. P.213 - 1950

(110) Eaton, W.W. Phys.Rev. 48, 921 - 1935

MacCarthy, J.T. Phys.Rev. 53, 80 - 1938.